Zenith of the quantum doctrine

Dissection of the uses and misuses of quantum theory in the quest for macroscopic mechanical quanta

Pereira Machado, João

DOI
10.4233/uuid:81bfc0a9-e4eb-4133-949b-c9ae0671c610

Publication date
2019

Document Version
Final published version

Citation (APA)
Pereira Machado, J. (2019). *Zenith of the quantum doctrine: Dissection of the uses and misuses of quantum theory in the quest for macroscopic mechanical quanta*. [Dissertation (TU Delft), Delft University of Technology]. https://doi.org/10.4233/uuid:81bfc0a9-e4eb-4133-949b-c9ae0671c610

Important note
To cite this publication, please use the final published version (if applicable).
Please check the document version above.

Zenith of the Quantum Doctrine

Dissection of the uses and misuses of Quantum Theory in the quest for macroscopic mechanical quanta

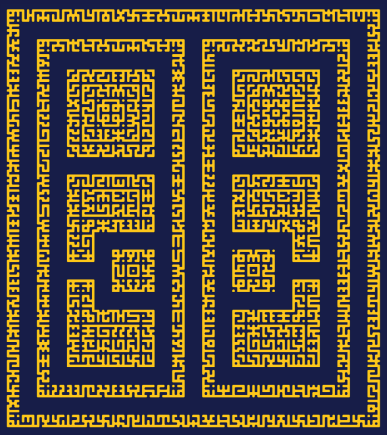

João Machado

ZENITH OF THE QUANTUM DOCTRINE

DISSECTION OF THE USES AND MISUSES OF QUANTUM THEORY IN THE QUEST FOR MACROSCOPIC MECHANICAL QUANTA

Zenith of the Quantum Doctrine

Dissection of the uses and misuses of Quantum Theory in the quest for macroscopic mechanical quanta

Proefschrift

ter verkrijging van de graad van doctor
aan de Technische Universiteit Delft,
op gezag van de Rector Magnificus Prof. dr. ir. T.H.J.J. van der Hagen,
voorzitter van het College voor Promoties,
in het openbaar te verdedigen op woensdag 27 februari 2019 om 10:00 uur

door

João Duarte Pereira Machado

Master of Science in Engineering Physics,
Technische Universiteit Delft, Delft, Nederland,
geboren te Lissabon, Portugal.

Dit proefschrift is goedgekeurd door de

promotor: Prof. dr. Y. M. Blanter

Samenstelling promotiecommissie:

Rector Magnificus,	voorzitter
Prof. dr. Y. M. Blanter,	Technische Universiteit Delft
Onafhankelijke leden:	
Prof. dr. R. Fazio	International Centre for Theoretical Physics, Italië
Dr. S. Gröblacher	Technische Universiteit Delft
Prof. dr. ir. T. H. Oosterkamp	Universiteit Leiden
Prof. dr. Y. V. Nazarov	Technische Universiteit Delft
Prof. dr. L. Kuipers	Technische Universiteit Delft
Prof. dr. A. F. Otte	Technische Universiteit Delft, reservelid

Keywords: Cavity Optomechanics, Mechanical quantum states, Quantum-Classical comparison

Printed by: IPSKAMP PRINTING

Casimir PhD Series, Delft-Leiden 2018-17

ISBN 978.90.8593.346.5

An electronic version of this dissertation is available at
http://repository.tudelft.nl/.

Voor mijn eerste leraar,
Een bloedoffergave,
Als proef van geletterdheid.

CONTENTS

SUMMARY / SAMENVATTING

The reflections composing this thesis examine the usage and necessity of quantum theory, with an emphasis on systems featuring mechanical resonators. The first chapter introduces the quantum formalism, reviews the historical motivation for the quantization of harmonic oscillators, and presents a derivation of the interaction between the electromagnetic field and mechanical motion in several distinct systems. The second chapter examines the nature of physical effects such as state transfer, squeezing, entanglement, and sideband asymmetry, and how they naturally emerge in non-quantum contexts. A dynamical statistical theory is introduced to aid the quantum/classical comparison, and standard measurement models are reviewed due to their strict connection to nonclassicality criteria. The third chapter deals uniquely with quantum effects occurring in systems with mechanical elements, such as phonon antibunching, parametric down-conversion in electromechanical systems, creation and interference of macroscopic superpositions in spin-cantilever systems, and collapse and revivals of mechanical motion and mechanical state dependent transmission in membrane-in-the-middle geometries. The fourth and last chapter discusses pervading issues with defining the classical limit, the quantum/classical comparison and definitions of nonclassicality.

Dit proefschrift is opgebouwd uit reflecties die het gebruik en de noodzaak van kwantumtheorie onderzoeken, met de nadruk op systemen met mechanische resonatoren. Het eerste hoofdstuk introduceert het kwantumformalisme en herziet de historische motivatie voor de kwantisering van harmonische oscillatoren. Verder wordt een afleiding van de interactie tussen het elektromagnetische veld en mechanische beweging in diverse verschillende systemen gepresenteerd. Het tweede hoofdstuk reflecteert op de aard van fysieke fenomenen zoals toestand overdragen, squeezing, verstrengeling en sideband-asymmetry, en hoe deze effecten zich vormen in niet-kwantum contexten. Een dynamische statistiektheorie wordt geïntroduceerd om de vergelijking tussen kwantum/klassieke verschijnselen te ondersteunen. De standaardmeetmodellen worden herzien vanwege het strikte verband met de nonclassicality criteria. Het derde hoofdstuk behandelt alleen kwantumeffecten die kunnen worden waargenomen in systemen met mechanische elementen, zoals phonon antibunching, parametrische down-conversie in elektromechanische systemen, creatie en interferentie van macroscopische superposities in spin-cantilever-systemen, en collapse & revivals van mechanische beweging en mechanische toestand-afhankelijke transmissie in membrane-in-the-middle geometrieën. Het vierde en laatste hoofdstuk analyseert de alomtegenwoordige problemen met de definities van het klassieke limiet en nonclassicality, net zoals de kwantum/klassieke vergelijking.

PREFACE

The hive is crammed. It is time to know ourselves. We, men of knowledge, are but foragers. Always struggling to find the next grain to ensure our survival. And in sunny days, we are zealous clerks, delighted with tending the gathered honey. We live obsessed with climbing up the tower, and our hastily life forgets that our heart craves to go down. Who among us has still a will to tackle prominent problems? Can we still believe in "greater questions" or do we deem what was once considered denuding the veils of nature as a naivety of yore?

We hear the surf of publications waves. Loud, massive, swarming and unimpressive. Only the simpleminded believe that truth or value can be measured in numbers. We hear how every day new wonderful groundbreaking discoveries are unclogging the path to the next technological revolution. We have no use nor need for another quantum-teleporting-topologically-entangled computer. Nature, Science, Gucci. The anthem of the vanity fair is too embedded in our ears. We hear the sermons of modern science preachers... but what is this smell they exhale? Depth, passion, commitment, rigor. They are all covered in dust. Are we also the last scientists?

The current state of Physics constrains every discussion to be dominated by linguistic traits nowadays. Never before were physicists so thrilled with semantic foreplay. The hermetic meaningless technicality, the self-referring and inconsistent definitions, the hunger for abstractedness, *chimeraconcepts* breeding other *chimeraconcepts*. What was once a science concerned with tangible entities has become a grammarian affair. Unclear? What does it mean quantum? What does it mean nonclassical? Surely such vocabulary is not unknown to anyone. It is now commonplace how quantum mechanics is a theory about the material consequences of sentimental indigestions. *Vox populi vox veritatis*. "Quantum" has become more than an attribute. It is now a mantra, or for more sensitive ears, a redundant definite article. Even past our gates, we find con men, lunatics and mystics selling holistic snake oils and other world panaceas. Decency has abandoned our domains. We no longer hold anything venerable, much less care for naming taboos. We would rather face lies, but we have to content ourselves with fairy-tales told with innocence and paternalistic affection. In our world of today, who does still deeply believe in science?

We abdicated asceticism for this. To become friendly, proselyte, reputable. A shadow of what we are supposed to be. We need to recall that there are no shortcuts to truth. Only serious, devoted, sober, lucid work. We need to acknowledge that candied porridge does not satiate us. We need to live education as scientific nurture. The futile accumulation and parroting of encyclopedic knowledge has no room in our vaults. Entertainers no longer amuse us and we learn nothing from human calculators. For there is only one thing we can ultimately conceive and value as science: speleology. Everything else is a mockery, and it should be left untouched. It is our duty, and what a repugnant one, to dive in the mud to search for the grains of truth. And by doing so, to face the danger of being nauseated with science.

1

ROOTS AND CORE OF QUANTUM OPTICS

First Myth of Physics: Intuition. What is learned through perception, it is never digested by the thought. At the dawn of the past century, a new age for physics began that utterly changed the notions about the nature of light and matter, giving birth to a completely new exotic world. As the revolution took place, manifestos were published. Once it ended, they metamorphosed into books. These remain mostly unread, only to occasionally whisper their provocative ideas.

Since my initiation, I have encountered two types of books on Quantum Optics: the prescriptive grammars, usually labeled as "formal", and the romantic novels, labeled as "intuitive". The first kind spur from authors with ascetic feelings towards mathematics alongside with a passion for etiquette, while the latter from a fear of mathematics and a desire for naturalness and connection to the material world. What is often observed in the first kind, is an obsession with formalism, where field quantization is introduced *ad hoc*, and mathematical properties and calculations are listed and derived without any deep discussion. The biggest danger of this sort of books, and an occasionally recurring trend in some fields of physics, is the desire to axiomatize physics, making it believe that the functioning of the entire universe could be derived from pure logic. The implications of such axiomatization are twofold: the imposition of dogma, where the underlying theoretical principles are revealed as divine truth; and the erasing of history. In fact, could anyone believe in any theory after witnessing its birth? Watching it crawl, gross and rickety, out of the sludgy chaos of concepts, struggling with constantly new discovered contradictions? No. It would be impossible.

On the other hand, against my deepest values and prejudices, I have never learned so much from the second kind. Despite the poor logical structure, depth of analysis, and unsubstantiated argumentation, had I not come across them, I would probably be more gullible. To these books, I am also grateful for inciting me in the pursue of the nature of light and matter, untainted by the urge to accept lesser truths.

The purpose of this work is to clarify several aspects regarding the quantum nature of

light and matter. From the inclined reader, it is expected familiarity with Quantum Optics, as the discussions exposed require a minimum of knowledge, and an indomitable will to understand. In the absence of such prerequisites, the content of this thesis will remain hermetic. For the ink that wrote it carries more than the desire to be read.

1.0.1. QUANTIZATION ABRIDGED

Consider a swinging pendulum in the presence of a gravitational field. The Hamiltonian describing the system is

$$\mathscr{H} = \frac{ml^2}{2}\dot{\theta}^2 + mgl(1-\cos(\theta)) \approx \frac{1}{2ml^2}L^2 + \frac{1}{2}mgl\theta^2, \tag{1.1}$$

where the approximation is valid for a small angle θ in respect to the equilibrium position. L is the angular momentum, m is the mass of the pendulum, g the local gravitational acceleration and l the pendulum's length. Within the approximation taken, the Hamiltonian of the system corresponds to a harmonic oscillator. Canonical quantization [1] dictates that canonical variables must be promoted to operators obeying the commutation relations $[\theta, L] = i\hbar$. This leads to the Hamiltonian $\mathscr{H} = \hbar\omega(b^\dagger b + 1/2)$, with the pendulum frequency $\omega = \sqrt{g/l}$, $\theta = \theta_{ZPF}(b + b^\dagger)$ and $L = iL_{ZPF}(b^\dagger - b)$, where

$$\theta_{ZPF} = \sqrt{\frac{\hbar}{2ml^{3/2}\sqrt{g}}} \quad \text{and} \quad L_{ZPF} = \frac{\hbar}{2\theta_{ZPF}}. \tag{1.2}$$

A classical pendulum swings with a precise amplitude and phase of motion determined by its initial conditions. So what is quantum in the quantum harmonic oscillator? The excitations. The energy of the resonator is proportional to integers of $\hbar\omega$, and these integers (the eigenvalues of the number operator $b^\dagger b$) correspond to the number of excitations present in the resonator. Further, the amount of excitations may be not well defined and when measured, the position (or angle, or angular momentum) of the pendulum returns a random outcome dependent on the state of the system. This summarizes the quantum properties of the pendulum and, as it is widely known, the classical limit occurs when $g \to \infty$, because the position of the pendulum becomes precisely defined. *N'est-ce pas?*

Not quite. How does gravity affect quantum mechanics? If the quantum uncertainties associated with the position of the pendulum are to be enhanced, it is best to avoid gravity and, as implied by θ_{ZPF}, a nearly free fall experiment should display a massive uncertainty. Thus, put a pendulum inside an elevator, sabotage the hoist, and watch its quantum nature flower. Although θ_{ZPF} increases with decreasing g, other uncertainties associated with the energy or angular momentum diverge as $g \to \infty$. Thus, by travelling to the closest black-hole, one would recover another fully quantum limit. How is the interplay between gravity and quantum mechanics then? Obscure.

Banters aside, contemporary General Relativity vs Quantum Mechanics quarrels shall not be touched upon. The example above serves only to portrait the essence of quantization trickery, even though it provides inspiration for the study of fundamental quantum uncertainties in altered gravity environments. But how to recover the classical dynamics then? Once the quantum leap has been taken, there is no going back. And is this quantization unique? I.e. are there alternative quantization procedures, and do they lead to

the same quantum nature for the system? Several distinct quantization methods exist, but they all suffer from their own pathologies and lack of equivalence between them [2]. Assigning quantum operators to classical variables easily leads to contradictions in the correspondence [3, 4], for multiparticle systems quantization can lead to a nonbosonic nature [5, 6], and even to a different spectrum for the harmonic oscillator [6, 7]. But such pathologies are asymptomatic.

But most importantly: why must the pendular motion be quantized? Why should the energy of such macroscopic object only take discrete values? Where did such idea come from? The origins of field quantization began with light, only to spread later to other forms of oscillations, due to the analogous physical behaviour. To understand the motivations for this quantization, one needs to look back to the conception of Quantum Optics. Although revisiting history is frightening and dangerous because it harms the belief of constant progress, let us nevertheless review the phenomena that triggered the quantization of the electromagnetic field, and ultimately led to the quantization of every harmonic oscillator.

1.1. FOUNDING PILLARS OF QUANTUM OPTICS

In this section, the original physical phenomena that led to the idea of an intrinsic discrete nature for the electromagnetic field are dissected in order to recall the necessity of quantizing light.

1.1.1. COMPTON EFFECT

Almost a century later, the Compton effect is still celebrated as a landmark proof of the existence of the photon [8], and the reason is simplicity. Compton [9] explains the frequency change of incident radiation in an absurdly simple manner by considering a single incident photon hitting an electron at rest, and losing momentum and energy (thus lowering its frequency) in the process. The price to pay for simplicity is leaving several apprehensions alive. In 1923, single-photon emitters did not exist, and even if the radiation beam has an arbitrarily low intensity, the radiation field still interacts with the electron with all the photons supported by the field's statistics *simultaneously*. Further, there is no reason for the photon number to be conserved, and the electron is able to emit any number of photons during the scattering process. The belief that the Compton effect is a manifestation of a particle nature for light is solely due to the comparison with billiards, and to the lack of frequency shift predicted by Thomson scattering. But like any classical field, the electromagnetic field carries energy and momentum, can exchange them with electrons, and scatter them. A photon-free explanation for this frequency shift was obtained by analysing the scattering process via the transition from a weakly bound state to a free electron state with momentum $\hbar\vec{k}$ with the Klein-Gordon equation[1] and a classical electromagnetic field [10, 11]. The Klein-Nishina formula as originally derived [12] did also not employ any quantized electromagnetic field. Such semiclassical explanations have reoccurred decades later [13, 14], and as emphasized by [13], the success of Compton's formula comes from the resonant form of the dipolar

[1] The Dirac equation was not known at the time; Klein-Gordon was the typical procedure for dealing with relativistic particles.

interaction, which makes the energy exchange between light and the electron peak at $\hbar\omega$, with $\hbar$ entering the formula through the Dirac [2] equation. Likewise, other scattering phenomena (such as Bremsstrahlung) say nothing regarding the nature of radiation, and that holds true for the following effect.

1.1.2. PHOTOELECTRIC EFFECT

Physical concepts do not have definitions, they have existence. And the living proof is the concept of photon, as the current one hardly shares any lineage with Einstein's original proposal of "spatially discontinuous distributions of energy" for light [15], nor entirely with Dirac's notion of a photon [1]. At the time, the photoelectric effect posed a puzzling problem mainly due to the lack of knowledge about the electronic structure of matter. When a metal is irradiated, electrons are ejected from the metal if the frequency of the incident radiation is above a characteristic threshold. For any frequency below this threshold, no photocurrent is created, even if the light intensity is drastically increased [3]. On the other hand, increasing the frequency above threshold only leads to an increase on the number of emitted electrons but not on their average kinetic energy. Further, it was expected to be a pronounced lag time between the irradiation and the emission, proportional to the build up energy time, but this time difference is not observed. All these features led to the proposal of "energy packets" for light [15] as an empirical way to explain the phenomenon. As time passed and more knowledge over the electronic behaviour of matter was gained, the "energy-packet" idea was dismissed in favour of a microscopically distinct model. With the advent of the Schrödinger equation, photoemission was modelled via the electronic transition from a bound state to a free electron state [16, 17], and treating the electromagnetic field classically. Einstein's rules for the photoelectric effect were once more rederived [18], with this formalism where light couples to matter via the Schrödinger equation cementing the modelling paradigm for photoemission [19, 20]. Despite a general understanding of the photoemission process, a full dynamical nonperturbative explanation still remains an open problem [21], motivating other approaches like quantum trajectories [22] and mathematical offshoots featuring Floquet theory [23].

1.1.3. SPONTANEOUS AND STIMULATED EMISSION AND RELATED EFFECTS

When an atom in vacuum is excited, its excited state is unstable and the atom decays spontaneously into a lower energy level emitting light with a frequency proportional to the energy difference between the atomic states. This phenomenon is named spontaneous emission and it is responsible for the atomic spectral lines. Despite the ubiquity of relaxation processes in the macroscopic world, the lack of knowledge on how to introduce decay in atomic systems made spontaneous emission another puzzle. Time-dependent perturbative QED calculations [24, 25] showed that the decay rate for a system in an excited state is proportional to $n+1$ (with n the photon number), and so when the light field is in its quantum vacuum state, decay still occurs. As this result does not hold for a classical field, spontaneous emission became an example of how quantum

[2] The results have been derived with the Klein-Gordon equation but they still hold for the Dirac equation.

[3] Except for ultra-intense light, when two photon-absorption can occur and photocurrent can be produced below threshold.

fluctuations of the electromagnetic field induce decay [25, 26], and of the necessity of the photon concept. However, the necessity of quantizing the electromagnetic field was once more questioned upon the discovery that radiation reaction causes spontaneous emission [27–30]. Incited by the QED divergence problems and the desire to test the limits of semiclassical approaches, the neoclassical theory launched a review of light-matter effects by taking the electromagnetic field in the Schrödinger equation to be classical, and considering the electrical current in Maxwell equations to be the quantum current $\vec{J} \propto Im(\psi^* \nabla \psi)$. Together with the backaction of the electron's own field, this leads to a natural decay term for an atom in an excited state, with the same decay rate [27–30] as in QED (the Einstein's A coefficient). As noted by [30], it is the selected use of retarded potentials that induces an "arrow of time" and enables the radiative decay. One could then think that there are two alternative explanations for the same phenomenon, and leading to the same results. However, the perturbative QED calculations [24, 25] only predict a transition for short periods of time, and do not guarantee that the system will remain in the ground state at $t \to +\infty$. As seen from the solution of the Jaynes-Cummings Hamiltonian [27], if the atom begins in its excited state and light in vacuum, the system simply experiences Rabi oscillations, but not irreversible decay. For the irreversibility of the decay process to be captured, the atom has to couple to a densely packed multimode electromagnetic field reservoir [26]. But in this situation, it is the coupling to all the radiation modes of the universe that forces the atom to decay, and the nature of the electromagnetic field is irrelevant.

Another related phenomenon is stimulated emission, where an excited atom decays to a lower energy state in the presence of an applied electromagnetic field, and amplifies the light in the process. Like all the preceding phenomena, the Maxwell-Schrödinger equations explain stimulated emission as well as optical nutations [29], and these equations form the primordial theory modelling the operation of masers [31] and lasers [32].

1.1.4. BLACK-BODY RADIATION

Occasionally, one wonders how the historical succession of scientific discoveries shapes our perception about the universe, and how that perception would differ had the breakthroughs happened in a different order. Black-body radiation was perhaps a premature phenomenon under this light. The Planck distribution for black-body radiation is regarded as the first evidence supporting the existence of light quanta. Yet, Planck's original idea was connected to "quantum oscillators" for the cavity's boundaries and not for the field itself, and the other explanation, stealthy and forsaken, relies on it. In the quantum statistical physics explanation of black-body radiation, light forms a non-interacting gas, where the interaction with its surroundings plays no role in the thermal state. But it is only through absorption and emission processes that light reaches its "thermal equilibrium", and the Planck distribution can be obtained from a detailed balance equation of the emission and absorption rates [30]. This can be seen from the following simplified argument of [30]: Consider a set of atoms or molecules interacting with classical light. For dipolar couplings ($\vec{E}.\vec{\mathscr{P}}$), the resonant interactions occur only when there is a frequency matching between the electromagnetic field frequency ω and the phase frequency $\epsilon/\hbar$ of the electronic dipolar moments (see Eq.(1.5)). Thus, one can simply approximate the whole system as a set of two-level systems (with a ground state $|g\rangle$ and

an excited state $|e\rangle$) that couple only to their corresponding resonant electromagnetic mode. Equilibrium is obtained by a detailed balance for the transition rates between the ground and excited states:

$$0 = \underbrace{A_{eg}p_e}_{\text{spontaneous emission}} + \underbrace{B_{eg}p_e\rho(\omega)}_{\text{stimulated emission}} - \underbrace{B_{ge}p_g\rho(\omega)}_{\text{absorption}}, \tag{1.3}$$

where $\{p_g, p_e\}$ are respectively the probabilities of finding an electron in the ground and excited states, $\{B_{ge}, B_{eg}, A_{eg}\}$ the Einstein's coefficients associated with absorption and spontaneous and stimulated emission, and $\rho(\omega)$ the electromagnetic energy density. With the Fermi golden rule, the absorption rate ($\propto \rho(\omega)|\langle e|\sigma_x|g\rangle|^2$) is found to be identical to the stimulated emission rate ($\propto \rho(\omega)|\langle g|\sigma_x|e\rangle|^2$), and so $B_{eg} = B_{ge}$. Further, in thermal equilibrium, $p_g = p_e e^{\beta\epsilon}$, where ϵ is the energy difference between the ground and excited states. With the resonant condition, Eq.(1.3) becomes

$$\rho(\omega) = \frac{A_{eg}}{B_{eg}} \frac{1}{e^{\beta\hbar\omega} - 1}, \tag{1.4}$$

which is the Bose-Einstein distribution. This illustrates how Planck's distribution naturally arises from a microscopic equilibrium between light-induced atomic transitions, making any granularity for light superfluous.

1.1.5. 1057 MHz

QED is not only about light, but also about its absence. Whenever a quantum field exists, even if there are no excitations present, it still interacts with the rest of the world. Such interaction with this new type of vacuum is occasionally blamed for several phenomena, among which the Lamb shift is occasionally found [26, 33]. The Lamb shift refers to the energy difference between the $2P_{1/2}$ and the $2S_{1/2}$ states of the hydrogen atom initially measured by Lamb [34], and it posed a problem to Dirac's electron theory because the latter predicts no energy difference between the $2P_{1/2}$ and the $2S_{1/2}$ states. Since experiments show that the $2S_{1/2}$ state is ≈1057 MHz above the $2P_{1/2}$ state, panic would have been installed if not for the recollection that much more is present than just an instantaneous point-like Coulomb potential. Quantum mechanics raised from the radiative consequences of orbiting electrons interacting with their own electromagnetic field, and so Dirac's hydrogen spectrum could never be the final prediction, as this interaction was not accounted for. The interaction of the electron with its own field gives rise to self-energy corrections to Dirac's spectrum, which have been repeatedly evaluated [35]. Despite divergence issues, necessity of arbitrary cutoffs or regulators, and new experimental deviant values [36], the interaction of the electron with its own field is taken to be the source of the Lamb shift. Electron self-energies already occur classically [37], they reoccur in the quantum theory for the electron, and they have no connection to zero-point fluctuations of the electromagnetic field. In any of the self-energy calculations mentioned [35] was the electromagnetic field ever quantized, but nevertheless enigmatic "vacuum fluctuations perturbing the position of the electron" [33] have come to make part of the folklore supporting the existence of photons. But like other spectral corrections testifying in favour of QED, they do it so by supporting Dirac's electron

theory rather than defending a particular nature for light. As it was formulated, Dirac's theory is simply a field theory for electrons.

Enough with the procession. Effect after effect, it has been clear that the photon concept is foreign to all of these phenomena, even if they constitute its homeland. If its genesis was a misconception, how come was it so fruitful? The answer lies in the particularities of the Schrödinger equation. A widely unnoticed fact is the existence of two $\hbar$'s: one arising from the Schrödinger (or Dirac) equation for the electron, and the other imposed for the electromagnetic field. However, there is nothing dictating *a priori* that the de Broglie's relations should be exactly equal for both matter and light. The resilience of the photon concept, the reason behind the apparent granularity of light where the energy of a mode is proportional to its frequency, comes from the condition for resonant interactions between light and matter. As noted repeatedly (see for example [13]), if an electronic transition between two states ($|1\rangle, |2\rangle$, with an energy difference ϵ between them) is induced by an electromagnetic field mode of frequency ω (and amplitude $\mathscr{A}$) via the dipolar interaction (in the interaction picture)

$$V_I = \lambda\Big(|1\rangle\langle 2| exp\Big[-i\frac{\epsilon}{\hbar}t\Big] + |2\rangle\langle 1| exp\Big[i\frac{\epsilon}{\hbar}t\Big]\Big)(\mathscr{A}_k e^{-i\omega t} + \mathscr{A}_k^* e^{i\omega t}), \tag{1.5}$$

the resonance condition occurs when $\epsilon = \hbar\omega$. This frequency matching condition for light-induced electronic transitions makes the energy exchange between light and matter occur in "quanta" of $\hbar\omega$, and it is this resonant feature that perpetuated the idea that light itself has a dicrete nature whose energy only exists in the form of integers of $\hbar\omega$. Thus, from the perspective of the neoclassical theory, "photons" arise as a by-product of an effective field theory of light-matter interaction, and have otherwise no real existence. But if such misconception has been objected, what else upheld the existence of photons?

1.2. BLOSSOMING OF QUANTUM OPTICS AND DEBUT OF ITS OFFSPRING

Truth be told, photons populated the physics folklore since their invention, and it was the fascination with them that secured them from oblivion. But what made them survive until today, what is in the heart of Quantum Optics, what lacked in Classical Electrodynamics and what the neoclassical theory could not provide, is the ability to portrait uncertainties and correlations for light. If a moment must be marked when Quantum Optics is ripe enough to be deemed needed, that moment is the first[4] direct observation of photon-antibunching [40]. The analysis of correlations between the intensity of a light beam split into two detectors was already a reality [41], but only with the discovery of anticorrelated intensities, impossible in a classical theory, could Quantum Optics have a *raison d'être*. These experimental observations were complemented with other types of correlations , such as Bell-like tests with entangled light [42–44]. Further, the analysis of statistical properties of light gave rise to the observation of uncertainty related effects

[4] It is sometimes found in the literature that the first observation of antibunching belongs to [38], but as also noted by [39], no direct measurement of $g^{(2)}$ was performed.

such as squeezing [45, 46], where the uncertainty of an electromagnetic field quadrature q was reduced below q_{ZPF}, at the expense of increasing the uncertainty on the other quadrature. Additionally, exotic states of light, such as Fock states [47], and cat-states [47, 48], were observed experimentally with tomography techniques.

And it is under this auspice that quantum theory reaches its zenith. Incited by its forerunner's successes, and dismissing the warnings of the neoclassical theory, the offspring of Quantum Optics proliferated into an initially forbidden territory: the land of things-we-can-see-with-the-naked-eye. As victory was achieved in the microscopic realm, there could be no reason for not attaining it in the macroscopic realm as well, since the latter is but a congregation of microscopic realms. And so, *mechanics* was emphasized in quantum mechanics, and the quest for phenomena exhibiting macroscopic quantum behaviour began. Not simply as mere emergent phenomena, but as genuine replicas of what was once confined to the microscopic world. For this mission, the most elementary paradigm of all played a central role: the harmonic oscillator. "All that oscillates has a quantum nature", so is proclaimed. And mechanical resonators, sharing a common oscillatory nature with light, constitute the primary tool and icon. And with them, Quantum Optomechanics attempts to conquer a seat for itself, in a territory where the $\hbar$, the superposition principle for probability amplitudes, and other related weaponry of its electrical ancestor are not immediately guaranteed. What led to the quantization of motion in mechanical resonators (like the quantization of any other form of oscillator) was the view that if, just like light, other bodies have an oscillatory nature, the quantization applied to light must also be applied to them. This forms essentially a speculation about the nature of mechanical motion. As light and mechanical motion have fundamentally different attributes, such quantized nature should not be taken for granted.

And this is how we have come to Quantum Optomechanics, where the quantum nature of both light and mechanical motion can be tested in systems coupling optical cavities to mechanical resonators. But what effects were observed in these systems that allude to a quantum nature? A non-exhaustive list [49, 50] includes: observation of shot noise in position sensing [51, 52], thus reaching the standard quantum limit (SQL); pushing the boundary further, SQL was passed [53], leading to detection sensitivites no longer limited by quantum fluctuations. Such feat is essentially possible because of squeezing. Reducing the uncertainty of the resonator's position (or of any other quadrature) is already a reality [54, 55] and it implies a manipulation of the resonator state. State manipulation has also been achieved in electromechanics, where mechanical and microwave resonators have been entangled [56], and displayed anticorrelations in the measurement of the quadrature fields. Further, transferring the (coherent) state of microwaves to the mechanical resonator and back has also been achieved [57], being dubbed "coherent quantum state transfer", and later extended to the optical domain. It was also observed in these systems that the optical (or microwave) sidebands created by the mechanical element were asymmetric [58–62], which has been attributed to quantum fluctuations.

In the meantime, other observed effects can be included in this list, such as phonon antibunching [63], where intensity anti-correlations were measured after swapping the light state with the mechanical state. Additionally, claims of direct phonon Fock state measurement [64] have also been made. The nature of (most of) these effects will be discussed in more detail in the following chapters, but for the moment a more pertinent

question arises: How does light couple to mechanical motion? To answer it, one needs to dive in the core of Optomechanics.

1.3. QUANTUM OPTOMECHANICS

1.3.1. OPTICAL CAVITIES AND THE NATURE OF PHOTONS

The energy of the electromagnetic field stored inside an optical cavity is given by

$$\mathscr{H} = \int \frac{\epsilon}{2}\left(||\vec{E}||^2 + c^2||\vec{B}||^2\right) d^3r\,, \tag{1.6}$$

where ϵ is the electric permittivity, c the speed of light, and $\vec{E}$ ($\vec{B}$) the electric (magnetic) field. As the fields only exist inside the cavity, the boundary conditions lead to a set of discrete modes. In a certain sense, this is a first quantization of the electromagnetic field, since the field cannot have arbitrary wavelenghts but only the allowed discrete set of wavelengths. This "quantization" arises from the imposed boundary conditions and it is essentially, geometric. But so it is with all quantizations.

From Maxwell's equations, one obtains the dispersion relation $\omega_k = |k|c$, where k is the angular wavenumber, ω_k the angular frequency, and c the light speed. The geometry of the cavity will only affect the spatial distribution of the mode and it has no consequences for the second quantization procedure. Decomposing the electric and magnetic fields as

$$\vec{E}(\vec{r},t) = -ic\sum_{\vec{k},\mu} |k|\mathscr{A}_{\vec{k},\mu} e^{i(\vec{k}.\vec{r}-kct)}\vec{e}^{\,||}_{\vec{k},\mu} - c.c.\,, \tag{1.7}$$

$$\vec{B}(\vec{r},t) = i\sum_{\vec{k},\mu} k\mathscr{A}_{\vec{k},\mu} e^{i(\vec{k}.\vec{r}-kct)}\vec{e}^{\,\perp}_{\vec{k},\mu} - c.c.\,, \tag{1.8}$$

where $\vec{k}$ labels the mode, μ the polarization, $\mathscr{A}$ the complex amplitude of the fields, and $\{\vec{e}^{\,||}_{\vec{k},\mu}, \vec{e}^{\,\perp}_{\vec{k},\mu}, \vec{k}\}$ form an orthogonal basis, one arrives at the Hamiltonian

$$\mathscr{H}_0 = 2\frac{V_{ol}}{\mu}\sum_{\vec{k},\mu} ||\vec{k}||^2 |\mathscr{A}_{\vec{k},\mu}|^2\,. \tag{1.9}$$

For simplicity, it is best to work with the rescaled variables $\alpha_{\vec{k},\mu} = \sqrt{2\epsilon c||\vec{k}||V_{ol}}\mathscr{A}_{\vec{k},\mu}$. In classical electrodynamics, the amplitude and phase of a field are always well-defined. If there are uncertainties associated with the amplitude and phase of a field, then we must endow the phase space with a probability distribution Q, so that the average energy becomes

$$\langle\mathscr{H}\rangle = \sum_{\vec{k},\mu}\omega_k \int |\alpha_{\vec{k},\mu}|^2 Q(\alpha_{\vec{k},\mu}, \alpha^*_{\vec{k},\mu})\, d^2\alpha_{\vec{k},\mu}\,. \tag{1.10}$$

Furthermore, the entire phase space can be covered with a countable set of concentric rings, i.e. a set of normalized functions strongly localized around a given anullar region in the complex plane, and decompose any function as a combination of the functions of this set. This idea is illustrated in Fig.1.1 for the set of functions $\left\{\frac{|\alpha|^{2n}}{\pi\, n!}e^{-|\alpha|^2}\right\}_n$.

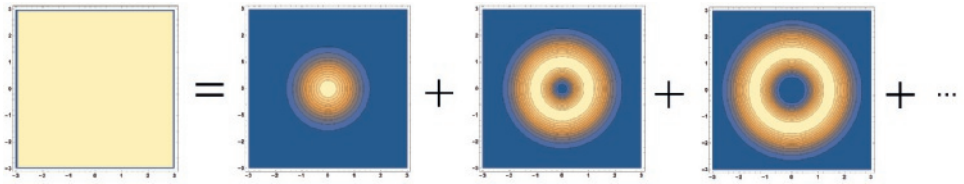

Figure 1.1: Decomposition of phase-space with the set of funtions $\{\frac{|\alpha|^{2n}}{\pi n!}e^{-|\alpha|^2}\}_n$.

So far the description was solely for a classical probability distribution. In quantum theory, two distinct points in phase space do not correspond to disjoint events, differentiating Q from a true probability distribution function. Additionally, in quantum theory, the basic block is the probability amplitude, i.e. a square integrable complex function Ψ containing all the information about the statistical properties of the system. In classical physics, if a field does not have a well-defined amplitude and phase, field correlations are obtained with the sum over the probabilities of finding the field at a given configuration, whereas in a quantum framework it is the probability amplitudes that are summed instead. Building on the procedure above, any probability amplitude can be decomposed in a basis $\{\Phi_n\}$, and factoring out the integration weight $e^{-|\alpha|^2}$ ($Q = e^{-|\alpha|^2}|\psi|^2$), ψ can be decomposed in the $\left\{\phi_n = \frac{\alpha^n}{\sqrt{\pi n!}}\right\}$ basis. It is straightforward to see that transitions between the basis' functions are accomplished via $\alpha\phi_n = \sqrt{n+1}\phi_{n+1}$ and $\partial_\alpha\phi_n = \sqrt{n}\phi_{n-1}$. With these, raising and lowering operators can be defined with the identification $a^\dagger \equiv \alpha$ and $a \equiv \partial_\alpha$. The factorization $Q = e^{-|\alpha|^2}\psi^*\psi$ is done such that ψ is solely a function of α, and so the average energy for a single mode and polarization (see Eq.(1.10)) is

$$\langle\mathscr{H}\rangle = \omega\int|\alpha|^2 e^{-|\alpha|^2}\psi^*(\alpha^*)\psi(\alpha)\,d^2\alpha = \omega\int e^{-|\alpha|^2}\psi^*\alpha\partial_\alpha\psi\,d^2\alpha + \ldots, \tag{1.11}$$

where partial integration was used, and zero-point contributions discarded. It is now natural to introduce an operator language. If $\langle\mathscr{H}\rangle$ is the average energy, and if the average value of an observable $\mathscr{O}$ is given by $\int e^{-|\alpha|^2}\psi^*\hat{\mathscr{O}}\psi\,d^2\alpha$ ($\hat{\mathscr{O}}$ is the operator representing the observable), then Eq.(1.11) implies that the Hamiltonian operator is $\hat{\mathscr{H}} = \omega\alpha\partial_\alpha \equiv \omega a^\dagger a$, which is the "second-quantized" version of the harmonic oscillator Hamiltonian. Using the Poisson bracket and the complex coordinates (α,α^*) to describe the time-evolution of ψ, one arrives at

$$d_t\psi = -i\omega\alpha\partial_\alpha\psi = -i\hat{\mathscr{H}}\psi\,, \tag{1.12}$$

which corresponds to the Schrödinger equation for the harmonic oscillator. This representation for the state ψ is called the Bargmann representation, and Q is called the Husimi Q-function. Despite the resemblance of this form of quantum mechanics to a classical statistical theory, the connection is however deceitful. This procedure does not immediately generalize to other Hamiltonians unless additional rules are provided, such as replacing the multiplication operation by the Moyal product.

Still, this provides the best position to understand the nature of Quantum Optics. The function $\phi_1 = \frac{\alpha}{\sqrt{\pi}}$ is commonly named "one photon", and the function ϕ_n is named "n

photons". And it is this the nature of photons: they are simply a basis for the functions describing uncertainties of the amplitude and phase of a field mode. Photons have as much physical meaning as a set of coordinates. The "granularity" of the electromagnetic field is nothing more than the discreteness of the basis covering the phase space for the field's complex amplitude. Thus, photons do not travel, because photons do not have an existence in real-space. Only the electromagnetic field can propagate. Photons do not bounce at reflecting surfaces, do not choose paths and do not behave as particles because photons do not have any existence outside the quasiprobability realm from which they are bound to. Having clarified the quantum nature of light, let us proceed to the coupling to a mechanical element.

1.3.2. STANDARD OPTOMECHANICS

As previously mentioned, the electromagnetic field carries momentum, and so mechanical motion can be induced by the radiation pressure force. To obtain this form of light-matter interaction, consider the case of a standard Fabry-Pérot cavity where one of the end-mirrors of the cavity can move in a direction perpendicular to the cavity electromagnetic fields (see Fig. 1.2).

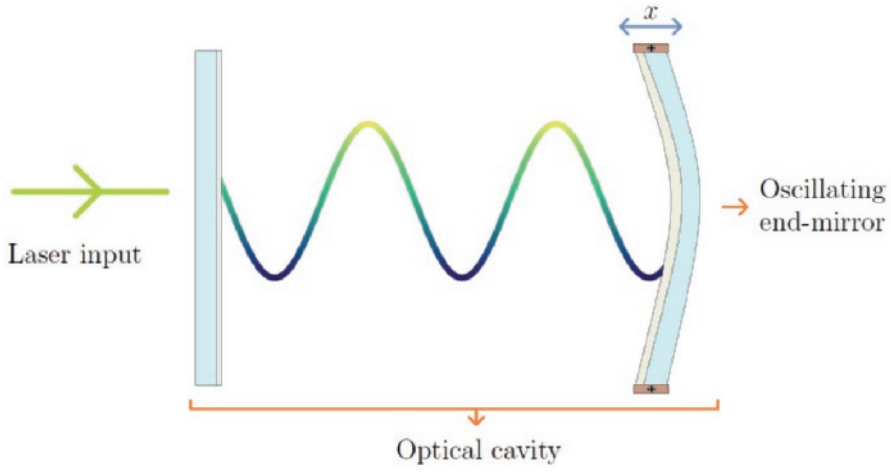

Figure 1.2: Standard optomechanical system composed by an optical cavity and an oscillating end-mirror.

The Hamiltonian is now

$$\mathscr{H} = \frac{\epsilon V_{ol}}{2L} \int_0^{L+X(t)} \left(||\vec{E}||^2 + c^2 ||\vec{B}||^2 \right) dx, \tag{1.13}$$

where V_{ol} is the rest volume of the cavity, and X the displacement of the end-mirror. If X is small in comparison to the unperturbed cavity length L, one can expand the energy in powers of X/L. Using the mode decomposition of Eqs. (1.7,1.8) for the unperturbed

cavity, the interaction becomes

$$\mathcal{H}_{int} = 2\epsilon c^2 V_{ol} \frac{X(t)}{L} \sum_{\vec{k},\vec{k}',\mu} (|k k'| + k k') Re\left\{ \mathcal{A}_{\vec{k},\mu} \mathcal{A}^*_{\vec{k}',\mu} e^{-i(|k|-|k'|)ct} - \mathcal{A}_{\vec{k},\mu} \mathcal{A}_{\vec{k}',\mu} e^{-i(|k|+|k'|)ct} \right\}. \tag{1.14}$$

If like the electromagnetic field, the position and momentum of the mirror are not precisely defined, the phase-space formulation must be extended to include the motional degrees of freedom. In a quantum framework, this is equivalent to bestow a wavefunction to the mechanical element (the moving mirror), namely a wavefunction for the centre of mass motion. In Optomechanics, this mechanical element is often a resonator, and so one can directly use the known operator formalism for this situation, and quantize this system of two interacting harmonic oscillators.

Optical frequencies are several orders of magnitude larger than any mechanical frequency, and so the last terms of the interaction in Eq.(1.14) provide rather fast rotating contributions (thus negligible). If the free spectral range is also much larger than the mechanical frequency, then the interaction between different modes is also far from resonance and it can be disregarded as well. Considering a single optical mode, the fully quantized Hamiltonian of Optomechanics becomes

$$\mathcal{H} = \omega_c a^\dagger a + \Omega b^\dagger b + g_0 a^\dagger a (b + b^\dagger). \tag{1.15}$$

The static terms of the Poynting vector at $x = L$ are proportional to the force created by the interaction in Eq.(1.15), and it is because of it that this form of coupling is named as "radiation pressure" interaction. However, other forms of interaction are possible. If the free spectral range matches the mechanical frequency for any pair of modes, the effective Hamiltonian (i.e. the Hamiltonian keeping only the resonant interactions) is the two-mode parametric amplifier Hamiltonian

$$\mathcal{H} = \omega_1 a_1^\dagger a_1 + \omega_2 a_2^\dagger a_2 + \Omega b^\dagger b + g(a_1^\dagger a_2 b + b^\dagger a_2^\dagger a_1). \tag{1.16}$$

1.3.3. ELECTROMECHANICS

Apart from the free radiation field, electrical excitations in LC circuits have also been tainted by quantization. Since a circuit composed by a capacitor and an inductor forms an electric harmonic oscillator, with the advent of second quantization, its nature was promptly deemed quantum. One particular point of view is that the electric circuit produces oscillating electric and magnetic fields, not differing from the oscillating electric and magnetic fields of light inside a cavity [65]. The quantization of LC circuits can be done using different possible combinations of generalized coordinates, namely the charge Q or the voltage V of the capacitor and the current I or the magnetic flux Φ through the inductor. The choices are (Q, Φ) or (V, I), but in order to relate properly to the free electromagnetic field, only electric or magnetic field variables should be chosen. For an infinitely long cylindrical inductor, the magnetic field $\vec{B}$ inside the coil is spatially uniform, as it is the electrical field $\vec{E}$ between the plates of a parallel plate capacitor. Like for optical cavities, the particular shape of the circuit elements is not relevant for the quantization, and the choice is made due to the simplicity. Using the relation between

the variables (V,Φ) and the electrical and magnetic fields, the Hamiltonian can be written as

$$\mathscr{H}_{LC} = \frac{1}{2}\frac{V_{ind}}{\mu N^2}B^2 + \frac{1}{2}\epsilon V_{cap}E^2\,, \tag{1.17}$$

where V_{ind} is the volume encapsulated by the inductor, N the number of loops and V_{cap} the volume between the capacitor plates. This choice of variables renders the comparison quite instructive and reveals that (apart from the N^2 factor) the stored electromagnetic field energy is the same as for light stored inside a cavity. And so, coincidently, the quantum excitations of the LC turn out to be of the same nature as the free radiation field ones. Using

$$\hat{E} \equiv \sqrt{\frac{\hbar\omega_{LC}}{2\epsilon V_{cap}}}(a+a^\dagger) \qquad , \qquad \hat{B} \equiv N\sqrt{\frac{\mu\hbar\omega_{LC}}{2V_{ind}}}\,i(a^\dagger - a)\,, \tag{1.18}$$

where ω_{LC} is the resonant frequency of the circuit, the quantized Hamiltonian becomes $\hat{\mathscr{H}} = \hbar\omega_{LC}a^\dagger a$. This shows that not only do the excitations in the LC circuit have the same nature has the optical modes in a cavity, but also that the only electromagnetic mode possible in a LC circuit is an electromagnetic mode with null momentum (hence the lack of several modes and polarisation, as well as the spatially uniformity of the fields). But by only employing the electric and magnetic fields, one thing was forgotten: electric charges and currents also participate in the motion. In this second-quantized picture, the charge at the capacitor plates is $Q = \sqrt{\frac{\hbar\epsilon\omega_{LC}}{2d_0}}(a+a^\dagger)$, which does not have a discrete spectrum of eigenvalues. Thus, although we are in possession of a fully quantum theory, the charged particles at the capacitor never have a discrete nature. This poses a question over the validity of this quantization, and the connection to a microscopic description in terms of electrons. I.e., there should be a regime where the discrete nature of the electric charge plays a role, and a quantum theory for such situation should be fundamentally different. A particular situation of interest clarifying this point would be a LC coupled in series to a single-electron transistor such that only one electron could hop to the capacitor.

Identically to the optical case, mechanical resonators can also be coupled to LC circuits, as depicted in Fig. 1.3. In these electromechanical systems, the coupling of the LC-resonator to a mechanical element is achieved by enabling one of the capacitor plates to move by using a drum as a capacitor plate. As the capacitor plate vibrates, the capacitance changes, and so does the energy and resonant frequency of the circuit. For a parallel plate capacitor, $V_{cap} = S(d_0 + x(t))$, where S is the plate surface area, d_0 the rest distance between the plates, and $x(t)$ the plate displacement. With the same quantization procedures, this capacitive coupling leads to the Hamiltonian

$$\mathscr{H}_{sys} = \omega_c a^\dagger a + \Omega b^\dagger b + g_0(a+a^\dagger)^2(b^\dagger + b)\,, \tag{1.19}$$

where $g_0 = \frac{\omega_{LC}}{4d_0}x_{ZPM}$. As a side note, this interaction is *exactly* linearly dependent on the displacement, in the sense that it does not matter if the displacement is large or small in comparison to d_0, the coupling is still proportional to x, contrary to standard optomechanical cavities. Electromechanical systems are often seen as a different physical realization of optomechanical systems but sharing the same physics, i.e. as 2 harmonic oscillators that couple via "radiation pressure". This is true for most situations, but the

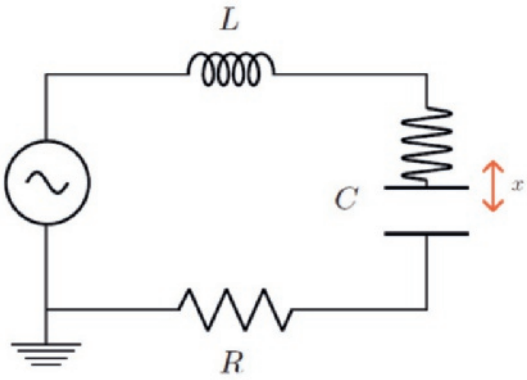

Figure 1.3: Schematics of an electromechanical system, where one of the capacitor's plates is a mechanical oscillator.

nature of the coupling mechanism is quite different. Specifically, the LC frequency is typically much larger than all other parameters, and so within RWA (rotating wave approximation), the "radiation pressure interaction" $a^\dagger a(b+b^\dagger)$ is the strongest form of the interaction. However, the true form of the interaction depends directly on the electric field intensity instead of the photon number. If the cavity frequency approaches the mechanical frequency ($\Omega \sim 2\omega_{LC}$), the effective interaction is essentially an electromechanical implementation of the degenerate parametric amplifier

$$\mathscr{H}_{eff} = \omega_c a^\dagger a + \Omega b^\dagger b + g_0(aab^\dagger + a^\dagger a^\dagger b)\,. \tag{1.20}$$

This represents a new and unexplored regime for electromechanics, to be discussed in Section 3.2.

1.3.4. QUADRATIC COUPLINGS

The interaction between light (or electric excitations) and motion is strongly dependent on the geometry of the system. So far the coupling forms presented are linear in displacement, but more exotic couplings can be achieved by strategically placing the mechanical element. The most common strategy to achieve this is to place the resonator at a symmetry point of the optical cavity, such as a node or an antinode (see Fig. 1.4).
At the symmetry points, the linear coupling vanishes, and the resulting interaction is quadratic in displacement (quartic couplings have also been proposed by an additional tilting of the membrane [66]). To illustrate how this quadratic coupling arises, consider the related example of levitated nanoparticles inside an optical cavity. Any physical object is composed by a myriad of atoms and its subatomic constituents, and the Schrödinger equation for a quantum system composed by N particles is

$$i d_t \psi(\vec{r}_1,...,\vec{r}_n) = \Big[\sum_{j=1}^{N} \frac{(-i\hbar\nabla_j)^2}{2m_j} + \sum_{j<l} V(\vec{r}_j - \vec{r}_l) + V_{ext}\Big]\psi(\vec{r}_1,...,\vec{r}_n)\,, \tag{1.21}$$

where $V(\vec{r}_j - \vec{r}_l)$ is the interparticle potential between particle j and l, while V_{ext} is an external potential. Changing to the relative coordenates $\vec{g}_n = \vec{r}_n - \vec{r}_{n+1}$ and to the centre

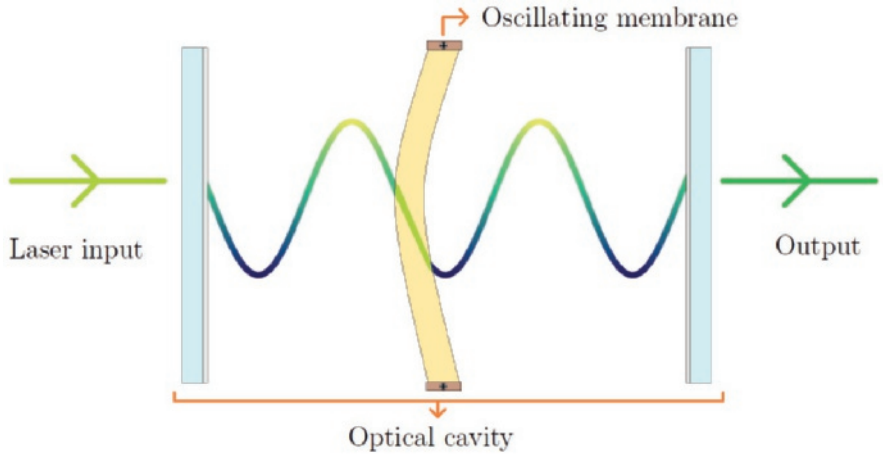

Figure 1.4: Example of a membrane-in-the-middle gemoetry. Placing a dielectric membrane in a cavity node leads to a coupling quadratic in displacement.

of mass coordinate $\vec{R}$, the centre of mass motion decouples from the internal dynamics. Naming ϕ the wavefunction for the centre of mass motion, and factorizing it in Eq.(1.21), the Schrödinger equation becomes

$$i d_t \phi(\vec{R}) = \left[-\frac{(i\hbar\nabla_R)^2}{2M} + V_{ext}(\vec{R}) \right] \phi(\vec{R}), \tag{1.22}$$

where M is the reduced mass. It is the wavefunction ϕ that represents the state of the nanoparticle (i.e. the centre of mass motion of the particle), and only the centre of mass motion is of interest here. To trap the nanoparticle, the external potential is created by an optical tweezer which creates a potential well for the particle. Treating the electromagnetic field of the optical tweezer as a classical Gaussian beam, the electric field intensity (in polar coordinates) is given by

$$I(\rho, z) = ||\vec{E}_0||^2 \left(\frac{k^2 W_0^4}{k^2 W_0^4 + 4z^2} \right)^2 e^{-\frac{2(W_0 k\rho)^2}{k^2 W_0^4 + 4z^2}}, \tag{1.23}$$

where W_0 is the beam waist, E_0 the electric field amplitude, and k the wavevector. The interaction of the optical tweezer with the levitating nanoparticle is a dielectric interaction, with the average energy

$$\langle V_{ext} \rangle = -\int d\vec{R} |\phi(\vec{R})|^2 \int_{B(\vec{R})} d\rho dz \, \epsilon_r \epsilon_0 I(\rho, z) \rho, \tag{1.24}$$

where ϵ_r is the dimensionless dielectric permittivity, and $B(\vec{R})$ the volume of the particle. Considering a point-like particle (i.e. $B(\vec{R})$ is small enough such that the field intensity is almost constant throughout the nanoparticle), the average energy becomes

$$\langle V_{ext} \rangle = -\epsilon_r \epsilon_0 V_B \int |\phi(\vec{R})|^2 I(\vec{R}) d\vec{R}, \tag{1.25}$$

where V_B is the particle's volume. Note also that the x, y, z coordinates decouple and so the motion is independent along each direction. Furthermore, V_{ext} has a potential minimum at the origin, and when the particle is well-trapped (i.e. the average displacement is small in comparison to W_0), Eq.(1.23) can be expanded in powers of ρ. Considering only a single direction (for e.g. x), the Schrödinger equation reads

$$i d_t \bar{\phi}(x) = \left[-\frac{\hbar^2}{2M} \partial_x^2 + \epsilon_r \epsilon_0 ||\vec{E}_0||^2 \frac{2V_B}{W_0^2} x^2 \right] \bar{\phi}(x) \,. \tag{1.26}$$

This shows that the trapped nanoparticle behaves like a harmonic oscillator whose frequency can be tuned by the laser intensity and spatial profile. Moreover, for this form of interaction to be valid and nontrivial, the amplitude of motion must be larger than the particle's size. One can now use the operator language from second quantization, even though the quantum excitations for this effective harmonic oscillator are not phonons. This effective mechanical oscillator can be coupled to light by trapping the particle inside an optical cavity. If the cavity is aligned perpendicular to the tweezer, then $\vec{E}_0.\vec{E}_{cav} = 0$ ensures that there is no direct coupling between the cavity and the optical tweezer, and the only surviving coupling is the coupling between the cavity mode and the particle due to its dielectric nature, namely

$$\langle V'_{ext} \rangle = \int d\vec{R} \, |\phi(\vec{R})|^2 \int_{B(\vec{R})} d\vec{r} \, (1-\epsilon_r) \epsilon_0 ||\vec{E}_{cav}(\vec{r})||^2 \,. \tag{1.27}$$

Using the same point-like approximation (now meaning that the cavity wavelength is large in comparison to the particle's size; analogous to the long-wavelength/dipole approximation in cavity QED) the potential becomes

$$V'_{ext}(\vec{R}) = (1-\epsilon_r) \epsilon_0 V_B ||\vec{E}_{cav}(\vec{R})||^2 \,. \tag{1.28}$$

Quantizing the electromagnetic field inside the cavity (and considering a Fabry-Pérot as before) leads to

$$V'_{ext}(x) = -\sum_{k,\mu} \frac{\hbar \omega_k}{2V_{cav}} (1-\epsilon_r) V_B (a_{k,\mu} - a^\dagger_{k,\mu})^2 \sin^2(kx) \,, \tag{1.29}$$

where $k = \frac{\pi n}{L}$, with L the cavity length. In physical implementations, cavity frequencies are at least a few THz, which is several orders of magnitude higher than any other characteristic frequency of the system. This implies that from $(a_{k,\mu} - a^\dagger_{k,\mu})^2$ only the slow oscillating terms $(2a^\dagger a + 1)$ govern the interaction. For small displacements, $\sin^2(kx)$ can be expanded in powers of x, which in general renders the standard optomechanical interaction. However, if the centre of the beam is located at a node/antinode of the cavity ($x = \{\frac{\pi}{k} m, \frac{\pi}{k}(m + 1/2)\}$, respectively), the linear interaction vanishes and the coupling becomes quadratic in displacement. Taking just one cavity mode into consideration, the resulting interaction becomes

$$\mathscr{H} = \omega_c a^\dagger a + \Omega b^\dagger b \pm \chi (a^\dagger a + 1/2)(b + b^\dagger)^2 \,, \tag{1.30}$$

where ± refers to the node/anti-node situation, and

$$\chi = (\epsilon_r - 1)\frac{V_B}{V_{cav}}\frac{x_{ZPM}^2}{c^2}\omega_c^3. \tag{1.31}$$

Additionally, for the anti-node situation, the cavity frequency has as additional contribution of $\chi/2$. Due to stability reasons, and because dielectric particles also provide a dissipation channel for light, it is better to place the nanoparticle around a node. The quantum effects enabled by this type of coupling will be addressed in Section 3.4.

With the knowledge of the interaction between light and motion, the analysis of the quantum effects present in these systems can now begin. The following chapters are the product of the research path pursued, and apart from sporadic discussions aimed at introducing the work in a wider context (which specify *what* is reviewed, with references to the relevant literature), they strictly contain independent and original work.

2

WHAT IS AND WHAT IS NOT QUANTUM

The question of whether a given phenomenon has a quantum nature is essentially a linguistic matter. It is the act of a new language attempting to exert its supremacy over a preexisting one. The interest is not to endow the old language with abilities to better describe newly discovered phenomena, but to denigrate it for its aphasia. Several features of quantum mechanics, such as squeezing and uncertainty principles, entanglement, and correlations, are often taken to be quantum properties/effects *an sich*. Such views arise from the fact that a classical formalism is often not equipped with tools allowing it to deal with uncertainties regarding the state of the fields involved. Thus, in most situations, the quantum-classical comparison is absurd because the classical theory cannot answer certain type of questions. In order to be able to make a proper comparison, one has to endow a classical theory with a classical probability distribution for the comparison to be done properly.

2.1. CONSEQUENCES OF DYNAMICAL STATISTICAL THEORY

To construct a classical statistical field theory, the phase-space must be dressed with a probability distribution $\mathbb{P}$, and random variables must be assigned to classical degrees of freedom. There are two possible prescriptions: the random variables evolve like the classical degrees of freedom (i.e. for a Hamiltonian system, the time evolution is given by the Poisson bracket $\{.,.\}$) and expected values are computed given the initial probability distribution of the random variable; or it is the probability distribution that evolves in time while the random variable remains static. As the two descriptions must produce the same outcomes, i.e. for any random variable $A(Q,P)$ ((Q,P) denote position and

momentum, but the following holds for any kind of conjugate phase-space variables),

$$\langle d_t A(Q,P)\rangle = \int dQdP\, d_t A(Q,P)\mathbb{P}(Q,P) = \int dQdP\,\{A(Q,P),\mathscr{H}\}\mathbb{P}(Q,P) =$$
$$= \int dQdP\, A(Q,P)(-\{\mathbb{P}(Q,P),\mathscr{H}\}) = -\int dQdP\, A(Q,P)d_t\mathbb{P}(Q,P)\,, \qquad (2.1)$$

and so the time-evolution for the probability distribution is given by $d_t\mathbb{P} = -\{\mathbb{P},\mathscr{H}\}$. These two possible descriptions (use of the dynamical random variables or the time-evolving probability distribution) have a striking connection to the Heisenberg picture and density matrix approach of quantum mechanics (respectively). Aided by this comparison, and because the probability distribution $\mathbb{P}$ provides knowledge about every property of the system, $\mathbb{P}$ shall henceforth be designated by the "state" of the system. Thus, $\mathbb{P}$ plays the classical role of quantum mechanical quasiprobability distributions such as the Husimi, Wigner or Sudarshan functions.

In order to determine what type of phenomena can now be described with a stochastic formulation, lets us consider the case of two coupled harmonic oscillators. Linearly coupled harmonic oscillators are not only an instructive example due to its simplicity, but they also constitute the backbone of many current physical devices probing quantum mechanics at a macroscopic scale [45, 54, 55, 57]. Although physical implementations may differ (i.e. the oscillators may be not only mechanical resonators but also LC circuits or electromagnetic modes inside an optical cavity), the nature of harmonic oscillators and the type of effects observed are universal, and so one can address the more abstract general case. If the positions Q_j or momenta P_j of a pair of oscillators are not precisely known and one wishes to make (statistical) predictions about the system, it is necessary to equip classical mechanics with a probability distribution $\mathbb{P}(Q_1,Q_2,P_1,P_2)$: $\mathbb{R}^{2d}\times\mathbb{R}^{2d}\to\mathbb{R}$ representing these uncertainties. For simplicity, only the $d=1$ case is considered. Instead of working in the (Q,P) phase-space, it is also possible to work in the complex plane instead, by making the change of variables $Q = \frac{1}{\sqrt{2m\omega}}(c+c^*)$ and $P = \sqrt{\frac{m\omega}{2}}\,i(c^*-c)$, or to use the rescaled coordinates $q = Re\{c\}$ and $p = Im\{c\}$. For two linearly coupled harmonic oscillators, the Hamiltonian can be written as

$$\mathscr{H} = \omega(p_1^2+q_1^2) + \Omega(p_2^2+q_2^2) + 2g\,q_1q_2\,, \qquad (2.2)$$

where ω and Ω are the resonators' frequencies and g a coupling parameter. The time-evolution for the probability distribution can be written as

$$\partial_t\mathbb{P} = -\{\mathbb{P},\mathscr{H}\} = x^T M(\partial_x)\mathbb{P}\,, \qquad (2.3)$$

where $x^T = \begin{bmatrix} q_1 & p_1 & q_2 & p_2\end{bmatrix}$, $(\partial_x)^T = \begin{bmatrix}\partial_{q_1} & \partial_{p_1} & \partial_{q_2} & \partial_{p_2}\end{bmatrix}$, T represents the transpose, and

$$M = \begin{bmatrix} 0 & \omega & 0 & g \\ -\omega & 0 & 0 & 0 \\ 0 & g & 0 & \Omega \\ 0 & 0 & -\Omega & 0 \end{bmatrix}. \qquad (2.4)$$

To solve Eq.(2.3), it is useful to make a change of variables. Since the equation could be brought to a quadratic form, a linear transformation $y = Rx$ suffices (where $y^T =$

$[u_- \quad v_- \quad u_+ \quad v_+]$). Using that $(\partial_x) = R^T(\partial_y)$, the time-evolution becomes

$$\partial_t \mathbb{P} = y^T (R^{-1})^T M R^T (\partial_y) \mathbb{P}\,. \tag{2.5}$$

The simplest and most interesting situation occurs when $\omega = \Omega$, and for this case, the use of symmetric and anti-symmetric combinations of the positions and momenta leads to

$$R = \frac{1}{2}\begin{bmatrix} 1 & 0 & -1 & 0 \\ 0 & 1 & 0 & -1 \\ 1 & 0 & 1 & 0 \\ 0 & 1 & 0 & 1 \end{bmatrix}, \tag{2.6}$$

which decouples the dynamics into

$$d_t \mathbb{P} = \Big[(\Omega - g)\, u_- \partial_{v_-} - \Omega v_- \partial_{u_-} + (\Omega + g)\, u_+ \partial_{v_+} - \Omega v_+ \partial_{u_+} \Big] \mathbb{P}\,. \tag{2.7}$$

Defining $\Omega_\pm = \Omega\sqrt{1 \pm \frac{g}{\Omega}}$ and $v_\pm = b_\pm \sqrt{1 \pm \frac{g}{\Omega}}$, Eq.(2.7) can be written as

$$d_t \mathbb{P} = \Omega_-(u_- \partial_{b_-} - b_- \partial_{u_-})\mathbb{P} + \Omega_+(u_+ \partial_{b_+} - b_+ \partial_{u_+})\mathbb{P}\,. \tag{2.8}$$

Using the coordinates accompanying the motion of the resonators instead of the static phase-space coordinates (u, b) immediately solves Eq.(2.8). I.e. by using $(U(t), B(t))$, where

$$U_\pm(t) = u_\pm \cos(\Omega_\pm t) - b_\pm \sin(\Omega_\pm t)\,, \quad B_\pm(t) = b_\pm \cos(\Omega_\pm t) + u_\pm \sin(\Omega_\pm t)\,, \tag{2.9}$$

Eq.(2.8) becomes $\partial_t \mathbb{P} = 0$. Therefore, the coordinates $\{U_j(t), B_j(t)\}$ fully describe the stochastic dynamics. For small coupling values ($g \ll \Omega$), the time-evolution of the positions and momenta of the resonators becomes

$$q_1(t) = (U_1 + U_2)(t) \approx q_1 \cos(\Omega t)\cos\Big(\frac{gt}{2}\Big) - q_2 \sin(\Omega t)\sin\Big(\frac{gt}{2}\Big)$$
$$+ p_1\Big[\frac{g}{2\Omega}\cos(\Omega t)\sin\Big(\frac{gt}{2}\Big) - \sin(\Omega t)\cos\Big(\frac{gt}{2}\Big)\Big] + p_2\Big[\frac{g}{2\Omega}\sin(\Omega t)\cos\Big(\frac{gt}{2}\Big) - \cos(\Omega t)\sin\Big(\frac{gt}{2}\Big)\Big], \tag{2.10}$$

$$p_1(t) = \Big(\sqrt{1 - \frac{g}{\Omega}}B_1 + \sqrt{1 + \frac{g}{\Omega}}B_2\Big)(t) \approx p_1 \cos(\Omega t)\cos\Big(\frac{gt}{2}\Big) - p_2 \sin(\Omega t)\sin\Big(\frac{gt}{2}\Big)$$
$$+ q_1\Big[\sin(\Omega t)\cos\Big(\frac{gt}{2}\Big) + \frac{g}{2\Omega}\cos(\Omega t)\sin\Big(\frac{gt}{2}\Big)\Big] + q_2\Big[\cos(\Omega t)\sin\Big(\frac{gt}{2}\Big) + \frac{g}{2\Omega}\sin(\Omega t)\cos\Big(\frac{gt}{2}\Big)\Big], \tag{2.11}$$

with an analogous relation for (q_2, p_2) obtained by interchanging the indices $1 \leftrightarrow 2$. The knowledge about the stochastic dynamics enables the direct comparison with the observed phenomena by evaluating the evolution of the probability distribution or any expectation value of an observable. Before proceeding, one should always have in mind that physical theories cannot be directly derived from experiment. Given an experimental observation of a certain effect, there is not necessarily a single theory describing it, and any theoretical interpretation of an experimental observation is always an embellishment of the *factum brutum*.

2.1.1. STATE TRANSFER

The goal of quantum engineering is the complete control of the quantum state of a system. If creating a particular quantum state in a given system is difficult, an alternative method is to transfer that quantum state from one system to another. State transfer has already been realized in optomechanics [57], where Gaussian states were transferred from one resonator to another. Such feat has been flagged as a landmark in the list of quantum effects in optomechanics [49], but what makes state transfer a quantum effect?

Consider the case of two resonators in an arbitrary disentangled state (i.e. the total probability distribution representing the system factorizes in a product of two probability distributions, each representing a single oscillator), then

$$\mathbb{P}(q_1, p_1, q_2, p_2, t=0) = \mathbb{P}_1(q_1, p_1, t=0)\,\mathbb{P}_2(q_2, p_2, t=0)\,, \tag{2.12}$$

$$\text{and} \quad \mathbb{P}(q_1, p_1, q_2, p_2, t) = \mathbb{P}_1\big(q_1(t), p_1(t)\big)\mathbb{P}_2\big(q_2(t), p_2(t)\big)\,, \tag{2.13}$$

with (q_j, p_j) given by Eqs. (2.10,2.11). After a period of T, such that $\Omega T = 2\pi(n \pm 1/4)$ and $gT = 2\pi(n' \mp 1/2)$ (with $n, n' \in \mathbb{Z}$), $q_1(T) \approx q_2(0)$, $p_1(T) \approx p_2(0)$ and vice-versa, and the state of the system becomes

$$\mathbb{P}(q_1, p_1, q_2, p_2, t=T) = \mathbb{P}_1(q_2, p_2, t=0)\,\mathbb{P}_2(q_1, p_1, t=0)\,, \tag{2.14}$$

meaning that after a time T, the probability distribution for resonator 2 is $\mathbb{P}_1$, and for resonator 1 is $\mathbb{P}_2$. Eq.(2.14) describes the effect of the state of the oscillator 1 being transferred to oscillator 2 and vice-versa. Therefore, the statistics of any measurement of resonator 1 will be faithfully reproduced for resonator 2. Consequently, state transfer is a simple consequence of the interaction and it has no quantum features.

2.1.2. SQUEEZING

The fact that quantum mechanics naturally features uncertainties puts it in the front line when it comes for systems requiring precision measurements. A lot of attention has been devoted to precise position measurements, and the inevitable intrinsic quantum uncertainties have triggered strategies to manipulate noise and reduce the imprecision beyond the standard quantum limit.

Whether working or not in a quantum framework, uncertainties in the measurement of a given observable are ultimately characterized by its variance. Another consequence of the interaction in this stochastic framework is that the quadratures' variance is no longer constant in time. Consider that the system starts in the state

$$\mathbb{P}(q_1, p_1, q_2, p_2, t=0) = G(q_1)G(q_2)G(p_1)G(p_2)\,, \tag{2.15}$$

where $G(x)$ is a Gaussian probability distribution centred around the origin and with variance δ^2. The interest now lies in what happens to one of the resonators (say resonator 1) after n_c oscillation cycles (i.e. $\Omega t = 2\pi n_c$), and not to the evolution of the whole system. Thus, the quantity of interest is the state of resonator 1, given by

$$\mathbb{P}_1(q_1, p_1, t) = \int dq_2 \int dp_2\, \mathbb{P}(q_1, p_1, q_2, p_2, t)\,. \tag{2.16}$$

Eqs. (2.10-2.11), together with Eq.(2.16) lead to

$$\mathbb{P}_1\Big(q_1, p_1, t = \frac{2\pi n_c}{\Omega}\Big) \approx \frac{1}{2\pi\delta^2} exp\left(-\frac{q_1^2 + p_1^2 + \frac{g}{\Omega} q_1 p_1 \sin\phi}{2\delta^2}\right), \tag{2.17}$$

where $\phi = 2\pi\frac{g}{\Omega} n_c$. Eq.(2.17) represents a deformed Gaussian (its level curves are ellipses) centred around the origin, squeezed along $\frac{1}{\sqrt{2}}(q_1 + p_1)$ and distended along $\frac{1}{\sqrt{2}}(q_1 - p_1)$. This squeezing is immediately visible from the variance of the quadratures $y = \frac{1}{\sqrt{2}}(q_1 - p_1)$ and $z = \frac{1}{\sqrt{2}}(q_1 + p_1)$, given by

$$Var(y) = \delta^2\Big(1 + \frac{g}{2\Omega}\sin\phi\Big), \quad Var(z) = \delta^2\Big(1 - \frac{g}{2\Omega}\sin\phi\Big). \tag{2.18}$$

This effect of decreasing the variance of a quadrature while enlarging the variance of the conjugate one is what is generally called squeezing. Squeezing is often considered a nonclassical macroscopic quantum effect [45], but its nature is devoid of any quantum properties. What is observed experimentally is an uncertainty trade between conjugate variables (the quadratures in [45, 54, 55]), which is fully characterized by changes in the variance as displayed in Eq.(2.18). Thus, squeezing is a simple consequence of the interaction in a stochastic framework, and does not possess an intrinsic quantum nature. Further, as far as linear couplings are concerned, the degree of squeezing is the same as in the respective quantum theory.

2.1.3. ENTANGLEMENT

Einstein's ghost wanders restlessly. It has become a widespread petty jest the "demonstration of his mistakes". He can never regain peace, but we can regain clarity. What began as an alert to certain counter-intuitive consequences of quantum mechanics, ended up in drawing the line where Physics acquires unjustified spiritistic hues. The term "entanglement" is often used to refer to the property that the outcome of the measurement of an observable A is deterministic, once the random outcome of a previous measurement of B is known (and where A and B are observables of distinct elements). But what is the nature of entanglement?

To answer this question, consider the case where the initial state of resonator 1 is a Gaussian distribution of width ϱ centred around the origin, while the state of resonator 2 is a precisely defined δ at $(q_2, p_2) = (X, 0)$. After n_c resonator cycles $\big($with $n_c = \frac{\Omega}{4g}\big)$, the state of the system is

$$\mathbb{P}(q_1, q_2, p_1, p_2) \approx \frac{1}{\pi\varrho^2}\delta(q_2 - p_1 - X)\delta(q_1 + p_2) Exp\Big[-\frac{(q_1 - p_2)^2 + (p_1 + q_2)^2}{4\varrho^2}\Big], \tag{2.19}$$

where terms of the order g/Ω were disregarded. The statistical properties between the random variables can be characterized by the Pearson correlation coefficient $PCC(x, y) = \frac{CoVar(x,y)}{\sigma(x)\sigma(y)}$, where $\sigma(x)$ is the standard deviation and $CoVar$ the covariance between the 2 variables. The values for PCC are displayed in Table 2.1, where it can be seen that $PCC = -1$ for (q_1, p_2) and (q_2, p_1).

PCC(x,y)	q_1	q_2	p_1	p_2
q_1	1	0	0	-1
q_2	0	1	-1	0
p_1	0	-1	1	0
p_2	-1	0	0	1

Table 2.1: Covariance matrix for the state in Eq. (2.19). The entries in the antidiagonal have a negative Pearson correlation coefficient, characteristic of anti-correlations between entangled quadratures.

The anticorrelations portrayed in Table 2.1 describe the experimental entanglement results of [56]. The significance of this perfect linear anticorrelation is that when the system reaches the state in Eq.(2.19), if p_1 is measured, the outcome will be a completely random value. Once the measurement of p_1 is done, its momentum is determined, and the position of resonator 2 is automatically fixed. Thus, if the random outcome of measuring the momentum of resonator 1 (p_1) is P, then the outcome of measuring the position of resonator 2 is $X+P$ with absolute certainty (see Eq.(2.19)). Then p_1 and q_2 fulfill the condition to be considered entangled. The nature of entanglement between two random variables (x, y) arises from the fact that the probability distribution $\mathbb{P}(x, y)$ describing the state of the system cannot be factorized into $\mathbb{P}_1(x)\mathbb{P}_2(y)$. Thus entanglement occurs because (x, y) are no longer independent random variables, and the physical origin for the loss of independence is the interaction between the resonators in a classical statistical description.

From this stochastic formalism, it follows an important consequence: even if the interaction is turned off at a given moment and the resonators are separated miles away, as long as the state is not perturbed, the anticorrelations still persist. If the position of resonator 1 is measured, then the momentum of resonator 2 is determined, and if the positions of both resonators are measured, it is possible to determine the positions and momenta of both resonators with complete precision. As the position operators of the 2 resonators commute, this set of commuting observables could determine the state of the system precisely, which from a quantum point of view, contradicts the complementarity between position and momentum operators.

This form of the EPR paradox has been subject to experimental tests under the fashionable form of inequality violations [68–70]. These violations are based on the premise that when the product [71] or the sum [72, 73] of the variances of entangled variables are below the zero-point uncertainty limit, then the variables must be entangled. It is also assumed that the entanglement criterion requires the negativity of a quasi-probability distribution [73] (the $\mathscr{P}$ function in these cases), and because of that negativity, the measured correlations have been deemed nonclassical [68]. However, analogous inequalities have been derived for particles undergoing Brownian motion [74], and it was shown that a form of classical entanglement was possible for this situation.

One of the quantum inequalities between entangled quadratures reads [72]:

$$Var(q_1+q_2)+Var(p_1-p_2)\geq 2\,. \tag{2.20}$$

For the state in Eq.(2.19),

$$Var(q_1+q_2)+Var(p_1-p_2)=2\varrho^2<2 \quad , \quad \text{for } \varrho<1\,. \tag{2.21}$$

Thus, not only the inequality can be violated in a classical context (thus making any claim of nonclassicality absurd), but it can also be violated for disentangled pairs of quadratures ($\{q_1, q_2\}$ and $\{p_1, p_2\}$). The meaning of Eq.(2.20) is that the uncertainties for $q_1 + q_2$ and $p_1 - p_2$ are below the zero-point uncertainty. From a classical point of view, concepts like intrinsic quantum noise, standard quantum limit or zero-point uncertainty are not a necessity nor a limitation, and classical states with low variance can easily break this kind of inequalities. Inequalities derived solely from a quantum formalism give plenty of room for classical violations, which make this type of experimental violations meaningless.

There are some subtleties around the EPR paradox and its implications for physical measurements, namely regarding locality. The assumption of locality means that if at the time of the measurement the two subsystems no longer interact, no real change can take place in the second system in consequence of anything that may be done to the first system. Even if such assumption is maintained (which does not need to be the case in a stochastic framework), the consequences for measurement correlations are null.

If the system is prepared in the state given in Eq.(2.19), performing a measurement in one of the resonators affects the outcomes of the measurements for the other, even if they no longer interact. This change in the outcome probability as a consequence of the measurement does not imply that a real change has taken place in the system, only that one has gained additional information about the system. Once the measurement is performed, there is a refinement of information over the state of the system, hence the correlations.

Any apparent disagreement between classical notions of locality or realism is because the EPR program was essentially intended to attack the stochastic nature of quantum mechanics, but this nature is not unique to quantum mechanics. The questions regarding complementarity have evolved beyond the EPR paradox, and are currently analysed under the framework of Bell-like inequalities. If the Bell inequalities should be true for any theory satisfying "the intuitively reasonable notions of reality and locality" [26], are they still valid when these are not satisfied?

Due to practical matters, a variant of the Bell inequality shall be analysed instead of the original one [1]. First, spins differ from other quantum variables in the independence of the components. For a quantum spin, $[\sigma^x, \sigma^y] \neq 0$, but for the momentum of a particle, $[p_x, p_y] = 0$. This introduces extra degrees of freedom that require the reassessment of the consequences of the perfect anti-correlation existent in the spin case. In the spin case, if the y component is measured and the spin is in a $\uparrow$ state along x, then the measurement outcome is $\uparrow$ or $\downarrow$ equiprobably, and the spin is projected to the y basis after the measurement. However, measuring the momentum of a particle along y can be completely independent of the particle's momentum along x.

Second, measuring spins is entirely different than measuring other physical variables. In particular, for the case of optical modes, measurements are often done via photodetection, which is a destructive process. Thus, it cannot be assumed that the system can be measured without disturbing it. This makes Bell's 3 detectors scheme unsuitable to analyse 2 particle correlations.

[1] Decent discussions of the Bell inequalities can be found in [75, 76], as well as a proposal for a test in the form of an equality [76].

To confirm whether Bell-like inequalities can or cannot be violated with a purely classical distribution function, consider the Clauser-Horne-Shimony-Holt (CHSH) inequality

$$|S| = |\mathbb{E}(\alpha_1,\beta_1) + \mathbb{E}(\alpha_1,\beta_2) + \mathbb{E}(\alpha_2,\beta_1) - \mathbb{E}(\alpha_2,\beta_2)| \leq 2\,. \tag{2.22}$$

The variables $\{\alpha_i,\beta_j\}$ in Eq.(2.22) correspond to the possible detection options, where the measurement outcome is binary (± 1). Although Bell-like inequalities featuring continuous variables have been proposed [77], only binary variables shall be considered due to their widespread used in entanglement tests. Eq.(2.22) can be tested experimentally for harmonic oscillators via homodyne measurement of quadratures, as displayed in Fig. 2.1. In this situation, the phase difference defined by the local oscillators plays the role of the polarization angle in the usual optical experiments.

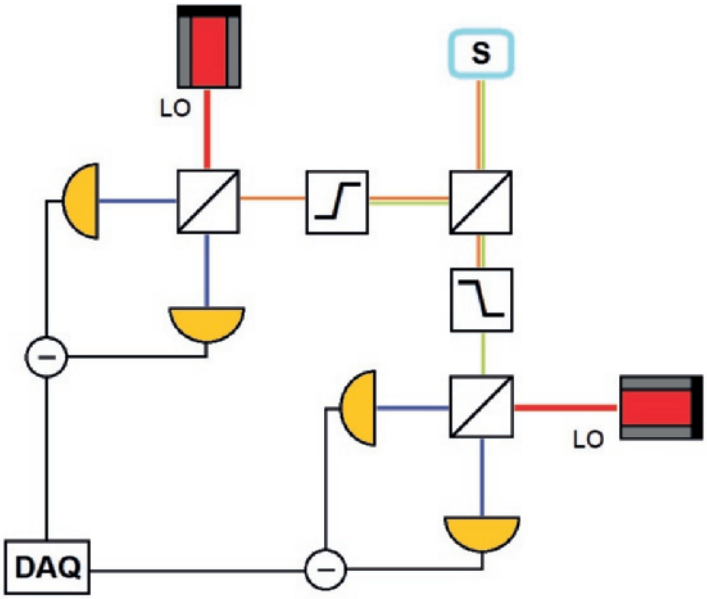

Figure 2.1: Depiction of an experimental scheme to violate CHSH with quadrature measurements. A source S emits 2 entangled optical modes, and the amplitudes of a pair of the modes' quadratures are measured via homodyne detection. The amplitudes α_j are converted to a binary outcome $\sigma(\alpha_j)$ and their product is analysed.

For binary measurement outcomes with homodyne detection, one must consider variables such as $\sigma(x) = 1-2\big(\Theta(b-x)+\Theta(x-a)\big)$ or $\sigma(x) = \Theta(x)$, where Θ is the Heavyside function. The probability distribution for the entire system can be partitioned in regions where the set $\{\sigma(\alpha_i),\sigma(\beta_i)\}$ takes a given value. Therefore, $S = \sum_{i,j,k,l=\pm 1} c_{i,j,k,l}\mathscr{I}_{i,j,k,l}$, with $\mathscr{I}_{i,j,k,l}$ the integral of $\mathbb{P}$ over the region where $\{i,j,k,l\}$ have a given value, and $c_{i,j,k,l}$ the value of $\sigma_1.\sigma_2$ in that region. The possible values that $c_{i,j,k,l}$ can take in any region are ± 2, as displayed in Table 2.2.

Normalization implies $\sum_{i,j,k,l=\pm 1}\mathscr{I}_{i,j,k,l} = 1$, and positivity $\mathscr{I}_{i,j,k,l} \geq 0$. Thus, $S \in [-2,2]$ and Eq.(2.22) cannot be violated classically. In quantum theory, on the other hand, the positivity condition $\mathscr{I}_{i,j,k,l} \geq 0$ does not exist as the Wigner function (the

$c_{i,j,k,l}$		$\sigma(\alpha_1)=-1$		$\sigma(\alpha_1)=+1$	
		$\sigma(\alpha_2)=-1$	$\sigma(\alpha_2)=+1$	$\sigma(\alpha_2)=-1$	$\sigma(\alpha_2)=+1$
$\sigma(\beta_1)=-1$	$\sigma(\beta_2)=-1$	2	2	-2	-2
	$\sigma(\beta_2)=+1$	2	-2	2	-2
$\sigma(\beta_1)=+1$	$\sigma(\beta_2)=-1$	-2	2	-2	2
	$\sigma(\beta_2)=+1$	-2	-2	2	2

Table 2.2: Value of $c_{i,j,k,l}$ for all possible combinations of σ_i.

quasiprobability function responsible for the quadrature measurement outcomes) can take negative values. If the negative regions of the Wigner function fall on the regions where $c_{i,j,k,l} < 0$ and the positive regions on $c_{i,j,k,l} > 0$ then, it is possible for S to be larger than 2. It is this feature that bestows a reason to attribute a nonclassical nature to the system whenever the Wigner function is negative.

Although the CHSH inequality has been experimentally violated, a violation with quadrature measurements has never been reported. The alternative implementations of the CHSH inequality tests typically rely on intensity or photocounting measurements. This is the case of measurements with double-cascade fluorescent atoms, where entangled pairs of photons are emitted [78, 79]. The violation of this sort of inequalities is associated with the negativity of another quasiprobability distribution for the quantum state (the $\mathscr{P}$ distribution), and this violation is only possible due to the peculiarities of photodetection and the strict connection with another physical effect: antibunching.

Besides the CHSH inequality, other inequalities have been proposed to treat the case of polarization correlations [80]. Although these inequalities were violated experimentally [42, 43, 81], the quantum/classical comparison is dubious due to the "localised photons" [42] and non-interfering classical cascade emissions [80] seasoning.

The overall landscape of testing Bell-like inequalities with light is dominated by cascade Fock states [2], which have peculiar properties for the usual photodetection measurements. It is thus desirable to test Bell-like inequalities using other types of states and measurements. Much of the meaning and value of these inequalities lie in the measurement procedure, as only through the theoretical modelling of the measurement process can theoretical bounds be placed. Without a theoretical frame, the significance of the measurements is diminished. To understand the essence of the measured object and to judge the meaning of the measured results, one always has to turn to measurement models.

2.2. STANDARD PHOTODETECTION THEORY

With the development of Quantum Optics, the problem of matching theoretical predictions to experimental measurements became prominent due to the noncommutative properties of operators. As different operator orders produce different outcomes, ordering rules have been sought to reproduce the uniqueness of the experimental observations. Currently, a widespread idea is that the measurement performed by photodetec-

[2] In some experiments, the entangled modes are produced using a parametric amplifier. The light state is therefore a 2-mode squeezed state that can be approximated to a pair of entangled photons for small squeezing.

tors must be described by normal ordered operators, but the reality is quite more complicated. Albeit normal ordering has become the rule, the operator order describing the measurement strictly depends on the detector model. In principle, any order respecting the properties of the measured observable (such as hermiticity) is valid, making even anti-normal ordering possible [82].

As with all theories, before any claim crystallizes into a postulate, a definition or a law, it has to undergo a process of redefinitions and argumentation to transit from debatable to defendable, and from the defendable to accepted. Let us inspect once more the roots of photodetection theory and advance in the cycle.

Here, a more general situation is considered than in [83]. To model photodetection, it is considered the standard picture of a system composed by $N+1$ energy levels, where all levels are closely packed (i.e. separated by an arbitrarily small ϵ) except the ground state, which is separated from the 1^{st} excited state by an extracting potential Φ. Additionally, the system starts in the ground state $|0\rangle$, and by coupling it to the electromagnetic field, it can make a transition to an excited state. This is meant to be a simple microscopic model for a detector for which an electron can go from the highest occupied band/orbital (here the ground state) to the conduction band. As the electron reaches the conduction band, detection takes place. The interaction between the system and the electromagnetic field has a dipolar nature, where the potential

$$V_I(t) = \sum_{j=1}^{N} g_j\left(|0\rangle\langle j|e^{-i\Delta_j t} + |j\rangle\langle 0|e^{i\Delta_j t}\right).\hat{E}(t)\,, \tag{2.23}$$

is in the interaction picture, $\Delta_j = \Phi+\epsilon(j-1)$, and $\{g_j\}$ are coupling parameters dependent on the polarizability of the energy level. The transition from the ground state to the conduction band is given by the excitation probability

$$\mathbb{P}_{exc}(t) = \sum_{j=1}^{N}\sum_{\phi}|\langle j,\phi|U(t)|0,\psi_i\rangle|^2 = 1 - Tr[U_I^{\dagger}(t)|0\rangle\langle 0|U_I(t)\rho] \tag{2.24}$$

where ψ_i (ϕ) is the initial (final) state of the electromagnetic field, ρ density matrix, and $U(t)$ ($U_I(t)$) is the time-evolution operator (in interaction picture) given by

$$U_I(t) = \mathscr{T}(e^{-i\int_0^t V_I(t')dt'}) = \sum_{n=0}^{+\infty}(-i)^n\int_0^t dt'_1\ldots\int_0^{t'_{n-1}} dt'_n V_I(t'_1)\ldots V_I(t'_n)\,. \tag{2.25}$$

For short time scales (or for weak-couplings g_j), the state evolution can be obtained by keeping just the lowest order terms of the Eq.(2.25) and together with Eq.(2.24), the excitation probability reads

$$\mathbb{P}_{exc}(t) \approx 2\int_0^t\int_0^t\sum_{j=1}^{N} g_j^2 e^{-i\Delta_j(t'-t'')}\langle E(t')E(t'')\rangle dt'\,dt''\,. \tag{2.26}$$

The coupling intensity g_j depends on the detailed electronic structure of the detector. It is assumed here that $|g_j|$ does not vary significantly for each energy level and so, it is taken to be constant ($|g_j| \approx g$). With this approximation, the sum over the energy levels

peaks at $t'-t''=\frac{2\pi z}{\epsilon}$, $z\in\mathbb{Z}$, where it attains the value $N+1$. As ϵ can be arbitrarily small so that the time-difference is outside the reach of validity, only the $z=0$ term is important in the band continuum limit ($\epsilon\to 0, N\to\infty$). This leads to $\sum_j e^{-i\Delta_j(t'-t'')}\to\frac{N}{\epsilon}\delta(t'-t'')$, and Eq.(2.26) reduces to

$$\mathbb{P}_{exc}(t)\approx\frac{Ng^2}{\epsilon}\int_0^t dt'\langle E^2(t')\rangle\,. \tag{2.27}$$

The integral in Eq.(2.27) acquires fast oscillating terms which are negligible in comparison to the static terms. Considering a single electromagnetic mode, the integration of these static terms leads to

$$\mathbb{P}_{exc}(t)\approx\frac{Ng^2E_{ZPF}^2}{\epsilon}t\langle a^\dagger a+aa^\dagger\rangle\,. \tag{2.28}$$

Despite the same procedure, there are several differences between Eq.(2.28) and the standard result. First, with the continuous band approximation, $\mathbb{P}_{exc}$ is proportional to t, instead of the usual resonant t^2 dependence [18]. This implies that $\eta=2Ng^2E_{ZPF}^2/\epsilon$ is a single-photon detection rate, and that the detection rate is constant in time in contrast to the standard result. Second, another consequence of the continuous band approximation is that detection does not select only light frequencies close to the extracting potential Φ as in the standard case. Third, because counter-rotating terms were kept (no RWA was used to simplify the interaction), the detector measures symmetrically ordered operators instead of the standard normal ordering [83]. The implication of this symmetric ordering is that even in vacuum, detection can occur due to zero-point fluctuations of the electromagnetic field. Consequently, all electromagnetic modes contribute to the detection process regardless of their state, as their zero-point fluctuations contribute to dark counts. Thus, the detection probability can be written as

$$\mathbb{P}_{exc}(t)\approx(\eta\langle a^\dagger a\rangle+r_{ZPF})t\,, \tag{2.29}$$

where r_{ZPF} is the dark count rate from the ZPFs of all the electromagnetic field modes. Because the number of modes contributing to the dark current is potentially infinite, r_{ZPF} may diverge.

2.2.1. HANBURY-BROWN-TWISS AND CORRELATIONS

Field amplitudes or intensities alone cannot tell much about the properties of the light state, and so higher order correlations of the electromagnetic field must be measured in order to infer the statistical properties of light. In order to analyse correlations, the probability for joint detection is considered. The question now is what is the probability for electrons in two separate detectors to be excited to the conduction band of both detectors simultaneously. This is given by

$$\begin{aligned}\mathbb{P}_{joint}(t)=&\sum_{j,l\geq 1}\sum_{\phi}|\langle j,l,\phi|U(t)|0,0,\psi_i\rangle|^2=1-Tr[U_I^\dagger(t)|0,0\rangle\langle 0,0|U_I(t)\rho]\\&-\sum_{l\geq 1}Tr[U_I^\dagger(t)|0,l\rangle\langle 0,l|U_I(t)\rho]-\sum_{j\geq 1}Tr[U_I^\dagger(t)|j,0\rangle\langle j,0|U_I(t)\rho]\end{aligned} \tag{2.30}$$

with $U_I(t)$ given by Eq.(2.25), but with the potential

$$V_I(t) = \sum_{j\geq 1, l\geq 0} g_j\left(|0,l\rangle\langle j,l|e^{-i\Delta_j t} + |j,l\rangle\langle 0,l|e^{i\Delta_j t}\right).\hat{E}^{(1)}(t) + \sum_{j\geq 0, l\geq 1} \gamma_l\left(|j,0\rangle\langle j,l|e^{-i\delta_l t} + |j,l\rangle\langle j,0|e^{i\delta_l t}\right).\hat{E}^{(2)}(t), \tag{2.31}$$

where $E^{(1)}$ ($E^{(2)}$) is the electric field impinging detector 1 (2). Combining Eqs.(2.31), (2.30) and (2.25) and using the same approximations as before ($|\gamma_j| \sim \gamma$, $|g_j| \sim g$, and the quasi-continuous band approximation), lengthly but straightforward calculations lead to

$$\mathbb{P}_{joint}(t) \approx \left(\frac{Ng\gamma}{\epsilon}\right)^2 \int_0^t dt_1 \int_0^{t_1} dt_2 \langle \hat{E}^{(2)}(t_2)\hat{E}^{(1)}(t_1)\hat{E}^{(1)}(t_1)\hat{E}^{(2)}(t_2)\rangle + \langle \hat{E}^{(1)}(t_2)\hat{E}^{(2)}(t_1)\hat{E}^{(2)}(t_1)\hat{E}^{(1)}(t_2)\rangle. \tag{2.32}$$

For the Hanbury-Brown-Twiss geometry depicted in Fig. 2.2, and for a 50/50 beam-splitter, $\hat{E}^{(1)}$ and $\hat{E}^{(2)}$ correspond to the reflected and transmitted light signal mixed with the vacuum. The corresponding relations between the signal and the vacuum fields ($E^{(s)}$ and $E^{(vac)}$ respectively), and the fields impinging detectors 1 and 2 are (for a particular choice of phase)

$$E^{(1)} = \frac{1}{\sqrt{2}}(E^{(s)} + E^{(vac)}) \quad \text{and} \quad E^{(2)} = \frac{1}{\sqrt{2}}(E^{(s)} - E^{(vac)}). \tag{2.33}$$

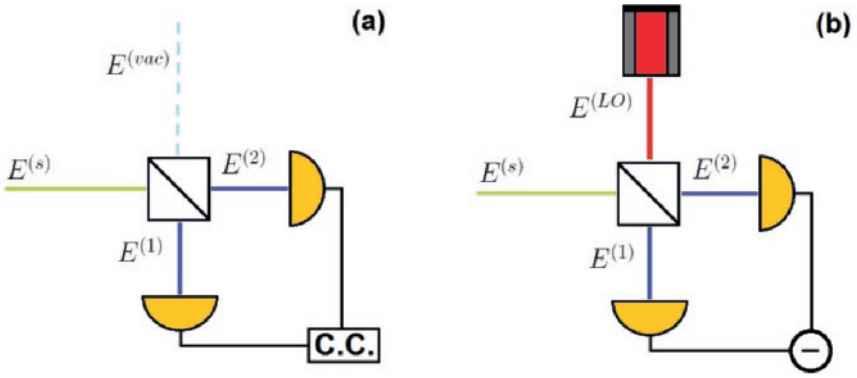

Figure 2.2: Depiction of the experimental scheme to measure $g^{(2)}$ **(a)** or the field quadrature $e^{i\phi_{LO}}\langle a_s^\dagger\rangle + e^{-i\phi_{LO}}\langle a_s\rangle$ (**b**). To measure $g^{(2)}$, the field $E^{(s)}$ is split into 2 detectors and the coincident detections are recorded. For quadrature measurements, the field $E^{(s)}$ is combined with a local oscillator $E^{(LO)}$ and the current produced at the 2 detectors is subtracted.

Substituting Eq.(2.33) into Eq.(2.32), considering a single mode for the signal beam, and keeping only the non-oscillating terms leads to

$$\mathbb{P}_{joint}(t) \approx \frac{t^2}{16}\Big\{\eta^2\langle a(aa^\dagger + a^\dagger a)a^\dagger\rangle + \langle a^\dagger(aa^\dagger + a^\dagger a)a\rangle + 2\eta\, r_{ZPF}\langle aa^\dagger + a^\dagger a\rangle - 4\eta^2\langle aa^\dagger\rangle + (d.c.)\Big\}, \tag{2.34}$$

where $d.c.$ stands for the dark coincidences' term, and for simplicity the single-photon detection rate η was considered equal for both detectors. It is now visible in Eq.(2.34) that for this case of a continuum detection band, without RWA, the operator order is the symmetric version of 4 possible operators orders. Note that symmetric combinations such as $aa^\dagger a^\dagger a + a^\dagger aaa^\dagger$ are not permitted. This symmetric ordering is completely distinct from the case of detection with a qubit, where normal order is the rule [83]. Further, ZPFs contribute here not only for coincidences in the detection, but also to induce extra coincidences in the presence of a signal. Writing Eq.(2.34) in a normal ordered way, one obtains

$$\mathbb{P}_{joint}(t) \approx \frac{t^2}{4}\left\{\eta^2\langle a^\dagger a^\dagger aa\rangle + \eta(\eta + r_{ZPF})\langle a^\dagger a\rangle + (d.c.)\right\}. \tag{2.35}$$

The importance of coincidence counting is that it gives direct access to measure higher order statistics of the electromagnetic field. However, dark counts lead to spurious coincidences that do not carry any information about the field. As they continue to exist in the absence of a signal beam, they can be estimated and subtracted from the total counts. Denoting by $\bar{\mathbb{P}}$ the probability with the dark counts subtracted, one can define a 2^{nd} order correlation function as the ratio between the probability of joint detections and the probability for single detections without dark counts by

$$\bar{G}^{(2)} = \frac{\bar{\mathbb{P}}_{joint}}{\bar{\mathbb{P}}_{det,1}\bar{\mathbb{P}}_{det,2}} = \frac{\eta\langle a^\dagger a^\dagger aa\rangle + (\eta + r_{ZPF})\langle a^\dagger a\rangle}{\eta(\langle a^\dagger a\rangle)^2}. \tag{2.36}$$

Note that for the H.-B.T. geometry, the intensity reaching detector 1 is $\propto (\hat{E}^{(1)})^2$, and so, using Eq.(2.33), the detection probability for detector 1 becomes $\mathbb{P}_{det,1}(t) \approx \frac{1}{2}t(\eta\langle a^\dagger a\rangle + 2r_{ZPF})$. Eq.(2.36) has additional contributions that do not occur in the normal ordered 2^{nd} order correlation

$$g^{(2)} = \frac{\langle a^\dagger a^\dagger aa\rangle}{(\langle a^\dagger a\rangle)^2}. \tag{2.37}$$

For a single-photon state, $g^{(2)} = 0$. This is an extreme case of antibunching ($g^{(2)} < 1$) and it means that no coincident detections ever occur. Or as usually said, "a photon can only be detected once" [40]. However, for a single-photon state in the quasi-continuous band scenario, $\bar{G}^{(2)} = 1 + \frac{r_{ZPF}}{\eta} > 1$, which means that the expected number of coincidence counts is higher than the single-detection counts. In this situation, ZPFs lead to additional coincidences and to single-photon bunching, where "a photon can be detected twice".

The difference between the quantum and classical situations is that for the latter, ZPFs do not exist and operator order is not an issue. For a classical field of amplitude α,

$$g^{(2)}_{class} = \frac{\langle|\alpha|^4\rangle}{(\langle|\alpha|^2\rangle)^2} = 1 + \frac{Var(|\alpha|^2)}{(\langle|\alpha|^2\rangle)^2}. \tag{2.38}$$

As the variance is always positive, $g^{(2)}_{class} \geq 1$, leading to the interpretation of antibunching as a nonclassical effect. It is important to be aware that a classical/nonclassical classification can only be meaningful within the theory describing the measurement. Attributing the nonclassical label to antibunching can only be done within the context of

a detection model. But then the question raises: is there a classical model that predicts antibunching? Despite the variety of detection models, antibunching constitutes to the present day one of the few phenomena in Quantum Optics without a (semi)classical explanation, and so being entitled to stand as "nonclassical".

Nevertheless, a classical explanation for antibunching would not be completely absurd. Standard photodetection theory predicts the existence of coincidences for a classical beam even if its energy is below the threshold energy necessary to excite 2 electrons. The contradiction between the predictions of the detection model and the basic principle of conservation of energy may be related to the fact that standard photodetection theory relies on time-dependent perturbation theory, and it does not describe the complete time-dynamics of the photodetection process. Currently, there are photodetection models that overcome the limitations of standard detection theory by using the machinery of quantum open systems [22, 84, 85], but so far this remains an open issue.

Some additional remarks should be made concerning antibunching. First, there are two distinct types of measurements: there are measurements with "click-detectors", meaning that the measurement outcome is binary (detection or nothing), and measurements which evaluate the correlations between the electric currents of the 2 detectors [86]. Although a simple extension is possible, the outcome of this last procedure is not what is usually modelled by standard photodetection theory, since the theory only predicts the joint excitation probability, and not correlations between the electrical currents. Second, standard photodetection theory also does not make predictions for correlations taken at different times. It is also a widespread belief that coincidences at different times can be described by the 2^{nd} order correlation function

$$g^{(2)}(t,\tau) = \frac{\langle a^\dagger(t)a^\dagger(t+\tau)a(t+\tau)a(t)\rangle}{\langle a^\dagger(t+\tau)a(t+\tau)\rangle\langle a^\dagger(t)a(t)\rangle}, \tag{2.39}$$

but that relies on misinterpretations of Eq.(2.32). Although correlation functions at different times can be computed in quantum theory, there is no formal way to derive the appropriate choice describing the real physical outcome [87], and no quantum formalism for this type of problem is known. It is not even known if simple properties like positivity for $g^{(2)}(\tau)$ are assured for $\tau \neq 0$.

Building upon antibunching, experimental variations were performed. Higher order correlations (8^{th} order in the fields) were tested experimentally [44, 79], breaking additional classical bounds. The interferometric nature of the H.-B. T. geometry also led to interference experiences with single and double-photon sources [40, 88–91]. Embedding interferometers in the H.-B. T. geometry led to the observation of oscillations in the coincidence rate as a function of the interferometer pathlength [40, 90, 91]. However, the nonclassical nature of this phenomenon is not fully clear cut, as it is thought to admit classical explanations [90, 91]. This interferometry has also been used to combine the double-slit experiment with the H.-B. T. geometry [88, 89], observing another kind of oscillation in the coincidences, but this time as a function of the position of the detectors.

All these antibunching experiments fueled the artistic view that when a photon reaches a beam-spliter, it takes only one path, inducing certain interpretations of propagating localised photons. Such localised photon notions motivated the combination of these interferometry schemes with double slit geometries to supposedly create which-path ex-

periments and test the wave-particle duality with trapped atoms [92]. The dependence of the observed interference pattern with the polarization of the emitted light was understood as light behaving as a particle or as a wave depending respectively on the absence or presence of an interference pattern [92]. Additionally, polarization served as an indicator of which atom (playing the role of the slit in the experiment) was light emitted from, triggering the interpretation that when a photon goes through a double slit, it takes both paths simultaneously, and only the conscious measurement forces it to choose a path, destroying the interference pattern.

Moving past the 19^{th} century interferometry and the cabalistic powers of consciousness, there is no quantum manifestation of any sort in optical double slit experiments. Such misinterpretations are based on misunderstandings between the quantum state and the field's spatial distribution, and the inability to conceive entanglement as a classical phenomenon. Quantum interpretations of photon paths are absurd because the lack of a wavefunction in real space for photons implies that the quantum state of light does not play any role regarding spatial properties of optical beams.

With the use of entangled light, the ladder was further climbed leading to what was coined as quantum eraser experiments [93, 94]. These experiments engaged in the long-standing discussions in quantum mechanics regarding the role of measurements and complementarity by making use of which-path schemes, but do not present any valid view on the topic. In [94], the spatial dependence of coincidences between 2 entangled optical beams were measured, where one of the beams goes through a double slit [3]. If after each slit there is a polarizer, with the polarizers oriented perpendicularly, and each beam does not have a well-defined polarization, then the interference pattern is broken due to the simple fact that the total intensity radiating from the 2 slits is the sum of the intensities coming from each slit. As the polarizers are set perpendicular to each other, the field amplitudes do not add and no interference occurs. When a polarizer is placed between the non-interfering beam and its detector, as the overall polarization of the system is well-defined, the measurement of the polarization of the non-interfering beam determines the polarization of the other beam. If the polarization of the interfering beam is determined to match one of the polarizers' orientations, then the interference is resurrected. Any quantum interpretation of such effects is an act of classical transvestism.

2.2.2. LINEAR MEASUREMENTS

A photodetector is able to measure the field intensity, and the H.-B. T. geometry opened the door to measure higher order correlations. But how to measure the field amplitudes? Consider the same H.-B. T. geometry above, with the exception that instead of mixing the signal with the vacuum, it is combined with an independent coherent field (a local oscillator LO) at the beam-splitter, as shown in Fig. 2.2. For a 50/50 beam-splitter, $E^{(vac)}$ is replaced by a nonzero average amplitude field $E^{(LO)}$ in Eqs. (2.33), and the single exci-

[3] An important observation made in [94] is that the order of the measurements is not irrelevant for the outcome.

tation probability for the two detectors are now

$$\mathbb{P}_{exc,1}(t) \approx \left[\frac{\eta}{2}\left(\langle a_s^\dagger a_s\rangle + |\alpha_{LO}|^2 + |\alpha_{LO}|(e^{i\phi_{LO}}\langle a_s^\dagger\rangle + e^{-i\phi_{LO}}\langle a_s\rangle)\right) + r_{ZPF}\right]t \tag{2.40}$$

$$\mathbb{P}_{exc,2}(t) \approx \left[\frac{\eta}{2}\left(\langle a_s^\dagger a_s\rangle + |\alpha_{LO}|^2 - |\alpha_{LO}|(e^{i\phi_{LO}}\langle a_s^\dagger\rangle + e^{-i\phi_{LO}}\langle a_s\rangle)\right) + r_{ZPF}\right]t\,, \tag{2.41}$$

$$\tag{2.42}$$

where $|\alpha_{LO}|^2$ and ϕ_{LO} are respectively the intensity and phase of the local oscillator. The difference between the outcome for the two detectors ($\propto \mathbb{P}_{exc,1} - \mathbb{P}_{exc,2}$) is then $\propto e^{i\phi_{LO}}\langle a_s^\dagger\rangle + e^{-i\phi_{LO}}\langle a_s\rangle$. Therefore, the field quadratures can be measured by combining a signal with a coherent field, and the measured quadrature can be selected by tuning the phase difference between the signal and the local oscillator. Linear measurements are a recurring tool in optics, and despite their simplicity, there are a few misunderstandings and enigmas surrounding them.

2.3. SIDEBAND ASYMMETRY[4]

Biased misconceptions often become dogmas provided that a blurry experimental connection is found. It is thus with the quantum interpretation of sideband asymmetry.

Sideband asymmetry (SA) refers to the difference in the spectral height of the side peaks accompanying a drive frequency. When a system is driven coherently at a frequency ω_L and it is coupled to an oscillator (such as a mechanical resonator), the spectrum acquires peaks (the sidebands) at $\omega_L \pm \Omega$, with Ω the mechanical frequency. This phenomenon was first observed with trapped ions [96] and neutral atoms [97], where laser cooling unveiled motional sidebands around atomic transitions. With the emergence of optomechanics, SA was observed in systems with larger mechanical elements such as nanobeams [58, 59], LC-resonators [60], ultracold atoms [61], and membranes [62]. In the absence of any symmetry breaking mechanism, it would be expectable for the sidebands to be equal. However, experimental observations reveal that one sideband is larger than the other. This imbalance has been justified by an asymmetric role of zero-point motion (ZPM) in the computed spectrum [98, 99]. Such quantum exegesis originates from proclaiming *ex cathedra* that the measurement outcome is described by

$$S_{XX}(\omega) = \int_{\mathbb{R}} e^{i\omega t}\langle \hat{x}(t)\hat{x}(0)\rangle_{th}\, dt = \delta(\omega+\Omega)\bar{n}_{th} + \delta(\omega-\Omega)(\bar{n}_{th}+1)\,, \tag{2.43}$$

where x is the displacement of the oscillator, and $\bar{n}_{th}$ its thermal occupancy. By identifying $\pm\Omega$ with the sidebands, SA would be naturally explained by ZPM. This would imply that the mechanical element had a truly quantum nature, regardless of its state. Thus, by cooling the resonator sufficiently, the asymmetry would become visible, ZPM unarguably established, and no classical theory explaining this phenomenon could exist [58]. Furthermore, it promised an experimental paradise where temperature could be determined without any calibration [61, 62]. Following such experimental observations, the quantum nature of SA was deemed true.

[4] The content of this section is part of a manuscript to be published. For a preprint see [95].

Developments in nanomechanics fed the desire to observe quantum effects at a macroscopic scale, which in turn raised the question of where does the quantum realm frontier lie. This question increased the necessity for a definition, where past a given borderline, certain phenomena would necessarily have a fundamental quantum nature. Once it was realised that the use of an operator formalism does not imbue a quantum nature for the system under consideration, deeper analyses on the nature of SA took place. This led to alternative interpretations and explanations such as interference between different noise channels [60, 100] and laser phase noise [101]. Despite certain flaws of the new interpretations [5], the claim of a quantum nature for SA became disputable [102].

Regarding SA, a pervasive problem plagues its interpretation: *a priori* definitions. The interpretation of SA differs for different operator orders (arising from different detector models [103]), and to assert that by definition, the experimental apparatus measures a particular operator order, does not force a detector to measure that specific order. Theoretical interpretations should be based on the physical situation, instead of the experimental validation being subdued to theoretical postulates. This constitutes a problem for experimental validation, as biased premises have been the starting point.

The problem over the nature of SA can be traced back to its measurement. In contrast to its classical counterpart, defining the power spectral density in a quantum framework poses a problem regarding the operators' order. Direct substitution of the fields by operators in classical formulas is dangerously arbitrary, as there is a multitude of possibilities and not all of them have a physical meaning. The problems with defining a quantum spectral density and the meaning of the distinct possibilities were raised before [87, 102] but remain unsolved. The usual way to address these issues is to take a specific measurement procedure into consideration.

SA can be measured using a linear detection scheme (such as homodyne or heterodyne detection, discussed in the previous subsection). The quantum description of these techniques [104] typically focuses on the quadrature measurement and noise response on the time-domain, leaving issues with the frequency domain unmentioned. A record of the measured field quadrature $X(t) = a_s(t) + a_s^\dagger(t)$ is constructed in the time domain, but it is in the frequency domain that the noise response is computed via the quadrature variance. This poses the problem of defining the variance of $X(\omega)$. As $X(\omega)$ is a complex operator, there are different possible orderings, namely $(\#1)\langle (X(\omega))^\dagger X(\omega)\rangle$ or $(\#2)\langle X(\omega)(X(\omega))^\dagger\rangle$ as well as any linear combination of the type $\lambda(\#1) + (1-\lambda)(\#2)$, with $\lambda \in [0,1]$. All these possibilities produce different outcomes, but the uniqueness of the spectrum implies that only one possibility should represent the observed spectrum.

The noise power spectral density is obtained with the Fourier transform of the average of the product between different measurement outcomes. As $X(t)$ is hermitian, the measurement outcome is a real number, and so is the product at different times. However $X(t)X(t')$ is not strictly hermitian, and therefore it can have non-real values as a possible outcome. Therefore $\langle X(t)X(0)\rangle$ cannot represent the physical measurement, and so can neither Eq.(2.43). The only hermitian possibility that can represent the measurement is the symmetric combination of $X(t)X(t')$ with its hermitian conjugate.

[5] For a comprehensive analysis of the problems of the distinct SA interpretations see Appendix A of [95].

Therefore, the most suitable spectral density to describe the measurement is

$$\bar{S}_{XX}(\omega) = \frac{1}{2}\Big\langle X(\omega)X(-\omega) + X(-\omega)X(\omega)\Big\rangle . \tag{2.44}$$

An alternative way to measure SA is with photodetection, and for this case the ordering issues are bypassed by choosing a detector model and establishing a link with the measurement outcomes. The typical detector model consists of a single qubit interacting briefly with the measured field via a weak dipolar coupling [83, 105]. The excitation probability P_{exc} of a qubit in the ground state for short time-scales and coupled to a stationary random field is computed with time-dependent perturbation theory as done in the previous Section, and it is [87]

$$P_{exc} \propto \int_{-t}^{t} e^{i\epsilon t'} \langle X(t')X(0)\rangle \, dt' . \tag{2.45}$$

By identifying the qubit energy splitting ϵ with the frequency ω, and P_{exc} with the measured signal, Eq.(2.45) has been employed as a quantum spectral density. However, such toy model is unable to completely model the measurement because: (1) spectrometers are not composed of a single qubit, and a single qubit alone cannot provide the spectral density for a wide frequency range. Models with several qubits lead to higher order correlation functions [83] and higher spin states do not lead to Eq.(2.45)[26]; (2) Eq.(2.45) is valid for short time-scales, where the transition rate is a constant given by the Fermi golden rule. To obtain the spectral density, the system has to be monitored for extended time-intervals, after which the validity of this result breaks down; (3) other detection models lead to different operator orders, such as anti-normal order in photon counters [82].

Irrespectively of the model and definitions considered, ZPM should not play a physical role in the asymmetry. Even though the measured field quadrature is associated with the operator X, the outcome of a measurement is a scalar x, and it is with the measurement record $x(t)$ that the spectrum is obtained. For the scalar $x(t)$, the order issue does not exist, the spectral density is well-defined, and there is no reason for ZPM to affect the sidebands differently. Nevertheless, ZPM plays a role in the variance of X, and there is a link between $X(t)$ and the measurement outcome. As X is monitored in time, a definite proof might rest in the theory of quantum continuous measurements. The formalism of continuous position measurements already exists in the literature [106], as well as analogous formalisms to model photodetection [22], but no suitable application to describe the spectral density is known. A closely related approach to describe homo- and heterodyne detection featuring quantum trajectories is also available in the literature [84] but it still relies on operator order postulates to evaluate the spectrum and not solely on the measurement record.

For the reasons exposed, Eq.(2.44) shall be used to compute the spectrum. To examine the nature of SA, it is considered the optomechanical case where the sidebands are measured via a signal coming from an optical (or microwave) cavity coupled to a mechanical resonator. From input-output relations, the signal amplitude is proportional to the cavity field, and for linear couplings, the cavity field yields a linear relation with the mechanical displacement. For this reason, when the cavity is driven, the coupling

to the mechanical resonator produces sidebands around the drive frequency that contain information about the mechanical motion. To compare with a typical experimental situation, 2 cavity modes are taken into account: a cooling mode, and a read-out mode with a frequency far away from the cooling mode. The equations of motion describing this system are [60]

$$i d_t b = \left(\Omega - i\frac{\Gamma}{2}\right)b - \sum_j g_j(a_j + a_j^\dagger) + \eta_b, \tag{2.46}$$

$$i d_t a_j = \left(-\Delta_j - i\frac{\kappa_j}{2}\right)a_j - g_j(b + b^\dagger) + \eta_j, \tag{2.47}$$

where Γ is the mechanical dissipation and Δ_j, κ_j, and g_j are the detuning, cavity linewidth and coupling strength for mode j. The detuning $\Delta_j = \omega_{L,j} - \omega_{cav,j}$ accounts for the shift of each mode j from their respective drive reference frame, i.e. a reference frame with frequencies displaced from the drive frequencies $\omega_{L,j}$. Here and onwards, the cavity frequency shift produced by the static displacement of the resonator is included in $\omega_{cav,j}$. Furthermore, b represents the phonon annihilation operator and a_r, a_c the photon annihilation operators for the read-out and cooling modes. At last, $\{\eta_j\}$ are the noise terms, with the properties

$$\langle \eta_j^\dagger(t)\eta_l(t')\rangle = \frac{\kappa_j}{2\pi}\bar{n}_j\delta_{jl}\delta(t-t') \quad \text{and} \quad \langle \eta_j(t)\eta_l^\dagger(t')\rangle = \frac{\kappa_j}{2\pi}(\bar{n}_j+1)\delta_{jl}\delta(t-t'), \tag{2.48}$$

where $\bar{n}_j$ is the thermal occupancy for mode j. An analogous relation holds for the mechanical noise. Note that the system behaves linearly as long as the interaction is weak enough to prevent entering the amplification regime. When this regime is reached, an instability takes place (primarily at $\Delta = \Omega$), leading to a behaviour very different than just the creation of sidebands. Moreover, in the strong coupling regime, hybridisation between the cavity and the mechanics occurs, leading to additional spectral features, such as a frequency splitting at $\Delta = -\Omega$. As we are only concerned in addressing the SA issue, only the case $g_j < \kappa_j, \Omega$ shall be considered, and since cooling occurs at the red-sideband, we set $\Delta_c = -\Omega$. Performing a Fourier transform in Eqs.(2.46-2.47) leads to the linear response function of the systems. The read-out field has the form

$$a_r(\omega) = q_1\eta_r(\omega) + q_2[\eta_r(-\omega)]^\dagger + q_3\eta_B(\omega) + q_4[\eta_B(-\omega)]^\dagger + q_5\eta_c(\omega) + q_6[\eta_c(-\omega)]^\dagger, \tag{2.49}$$

where $\{q_j\}$ are

$$\begin{aligned} q_1 =& \beth(\omega)\Big[\Big(\Big(\Omega^2 - \big(\omega + i\frac{\Gamma}{2}\big)^2\Big)\big(\Delta_r - \omega - i\frac{\kappa_r}{2}\big) + 2\Omega g_r^2\Big)\times \\ &\times\Big(\Omega^2 - \big(\omega + i\frac{\kappa_c}{2}\big)^2\Big) - 4g_c^2\Omega^2\Big(\Delta_r - \omega - i\frac{\kappa_r}{2}\Big)\Big], \end{aligned} \tag{2.50}$$

$$q_2 = -\beth(\omega)2\Omega g_r^2\Big(\Omega^2 - \Big(\omega + i\frac{\kappa_c}{2}\Big)^2\Big), \tag{2.51}$$

$$q_3 = \beth(\omega)g_r\Big(\Delta_r - \omega - i\frac{\kappa_r}{2}\Big)\Big(\Omega + \omega + i\frac{\Gamma}{2}\Big)\Big(\Omega^2 - \Big(\omega + i\frac{\kappa_c}{2}\Big)^2\Big), \tag{2.52}$$

$$q_4 = \beth(\omega)g_r\Big(\Delta_r - \omega - i\frac{\kappa_r}{2}\Big)\Big(\Omega - \omega - i\frac{\Gamma}{2}\Big)\Big(\Omega^2 - \Big(\omega + i\frac{\kappa_c}{2}\Big)^2\Big), \tag{2.53}$$

$$q_5 = \beth(\omega) 2\Omega g_r g_c \Big(\Delta_r - \omega - i\frac{\kappa_r}{2}\Big)\Big(\Omega + \omega + i\frac{\kappa_c}{2}\Big), \tag{2.54}$$

$$q_6 = \beth(\omega) 2\Omega g_r g_c \Big(\Delta_r - \omega - i\frac{\kappa_r}{2}\Big)\Big(\Omega - \omega - i\frac{\kappa_c}{2}\Big), \tag{2.55}$$

with

$$\begin{aligned}\big(\beth(\omega)\big)^{-1} = &\Big(\Omega^2 - \Big(\omega + i\frac{\Gamma}{2}\Big)^2\Big)\Big(\Delta_r^2 - \Big(\omega + i\frac{\kappa_r}{2}\Big)^2\Big)\Big(\Omega^2 - \Big(\omega + i\frac{\kappa_c}{2}\Big)^2\Big)\\ &+ 4\Omega\Delta_r g_r^2\Big(\Omega^2 - \Big(\omega + i\frac{\kappa_c}{2}\Big)^2\Big) - 4\Omega^2 g_c^2\Big(\Delta_r^2 - \Big(\omega + i\frac{\kappa_r}{2}\Big)^2\Big).\end{aligned} \tag{2.56}$$

In general, the read-out field does not have the same intensity at the red- and blue-sidebands because of the backaction from the cooling and read-out modes. This can be verified by evaluating, for example, the case with $\Delta_r = 0$ (corresponding to the experimental situation in [62]) in the limit $\Gamma \ll g_j, \kappa_j, \Omega$, which gives

$$\left|\frac{q_1(\Omega)}{q_1(-\Omega)}\right| = \left|\frac{A_- + iB_-}{A_+ - iB_+}\right| \neq 1, \tag{2.57}$$

where $A_\pm \approx 2(1+C_c)\Omega - \frac{\kappa_2}{4\Omega}(\kappa_r \pm \kappa_c C_r)$, $B_\pm \approx \kappa_r(1+C_c) + \kappa_c\big(\frac{1}{2} \pm C_r\big)$, and $C_j = \frac{4g_j^2}{\Gamma\kappa_j}$ is the cooperativity for mode j. Thus, the asymmetry does not present a method for absolute self-calibrated thermometry.

A method to measure SA is to send a probe beam at $\omega_{cav} - \Omega$ and measure the red-sideband at ω_{cav}, and then change the probe frequency to $\omega_{cav} + \Omega$ to measure the blue-sideband at ω_{cav} (see Fig.2.3). This way, each sideband can be enhanced at a time (while the other sideband is off-resonant) and measured more easily. At the enhanced red-sideband+cavity peak, the field amplitude for the read-out mode at $\Delta_r = -\Omega$ is

$$a_r(\omega) \approx Q_- \eta_r(\omega) - R_-\Big(\eta_B(\omega) - 2i\xi_c\eta_c(\omega)\Big), \tag{2.58}$$

while at the enhanced blue-sideband+cavity peak, the field amplitude of the probe at $\Delta_r = \Omega$ is

$$a_r(\omega) \approx Q_+ \eta_r(\omega) - R_+\Big([\eta_B(-\omega)]^\dagger - 2i\xi_c[\eta_c(-\omega)]^\dagger\Big), \tag{2.59}$$

with

$$Q_\pm \approx \frac{\Big(1 - i\frac{\kappa_r}{4\Omega}C_r + C_c\Big)}{\omega \pm \Omega + i\frac{\kappa_r}{2}(1 + C_{eff}^\pm)} \quad , \quad R_\pm \approx \frac{2i\xi_r}{\omega \pm \Omega + i\frac{\Gamma}{2}(1 + C_{eff}^\pm)} \quad , \tag{2.60}$$

$$C_{eff}^\pm = C_c \mp C_r, \tag{2.61}$$

and $\xi_j = g_j/\kappa_j$, and considering the limit $g_j \ll \kappa_j \ll \Omega$. With Eqs. (2.44) and (2.58-2.61), the spectral density for each enhanced sideband is found to be

$$\tilde{S}_{XX}^\pm \approx \frac{(1+C_c)^2 + \frac{\kappa_r^2}{16\Omega^2}C_r^2}{(\omega \pm \Omega)^2 + \frac{\kappa_r^2}{4}(1 + C_{eff}^\pm)^2}\kappa_r(\bar{n}_r + {}^1\!/_2) + \frac{4\xi_r^2\Gamma(\bar{n}_B + {}^1\!/_2 + C_c(\bar{n}_c + {}^1\!/_2))}{(\omega \pm \Omega)^2 + \frac{\Gamma^2}{4}(1 + C_{eff}^\pm)^2}, \tag{2.62}$$

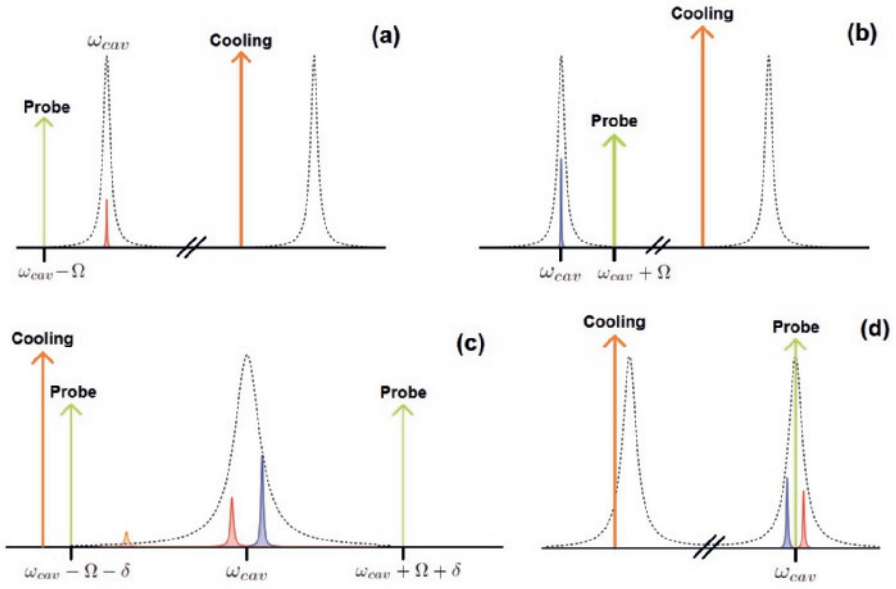

Figure 2.3: Different schemes to measure sideband asymmetry. The sidebands can be measured one at a time by placing the probe red(blue)-detuned (panel **a** (**b**)). Alternatively, a single cavity mode can be probed with 2 tones, which create sidebands within the cavity linewidth (panel **c**). The sidebands can also be measured directly with a probe tone on resonance (panel **d**). Cooling tones are also represented for completeness.

where $X = a + a^\dagger$ and $\pm$ correspond to the blue(+) or red(−) sidebands. As it can be seen from Eq.(2.62), the only difference in the expression for the sidebands lies in the denominator, where the interaction gives a different contribution for the linewidth of each sideband. It is also clear that there is no zero-point contribution to the imbalance, and that the origin of the asymmetry for the weak-coupling and resolved sideband regime is the distinct effective optomechanical dampings for each sideband. Thus, contrary to the standard result where the height of the sidebands is $n/n+1$, we find that the height of both sidebands is proportional to $n+1/2$, with n the number of thermal excitations. A consequence of this difference is that at $T = 0$, the red sideband does not vanish. One could think that at $T = 0$, the absence of phonons would prevent the sideband to exist. However, as we are considering quadrature measurements instead of photon counting, the zero-point motion of the resonator affects the measurement of its position, and allows for the existence of the red sideband.

The asymmetry is quantified experimentally via the noise power $I^\pm$, which is obtained by integrating the area of the resonant sidebands $S^\pm$ over all frequencies. The asymmetry factor ζ is then

$$\zeta = \frac{I^+}{I^-} - 1 = \frac{2C_r}{1 - C_r + C_c}. \tag{2.63}$$

As backaction is not strictly quantum, Eq.(2.63) shows that the asymmetry already arises in a classical framework. Although not explicitly visible from Eq.(2.63), the asymmetry ζ may depend on the temperature. For real physical systems, the mechanical quality

factor is temperature dependent, leading to a temperature dependent asymmetry. For small cooperativities, the asymmetry is directly proportional to the quality factor, and if the latter decreases linearly with temperature around a given temperature range, then the qualitative temperature dependence of the asymmetry matches the standard result.

An alternative way to measure SA with only one cavity mode is to simultaneously drive the system with two probe tones (see Fig. 2.3). These two tones are slightly detuned by δ from $\omega = \omega_{cav} \pm \Omega$ such that the sidebands do not overlap at ω_{cav}. Thus, to make the sidebands distinguishable and enhanced (so well within the cavity linewidth), δ must obey $\Gamma \ll \delta \ll \kappa$. To fully describe the experimental situation, we consider once more a cooling tone of frequency $\omega_{cav} - \Omega - \delta_c$, with $\delta_c \gg \delta + \Gamma$ so that the cooling tone does not provide an undesired contribution to the asymmetry. In this multi-tone case, the appearance of beats between the different tones ϖ_j is inevitable, and the linear interaction of Eq.(2.47) can no longer be made time-independent. Thus, the original form of the interaction must be considered, and the equations of motion for the system are now [60]

$$i d_t a = \left(\omega_{cav} - i\frac{\kappa}{2}\right)a - g_0(b + b^\dagger)a + \eta_A(t) + \sum_j s_j e^{-i\varpi_j t}, \tag{2.64}$$

$$i d_t b = \left(\Omega - i\frac{\Gamma}{2}\right)b - g_0 a^\dagger a + \eta_B(t), \tag{2.65}$$

where the sum in j is over the ϖ_j frequencies $\{\omega_{cav} \pm (\Omega + \delta), \omega_{cav} - \Omega - \delta_c\}$. The driving terms can be removed with the shift

$$a(t) = A(t) + \sum_j e^{-i\varpi_j t}\alpha_j \quad , \quad b = \beta + B(t), \tag{2.66}$$

where

$$\alpha_j = \frac{s_j}{\Delta_j + i\frac{\kappa}{2}} \quad , \quad \beta = \frac{g_0}{\Omega - i\frac{\Gamma}{2}} \sum_j |\alpha_j|^2. \tag{2.67}$$

With this shift, the resonant part of the interaction is enhanced by α_j, and it becomes linear in A and B. As g_0 is negligible in comparison to the other parameters, the terms linear in A and B suffice to account for the effects of the interaction. Disregarding the nonlinear terms, and performing a Fourier transform at the equations of motion, we find the cavity field to be

$$A(\omega)\mathscr{D}(\omega) = \beth(\omega) - \sum_{p \neq q} \alpha_q^* G(\omega - \varpi_p) A(\omega - \varpi_p + \varpi_q) - \sum_{p,q} \alpha_q G(\omega - \varpi_p)(A(\varpi_p - \omega + \varpi_q))^\dagger, \tag{2.68}$$

where

$$\begin{aligned}\beth(\omega) = &-\sum_q \left(\frac{g_0 \alpha_q \eta_B(\omega - \varpi_p)}{\omega - (\varpi_p + \Omega) + i\frac{\Gamma}{2}} - \frac{g_0 \alpha_q (\eta_B(\varpi_p - \omega))^\dagger}{\omega - (\varpi_p - \Omega) + i\frac{\Gamma}{2}}\right) \\ &- \eta_A(\omega) - \sum_{p,r \neq q} g_0 G(\omega - \varpi_p)\alpha_q^* \alpha_r \delta(\omega - \varpi_p + \varpi_q - \varpi_r),\end{aligned} \tag{2.69}$$

$$\mathscr{D}(\omega) = \omega - \omega_{cav} + i\frac{\kappa}{2} - \sum_q \alpha_q^* G(\omega - \varpi_q) \quad , \quad G(\omega - \varpi_p) = \frac{2 g_0 \alpha_p \Omega}{\Omega^2 - (\omega - \varpi_p + i\frac{\Gamma}{2})^2}. \tag{2.70}$$

Eq.(2.68) provides a general framework for the cavity spectrum when linearly coupled to another oscillator and driven by multiple tones. Obtaining an analytical solution for this system is impractical, because the presence of several tones implies that all arbitrary integer combinations of the tones' frequencies must be evaluated. However, the higher harmonics are off-resonant and they can be disregarded in the weak-coupling regime. Using Eqs.(2.68-2.70), the same procedure leads to an equation analogous to Eq.(2.62), with an effective cooperativity given by

$$C_{eff}^{\pm} = C_c \frac{\Gamma^2}{4(\delta_c \pm \delta)^2 + \Gamma^2} \mp C_{\pm} \pm C_{\mp} \frac{\Gamma^2}{16\delta^2 + \Gamma^2}, \tag{2.71}$$

where $\pm$ stands for the sideband at $\omega_{cav} \pm \delta$. Since C_{eff} is different for each sideband, an imbalance occurs even if the red and blue-sideband tones have the same intensity ($C_+ = C_-$). This difference between C_{eff}^{+} and C_{eff}^{-} is due to the δ frequency shift from the resonance. Identically to the multimode case, backaction leads to an asymmetry in the spectrum.

Thus, the undisputed existence of SA is not a proof of any quantum nature for the system. The use of a symmetric noise power spectral density shows that SA arises from the backaction caused by the cooling and probe drives, and that no ZPM contributes to the asymmetry. The symmetric spectral density was already employed in [60, 102], but the asymmetry was attributed to quantum interference between the cavity noise and the mechanical resonator's noise. Such misinterpretation sprouts from miscalculations [6]. Though only white noise was considered here, the analysis can be extended for any type of noise. However, since only frequencies within a bandwidth of Γ contribute to the sidebands' peaks, coloured noise is expected to be unimportant.

Although the present analysis is restricted to coupled harmonic oscillators, the same procedure can be generalized to analyze the trapped ions and neutral atoms [96, 97] case. The role of backaction has not yet been investigated in these systems, and a thorough analysis would clarify the nature of the asymmetry for this case. Note that for the case of trapped ions and atoms, their electronic quantum nature may lead to quantum signatures for the output light that are not an intrinsic feature of the light field (neither of the mechanical motion), much like in the case of Raman scattering [107].

[6] For the specific problems see Appendix A of [95].

3

WHERE TO LOOK FOR QUANTUM

The most honourable reason for the prevalence of quantum theory is what it represented. The introduction of a new paradigm, the uncommon and complex machinery, the bizarre and exotic features. All of this provided a breath of fresh air to Physics, and it should never be underestimated how every cultural endeavour needs a periodic stirring in order to stay alive. And what better than a theory that questions the most basic perceptions and overthrows old canons? A new theory with fertile and unexplored lands, with seemingly endless possible avenues to pursue. Who can resist such paradisaic gardens? "What is truth?" they chant. And we undress ourselves from convictions and indulge in getting lost in the labyrinth.

What quantum phenomena are to be found in macroscopic mechanical systems?

3.1. PHONON ANTIBUNCHING IN STANDARD OPTOMECHANICS[1]

As discussed in subsection 1.3.2, light couples to mechanics in standard optomechanical systems via radiation pressure. Because of the simplicity of the interaction and for symmetry reasons ($a \to ae^{i\phi}$ leaves Eq.(1.15) invariant), the system is integrable, and the exact solution for the isolated system has already been found [109, 110]. For an isolated system, radiation pressure simply leads to a constant force acting on the mechanical resonator, and to a coherent displacement of the resonator depending on the photon statistics:

$$b(t) = e^{-i\Omega t}\left(b(0) + \frac{g_0}{\Omega}a^\dagger a\right) - \frac{g}{\Omega}a^\dagger a\,. \tag{3.1}$$

Sadly, the exact solution does not bring quantum phenomena along with it. The effects of the interaction are more prominent at half of a mechanical period, where $b(t = \pi/\Omega) = -b(0) - 2g_0/\Omega a^\dagger a$, and if the mechanical resonator starts in the ground state, the mechanical state after a half period is fully determined by the cavity state. Under these

[1] The content of this section is based on the published work [108].

conditions, the mechanical second order correlation function is

$$g^{(2)}\left(t=\frac{\pi}{\Omega}\right)=\frac{\langle b^\dagger b^\dagger bb\rangle}{(\langle b^\dagger b\rangle)^2}\left(t=\frac{\pi}{\Omega}\right)=1+\frac{Var(n_a^2)}{\left(\langle n_a^2\rangle\right)^2}, \tag{3.2}$$

where n_a is the photon number. As the photon number distribution is always positive, $g^{(2)}\geq 1$, and no phonon antibunching occurs. The reason behind the absence of dynamical quantum effects is that the interaction changes the mechanical state in a trivial way (it mainly displaces the state, if the initial mechanical state is a Gaussian state [110]).

In order for the interaction to produce more interesting effects, namely to be able to observe quantum effects, the photon number should not remain constant. The best way to do this is to drive the optical cavity with a coherent laser. The price of driving is that the integrability of the isolated system is lost, as it relied on a constant photon number. Including driving in the Hamiltonian leads to

$$\mathscr{H}=-\Delta a^\dagger a+\Omega b^\dagger b-g_0 a^\dagger a(b^\dagger+b)+\mathscr{E}(a^\dagger+a), \tag{3.3}$$

where $\Delta=\omega_L-\omega_c$ is the detuning of the laser frequency ω_L from the cavity frequency ω_c, $\mathscr{E}$ is the driving strength, and a is the cavity's photon annihilation operator in the frame rotating with the driving frequency ω_L. In order to sweep away the direct influence of the driving term, the operator shifts $a=A+\alpha$ and $b=B+\beta$ are performed, with $\alpha=\mathscr{E}/\Delta$ and $\beta=\alpha^2 g_0/\Omega$. The shifted operators A,B represent the field displacements around the coherent components α,β produced by the drive.

The effects of driving the system have been analyzed theoretically by treating the driving as a perturbation [111]. For this weak driving regime, it was found that mechanical states with sub-Poissonian statistics can be created in the single-photon strong coupling regime (g_0 bigger than the cavity linewidth), which was corroborated by numerical simulations [112]. Other works reported similar quantum states in this regime, and signalled a connection to self-sustained oscillations [113].

However, the yet experimentally achievable regime is the multi-photon strong coupling, where driving enhances the single-photon coupling by a factor of $\sqrt{N_{photons}}$. Although quantum fluctuations are usually negligible in this regime, and the lineared interaction usually suffices to describe the behaviour of the system, a nonlinear interaction is a prerequisite for the occurrence of nontrivial quantum phenomena. The existent theoretical description of the nonlinear system featuring strong driving is mostly classical but there has been recently a growing interest in its quantum counterpart. Nonlinear corrections to optomechanically induced transparency were obtained for this regime (through standard perturbation theory [114] and resorting to Keldysh techniques [115]). The nonlinear interaction can also lead to parametric down-conversion between hybrid excitations of photons and phonons, the polaritons, if the system is driven at the red sideband [116].

To be able to look for quantum effects in these systems, it is desirable to retain the nonlinear character of the interaction while taking a strong coherent drive into account. As the coupling g_0 is typically smaller than all other physical parameters (for most experiments, $\eta=g_0/\Omega\sim 10^{-3}$ or less [50], though $g_0>\Omega$ in [117] or close to it [118]), a possible strategy to deal with the nonlinearity is to diagonalize the Hamiltonian perturbatively in

η. One can then perform a unitary transformation to obtain an effective Hamiltonian $\mathscr{H}_{eff} = U\mathscr{H}U^\dagger$ for which the effective interaction is even weaker (of the order of η^2). The Hamiltonian in Eq.(3.3) has the form $\mathscr{H} = \mathscr{H}_0 - \eta V$ with

$$V = \Omega\Big[A^\dagger A(B^\dagger + B) + (\alpha A + \alpha A^\dagger)(B + B^\dagger)\Big]. \tag{3.4}$$

It is clear from the above equation that by driving the system with a strong coherent source, some interaction terms are enhanced by a factor of α. These enhanced terms lead to a linear coupling between light and mechanics, and they suffice to describe the physics of these systems as long as the driving is not strong enough to cause amplification. Acting with the unitary transformation $U = e^{-\eta^2 T}e^{-\eta S}$ (S and T are anti-Hermitian operators) on the Hamiltonian above leads to

$$\mathscr{H}_{eff} = \mathscr{H}_0 - \eta^2\Big(\frac{1}{2}[V,S] + [T,\mathscr{H}_0]\Big) + o(\eta^3), \tag{3.5}$$

where the condition $[\mathscr{H}_0, S] = V$ was imposed in order to eliminate the first order contributions of η (which corresponds to a Schrieffer-Wolff transformation). Choosing S and T properly enables the diagonalization of the Hamiltonian up to η^2, forcing S and T to be

$$S = \frac{\alpha\Omega}{\Delta-\Omega}AB - \frac{\alpha\Omega}{\Delta+\Omega}A^\dagger B - A^\dagger AB - h.c., \tag{3.6}$$

$$T = c_0 A + c_1 AA + c_2 A^\dagger AA + c_3 ABB + c_4 A^\dagger BB + c_5 AB^\dagger B + c_6 BB - h.c., \tag{3.7}$$

where h.c. stands for the Hermitian conjugate. The coefficients $\{c_j\}$ for the T operator are shown in Table 3.1.

c_0	c_1	c_2	c_3
$\frac{\Omega\alpha}{\Delta}\frac{\Delta-2\Omega}{\Delta-\Omega}$	$-\frac{\Omega^3\alpha^2}{2\Delta(\Delta^2-\Omega^2)}$	$-\frac{\Omega\alpha(2\Omega^2-\Delta^2)}{\Delta(\Delta^2-\Omega^2)}$	$-\frac{\Delta\Omega\alpha}{2(\Delta-2\Omega)(\Delta-\Omega)}$
c_4	c_5	c_6	
$-\frac{\Delta\Omega\alpha}{2(\Delta+2\Omega)(\Delta+\Omega)}$	$-\frac{\Omega^2\alpha}{\Omega^2-\Delta^2}$	$\frac{\Delta\Omega\alpha^2}{2(\Delta^2-\Omega^2)}$	

Table 3.1: Coefficients of T

Despite the apparent general character of the transformation, it is seen from Tab. 3.1 that it is not possible to perform the transformation around the points $\Delta = \{0, \pm\Omega, \pm 2\Omega\}$. The reason for the exclusion of the sidebands is that the interaction is resonant for these particular detunings. Whenever resonant conditions are met, the interaction cannot be treated perturbatively, and each resonant case must be assessed separately. At these detunings, the spectrum is linearly dependent on the coupling and the photon and phonon degrees of freedom hybridize. This hybridization is the essence of polaritons, and to address the system at the sidebands, a description in terms of these quasi-particles must be employed.

The explicit form of the effective Hamiltonian in Eq. (3.5) is then

$$\mathscr{H}_{eff} = -\tilde{\delta} A^\dagger A + \eta^2 \Omega (A^\dagger A)^2 + \tilde{\Omega} B^\dagger B\,, \tag{3.8}$$

and $\tilde{\delta}$ and $\tilde{\Omega}$ are

$$\tilde{\delta} = \Delta + 2\frac{g^2\Omega}{\Delta^2 - \Omega^2}\,, \quad \tilde{\Omega} = \Omega - 2\frac{g^2\Delta}{\Delta^2 - \Omega^2}\,, \tag{3.9}$$

with the multi-photon coupling $g = g_0\alpha$. The effective Hamiltonian presented in Eq. (3.8) reveals that the mechanical coupling leads to a Kerr nonlinearity for the photons (the $(A^\dagger A)^2$ term), as well as mechanical and cavity frequency shifts.

Apart from the particular detunings mentioned above, the approach also does not hold for arbitrarily high coupling values g. The validity region of the transformation can be seen in Fig. 3.1, where it is plotted the ratio r between the disregarded higher order terms and the lower order terms (up to η^2). It is seen that the higher order terms reach the magnitude of the lower order terms almost everywhere as $g \sim \Omega$. Therefore, the analysis must be restricted to weak multi-photon coupling values.

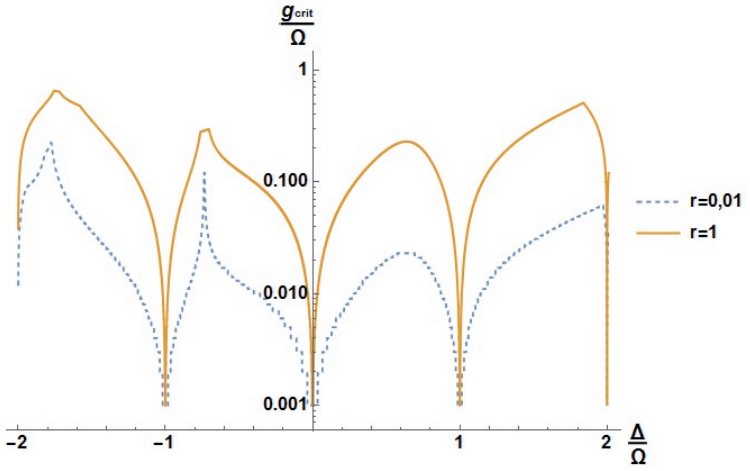

Figure 3.1: Ratio r between higher order terms and lower order terms as a function of detuning. The transformation is not valid at $\Delta = 0, \pm\Omega, \pm 2\Omega$, as well as for $g > \Omega$, since the magnitude of the disregarded higher order terms becomes non-negligible.

With Eq. (3.8), the solutions for the operator equations of motion in the new (diagonalized) basis are straightforward to obtain, and the time-evolution for the operators $\{A_N, B_N\} = \{UAU^\dagger, UBU^\dagger\}$ is given by

$$A_N(t) = e^{i(\tilde{\delta} - 2\eta^2\Omega A^\dagger A)t} A_N(0) \quad \text{and} \quad B_N(t) = e^{-i\tilde{\Omega}t} B_N(0)\,. \tag{3.10}$$

Returning to the original basis, the mechanical resonator evolves as

$$B(t) \approx \Xi_0(t)B(0) + \Xi_1(t)A(0) + \Xi_2(t)A^\dagger(0) + \Xi_3(t)A^\dagger(0)A(0) + o(\eta^2), \tag{3.11}$$

with

$$\Xi_0(t) = e^{-i\tilde{\Omega}t}, \tag{3.12}$$

$$\Xi_1(t) = \frac{g\Omega}{\Delta+\Omega}(e^{-i\tilde{\Omega}t} - e^{(i\tilde{\delta}-2i\eta^2\Omega(A^\dagger A)(0))t}), \tag{3.13}$$

$$\Xi_2(t) = \frac{g\Omega}{\Delta-\Omega}(e^{(i\tilde{\delta}-2i\eta^2\Omega(A^\dagger A)(0))t} - e^{-i\tilde{\Omega}t}e^{(i\tilde{\delta}-2i\eta^2\Omega(A^\dagger A)(0))t}), \tag{3.14}$$

$$\Xi_3(t) = \eta(1-e^{-i\tilde{\Omega}t}). \tag{3.15}$$

After a complete mechanical cycle ($t = 2\pi/\Omega$), $\Xi_0 = 1$ and $\Xi_3 = 0$. Furthermore, the action of $exp\big(-2i\frac{g_0^2}{\Omega}(A^\dagger A)(0)t\big)$ on a coherent state $|q\rangle$ is to impart a phase $\phi = -2i\eta^2\Omega t$. For simplicity, it is chosen $\eta = 10^{-3}$ such that $\phi = 0$ after 10^6 cycles, and use this choice from here on. If the mechanical state starts in the ground state (the physical state, not the displaced one), it is then possible to control the state of the mechanical resonator by tailoring it with the cavity state. This control over the mechanical state can be exploited to observe quantum phenomena for the mechanical element, in particular phonon antibunching. Consider that the cavity starts in the groundstate (no light inside the cavity), and that the laser driving creates a coherent state for the cavity with amplitude q. The second order correlation function for the mechanical field is then given by

$$g^{(2)}(t_m^*) = 1 + \frac{|X_2|^2\big(|X_2|^2(1+2|q^2|) + |X_1|^2(1+6|q|^2)\big) + 2(|X_1|^2+3|X_2|^2)Re\{X_1X_2^*q^2\}}{\big(|qX_1|^2+|X_2|^2(|q|^2+1)+2Re\{X_1X_2^*q^2\}\big)^2}. \tag{3.16}$$

The behaviour of Eq.(3.16) with the detuning is displayed in Fig. 3.2. It is seen that for small coherent states, it is possible for phonon antibunching to occur close to $\Delta = -\Omega$. As the antibunching tends to vanish with the increase of the driving amplitude, the antibunching behaviour is most likely caused by the creation of a small squeezed state for the mechanical resonator. This phonon antibunching effect can be observed by swapping the mechanical and the optical states, and then perform a Hanbury-Brown Twiss experiment as displayed in Fig. 2.2.

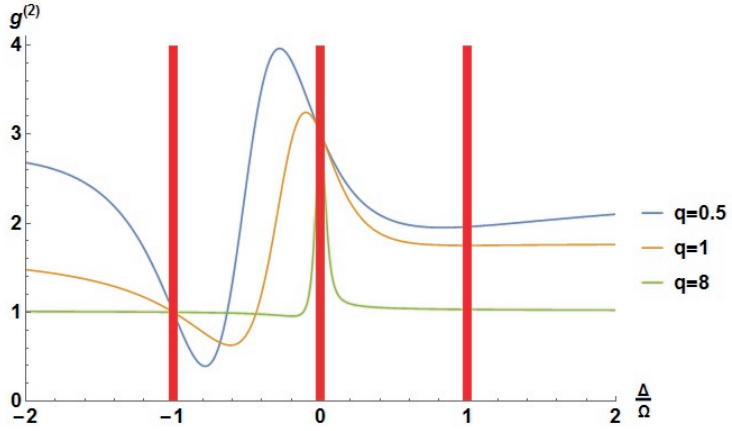

Figure 3.2: Dependence of the mechanical second order correlation function with detuning for coherent states of different amplitude q. It is seen that for small coherent cavity states ($|q| < 1$), it is possible for the system to display phonon antibunching close to $\Delta = -\Omega$. The red vertical lines mark the regions where the approach is not valid.

3.2. CAPACITIVE COUPLING [2]

As discussed in subsection 1.3.3, mechanical resonators can be coupled to LC resonators, and when the LC frequency is half of the mechanical frequency, a new type of interaction is possible in electromechanics. This is the parameter regime to be investigated in this section. Although this condition has never been reported in any electromechanical device, it should be feasible to attain it with current technology, since circuit electromechanical realizations with GHz mechanical resonators have already been reported [119] and with large coupling strengths[120]. Alternatively, the LC resonance frequency can be brought down by using a large inductance or capacitance, at the expense of a weaker coupling.

This parametric coupling already occurs in quantum optics, where it describes the process of parametric down-conversion, but it can be also implemented in electromechanics. The lowest energy levels of the degenerate parametric amplifier are known and some exact results exist for related Hamiltonians [121], but no full diagonalization was ever found.

3.2.1. INTEGRABILITY AND THE UNSTABLE VACUUM

The structure of quantum mechanics is linear algebra. In an ideal scenario, any physical problem reduces to solving the eigenproblem $\mathscr{H}|\psi\rangle = \epsilon|\psi\rangle$, and with the full spectrum and set of eigenstates, everything can be known about the system. Thus, the problem of interest is how to diagonalize exactly the degenerate parametric amplifier Hamiltonian

$$\mathscr{H} = \omega a^\dagger a + \Omega b^\dagger b + g(aab^\dagger + a^\dagger a^\dagger b)\,. \tag{3.17}$$

[2] The content of this section is based on a project with E. Jansen.

Eq.(3.17) reveals that the Hamiltonian is invariant under the transformations $a \to ae^{i\phi}$ and $b \to be^{2i\phi}$. This continuous symmetry is intimately connected to the conservation of excitation number $\hat{C} = a^\dagger a + 2b^\dagger b$, as seen from the following reasoning: If $\hat{C}$ is a conserved quantity, then it commutes with $\mathscr{H}$, and so does any linear combinations of powers of $\hat{C}$. Thus, one can construct a group of unitary transformations $U_\phi = e^{-i\phi\hat{C}}$, whose action on a and b produces the aforementioned phase shift. On the other hand, if T is an invertible transformation that leaves the Hamiltonian invariant, then

$$T\mathscr{H}T^{-1} = (\mathscr{H}T + [T,\mathscr{H}])\,T^{-1} = \mathscr{H} + [T,\mathscr{H}]\,T^{-1} = \mathscr{H}, \tag{3.18}$$

which implies that T is a constant of motion ($[T,\mathscr{H}] = id_t T = 0$). A unitary transformation T_ϕ belonging to a continuous 1D group can always be written as $T_\phi = e^{-i\phi\hat{C}}$, and iff $\forall\phi \in \mathbb{R}$, T_ϕ leaves the Hamiltonian invariant, then the group generator $\hat{C}$ is also a constant of motion, as seen from the relation $\hat{C} = iT_{-\phi}\partial_\phi T_\phi$.

The phase shift for the a and b fields that leaves the Hamiltonian invariant is obtained respectively with $\Phi_a = e^{-i\phi a^\dagger a}$ and $\Phi_b = e^{-2i\phi b^\dagger b}$. Therefore, $\left\{U = \Phi_a\Phi_b = e^{-i(a^\dagger a + 2b^\dagger b)\phi}\right\}_\phi$ is the unitary group of transformations leaving the Hamiltonian invariant, certifying that $\hat{C}$ is a constant of motion. If a transformation T leaves the Hamiltonian invariant, and $|\psi\rangle$ is an eigenstate of $\mathscr{H}$, then $T|\psi\rangle$ is also an eigenstate with the same energy. Thus, the eigenstates of $\hat{C}$ can be used as a basis to represent the eigenstates of $\mathscr{H}$, and the eigenstates can be expressed in the basis $\{|\phi_m^{(C)}\rangle = |C-2m,m\rangle\}$ (with m the phonon number), where $C, m \in \mathbb{N}$ and $C \geq 2m$. Eq.(3.17) can be rewritten as

$$\mathscr{H} = \omega\hat{C} + (\Omega - 2\omega)b^\dagger b + g(aab^\dagger + a^\dagger a^\dagger b)\,. \tag{3.19}$$

The usefulness of the symmetry observation is that the interaction only acts between states with the same C. This decomposition reduces the number of relevant degrees of freedom, since now only m matters for the diagonalization problem. Consequently, the Hamiltonian becomes block diagonal, and the eigenstates are grouped into "closed" classes for each C, in the sense that if the system starts in a state inside a class with a given C, then the state will never evolve into another state outside of its class.

The particular case of interest is the spectrum for $\Omega = 2\omega$. When this resonance condition is fulfilled, the effects of the interaction are more prominent and cannot be treated perturbatively, the explicit dependence on the excitation number $b^\dagger b$ vanishes and the free energy depends only on $\hat{C}$. The eigenvalue problem associated with obtaining the spectrum of Eq.(3.19) can be written as

$$\mathscr{H}|\psi\rangle = E|\psi\rangle \Leftrightarrow (aab^\dagger + a^\dagger a^\dagger b)|\psi\rangle = \frac{1}{g}(E - \omega\hat{C})|\psi\rangle\,, \tag{3.20}$$

making now evident that the energy spectrum is a linear function of g. The Hamiltonian can then be decomposed in the $\mathscr{H}_C$ subspaces ($\mathscr{H} = \bigoplus_{C\in\mathbb{N}}\mathscr{H}_C$), which in the $\{|\phi_m^{(C)}\rangle\}$

basis, $\mathscr{H}_C$ corresponds to a tridiagonal matrix of dimension $\lfloor \frac{C}{2} \rfloor$ given by

$$\mathscr{H}_C \equiv \begin{bmatrix} 0 & b_0 & 0 & \dots & 0 \\ b_0 & 0 & b_1 & & \vdots \\ 0 & b_1 & 0 & \ddots & 0 \\ \vdots & & \ddots & \ddots & b_{\lfloor \frac{C}{2} \rfloor} \\ 0 & \dots & 0 & b_{\lfloor \frac{C}{2} \rfloor} & 0 \end{bmatrix}. \tag{3.21}$$

where $b_m = \sqrt{(m+1)(C_2 m)(C-2m-1)}$. To illustrate the idea behind the diagonalization procedure, consider the case $C = 2$. The class for $C = 2$ is given by states of the form $|\psi\rangle = c_0|2,0\rangle + c_1|0,1\rangle$, and the eigenvalue problem becomes

$$\begin{bmatrix} 0 & \sqrt{2} \\ \sqrt{2} & 0 \end{bmatrix} \begin{bmatrix} c_0 \\ c_1 \end{bmatrix} = \frac{E-2\omega}{g} \begin{bmatrix} c_0 \\ c_1 \end{bmatrix}. \tag{3.22}$$

The spectrum for $C = 2$ is then $E = 2\omega \pm \sqrt{2}g$. The procedure is identical for higher C, and the spectrum can be obtained in this manner up to $C = 17$. Beyond $C = 17$, no analytical expressions for the energies or the eigenstates could be found. These energy levels are shown in Fig. 3.3, and the precise values for the energy can be found in [122]. Tridiagonal matrices like the one in Eq.(3.21) have been linked to the theory of finite orthogonal polynomials [121], and the eigenvalue problem of Eq.(3.20) can be expressed in terms of polynomial equations using the Bargmann representation, but no further progress was accomplished.

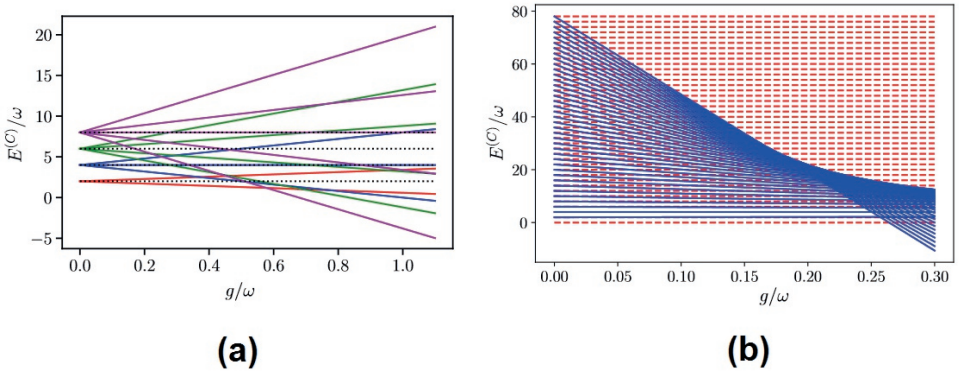

Figure 3.3: **(a)** Energy spectrum as a function of g for the even lower C's (red C=2; blue C=4; green C=6; purple C=8). Odd C's have the same behaviour but are shifted upwards by ω; **(b)** Lowest energy of each class C as a function of g (determined numerically). The observed tendency is that the absolute value of the slope increases with C, suggesting that higher C have lower energy states.

As seen from Fig. 3.3, the aperture of the energy levels increases with C, and as the coupling increases, level crossings occur and the lowest energy level is no longer the vacuum, but a state containing C excitations. Numerical determination of the spectrum for

higher C's suggests that for each C, the energy levels are symmetric in respect to $E-\omega C$, and that the maximum slope of the energy levels with g increases with C. This seems to imply that for any non-null g and for any given energy level, there exists always another level with a lower energy. If that is the case, then the system does not have a ground state. The inclusion of the counter-rotating terms of Eq.(1.19) only aggravates this behaviour [122]. If the system does not have a ground state, several important questions arise, namely, without a ground state, the partition function as normally defined in statistical physics diverges. Thus, to what kind of distributions does the system thermalize into?

The interest in the exact solution laid on enlightening the properties of the system. It is clear that even for low coupling values, the vacuum is not the ground state of the system, and so this electromechanical system, by the simple fact that it exists, and even if there are no initial mechanical and electric excitations, will host electrical currents and mechanical vibrations created spontaneously from the vacuum. Such vacuum instabilities and superradiative transitions are already known in cavity QED, but contrary to cavity QED, there is no clear mechanism preventing this vacuum instability for electromechanics. A possible natural prevention mechanism for the associated divergences is the limit when the displacement is such that the capacitor plates touch each other.

Is this vacuum instability a quantum effect? No. The complete energy of the system in terms of the fields is (see Eq.(1.19))

$$\mathscr{F} = \frac{1}{2}\frac{V_{ind}}{\mu N^2}B^2 + \frac{1}{2}\epsilon S(d_0+x)E^2 + \frac{p^2}{2m} + \frac{1}{2}m\Omega^2 x^2\,, \tag{3.23}$$

and using $X = x + \frac{\epsilon S E^2}{2m\Omega^2}$, the energy can be written as

$$\mathscr{F} = \frac{1}{2}\frac{V_{ind}}{\mu N^2}B^2 + \frac{p^2}{2m} + \frac{1}{2}m\Omega^2 X^2 + \frac{1}{2}\epsilon S d_0 E^2 - \frac{\epsilon^2 S^2}{8m\Omega^2}E^4\,. \tag{3.24}$$

From the last terms, it is clear that the free energy of the (classical) system has the shape of an inverted E^4 potential, and the energy has its minimum at $E\to\infty$. But in a classical system, for certain parameters and initial conditions, the system can be trapped inside the inverted double well potential and be stable as long as there are no fluctuations perturbing the system's stability. The difference for the quantum case is that, due to quantum fluctuations, the system can always tunnel through the double well, and the false vacuum would inevitably meet its fate.

3.2.2. DYNAMICAL CASIMIR EFFECT IN ELECTROMECHANICS [3]

The main feature of the parametric amplifier interaction is that it is able to exchange excitations between systems with very distinct natures. In comparison to the parametric down-conversion process in quantum optics, this interaction in the context of electromechanics describes the conversion of a mechanical phonon (the harmonic mode) created by the pump to two microwave photons (the subharmonic mode). Thus, if the mechanical resonator is driven, the motion of the capacitor plate induces a current in

[3] The content of this subsection is based on the published work [123].

the LC circuit. In order to maximize this effect, the mechanical motion should be driven at its resonant frequency. Including the resonant mechanical driving, the Hamiltonian becomes

$$H = \omega a^\dagger a + 2\omega b^\dagger b - g\left(a^\dagger a^\dagger b - b^\dagger aa\right) + \mathscr{E}\left(b^\dagger e^{-2i\omega t} + be^{2i\omega t}\right), \tag{3.25}$$

where $\mathscr{E}$ is the driving amplitude. The explicit time dependence of the Hamiltonian can be swept away by transforming to the rotating frame with $U = \exp[-2i\omega t(a^\dagger a + 2b^\dagger b)]$, and rotating the b-field by $-\pi/2$, making the Hamiltonian (3.25)

$$H = ig\left(a^\dagger a^\dagger b - aab^\dagger\right) + i\mathscr{E}\left(b^\dagger - b\right), \tag{3.26}$$

With this rotation, the deterministic parts of the resulting equations of motion are real. Taking dissipation into account, the quantum Langevin equations (QLEs) for the Hamiltonian (3.26) are

$$\begin{aligned} \partial_t a &= -\frac{\kappa}{2}a + 2ga^\dagger b + i\eta_A, \\ \partial_t b &= -\frac{\Gamma}{2}b - ga^2 + \mathscr{E} + i\eta_B, \end{aligned} \tag{3.27}$$

where κ (Γ) is the LC (mechanical) decay rate and $\{\eta_i\}$ are stochastic Gaussian noise operators. The nonlinear operator character of Eqs. (3.27) hinders the search for an exact solution, so in order to understand the basic properties of the system, let us start by finding the noiseless steady-state solutions to the QLEs (3.27). These are

$$(\alpha,\beta)_{\rm ss} = \left(0, \frac{2\mathscr{E}}{\Gamma}\right) \quad \text{and} \quad (\alpha,\beta)_{\rm ss} = \left(\pm\sqrt{\frac{\mathscr{E}-\mathscr{E}_c}{g}}, \frac{\kappa}{4g}\right), \tag{3.28}$$

where $\mathscr{E}_c = \frac{\kappa\Gamma}{8g}$ is the critical driving. As the second solution above only exists when $\mathscr{E} > \mathscr{E}_c$, an above-threshold and a below-threshold phase can be defined. For an electromechanical system, this transition takes place when the phonon number created by the mechanical driving reaches the value $(8g/\kappa)^{-2}$, which requires at least $\sim 10^4$ pump phonons for current devices [50]. Below threshold, the LC field amplitude is constantly null, whereas the mechanical amplitude increases linearly with the driving. Above threshold, the mechanical amplitude saturates (a phenomenon known as pump depletion [84, 124]) and all energy pumped into the system is transfered to the LC circuit. One could then proceed with a simple linearization around the stationary points, but because of the phase transition character, this yields diverging results at the threshold $\mathscr{E}_c$ [122]. A way to overcome this problem is the use of a self-consistent linearization [126].

To do this, it is more convenient to express the QLEs (3.27) in terms of the scaled variables $\tau = \frac{1}{2}\Gamma t$, $\epsilon = \mathscr{E}/\mathscr{E}_c$, $\gamma = \Gamma/\kappa$, $\mu = 4g/\kappa$, $\tilde{a} = \sqrt{2\mathscr{C}}a$, $\tilde{b} = \mu b$, $\eta_A = \sqrt{\kappa}\xi_A$ and $\eta_B = \sqrt{\Gamma}\xi_B$, as well as the single photon cooperativity $\mathscr{C} = \frac{4g^2}{\kappa\Gamma}$. With this scaling, the critical point is fixed at $\epsilon_c = 1$, thus facilitating the comparison of solutions with different parameters, and the evaluation of the stochastic fluctuations in the diabatic regime ($\Gamma \ll \kappa$). In terms of the scaled variables, the QLEs (3.27) are

$$\begin{aligned} \gamma\partial_\tau \tilde{a} &= -\tilde{a} + \tilde{a}^\dagger\tilde{b} + 2i\sqrt{\mathscr{C}}\,\xi_A(\tau/\gamma), \\ \partial_\tau \tilde{b} &= -\tilde{b} - \tilde{a}^2 + \epsilon + i\sqrt{2}\mu\,\xi_B(\tau), \end{aligned} \tag{3.29}$$

and where $\langle \xi_i(t)\xi_i^\dagger(t')\rangle = (\bar{n}_i+1)\delta(t-t')$. Here and onwards, it is considered that there are no thermal fluctuations affecting the LC ($\bar{n}_A = 0$).

In the usual quantum optical case of a fast-decaying pump mode, the system dynamics is typically solved through adiabatic elimination of the pump mode [124, 127]. However, in electromechanics, the pump mode (the mechanical mode) decays much slower than the subharmonic mode (LC), making adiabatic elimination impossible. This regime is known as the diabatic regime $\gamma \ll 1$, and for microwave resonators, γ is rather low ($\gamma \sim 10^{-4}$ in [125]). Here, it is considered the diabatic limit $\gamma \to 0$. In terms of the scaled variables, the diabatic limit is $\gamma = \frac{\mu^2}{4\mathscr{C}} \to 0$, implying the limit $\mu \to 0$ (the highest μ for microwave resonators is $\sim 10^{-3}$ and $\mathscr{C} > 1$ was not yet obtained [50]).

Although adiabatic elimination is not valid in this regime, it is still possible to eliminate the mechanical mode by considering the steady-state case. In this limit, the mechanical noise contribution ξ_B is negligible for thermal phonon numbers $\bar{n}_B \ll \mu^{-2}$ (which is the case for MHz resonators at mK temperatures). The second noise contribution to the dynamics of the mechanical mode $\tilde{b}$ comes from the fluctuations of the coupling term: $\tilde{a}\tilde{a} - \langle \tilde{a}\tilde{a}\rangle$. These fluctuations are proportional to the quantum noise introduced by ξ_A and scale with $\langle \xi_A \xi_A^\dagger\rangle = \gamma\delta(\tau-\tau')$. Thus, in the diabatic limit, these fluctuations vanish as well.

Writing $b = \tilde{\beta}_{ss} + \delta b$ and keeping only terms linear in the operators leads to

$$\gamma\partial_\tau \tilde{a} = -\tilde{a} + \tilde{\beta}_{\rm ss}\tilde{a}^\dagger + 2i\sqrt{\mathscr{C}}\xi_A, \tag{3.30}$$

with $\tilde{\beta}_{\rm ss} = \epsilon - \tilde{\alpha}_{\rm ss}^2$, and where $\tilde{\alpha}_{\rm ss}$ must be determined self-consistently. Solving Eq.(3.30), one finds

$$\langle \tilde{a}^\dagger\tilde{a}\rangle_{\rm ss} = \tilde{\beta}_{\rm ss}\langle \tilde{a}^2\rangle_{\rm ss} = \frac{\tilde{\beta}_{\rm ss}^2}{(1-\tilde{\beta}_{\rm ss}^2)}\mathscr{C}, \tag{3.31}$$

where $\tilde{\beta}_{\rm ss}$ is determined by the self-consistency relation

$$\tilde{\beta}_{\rm ss} = \epsilon - \frac{\tilde{\beta}_{\rm ss}}{(1-\tilde{\beta}_{\rm ss}^2)}\mathscr{C}. \tag{3.32}$$

The solution to Eq. (3.32) is

$$\begin{aligned}\beta_{ss} = \frac{\epsilon}{3} &- \frac{\left(1-i\sqrt{3}\right)\left(\epsilon^2+3(\mathscr{C}+1)\right)}{6\sqrt[3]{\epsilon(\epsilon^2+\frac{9}{2}(\mathscr{C}-2)) + i\sqrt{\left(\epsilon^2+3(\mathscr{C}+1)\right)^3 - \epsilon^2\left(\epsilon^2+\frac{9}{2}(\mathscr{C}-2)\right)^2}}} \\ &- \frac{\left(1+i\sqrt{3}\right)}{6}\sqrt[3]{\epsilon(\epsilon^2+\frac{9}{2}(\mathscr{C}-2)) + i\sqrt{\left(\epsilon^2+3(\mathscr{C}+1)\right)^3 - \epsilon^2\left(\epsilon^2+\frac{9}{2}(\mathscr{C}-2)\right)^2}}.\end{aligned} \tag{3.33}$$

Plugging Eq.(3.33) in Eq. (3.31), the self-consistent photon number is obtained. Fig. 3.4 shows the scaled mechanical amplitude $\tilde{\beta}_{\rm ss}$ and scaled mean photon number $\langle \tilde{a}^\dagger\tilde{a}\rangle$ as a function of ϵ. It is seen that when $\mathscr{C} \to 0$, the self-consistent result tends towards the noiseless classical solution. This happens because the fluctuations introduced by the noise operator are suppressed, as seen from Eq. (3.30). For higher $\mathscr{C}$, the quantum LC

noise starts to play a significant role, and the self-consistent result deviates significantly from the classical prediction near ϵ_c. The most important difference from the noiseless classical picture is that microwave photons are still created below threshold due to zero-point fluctuations.

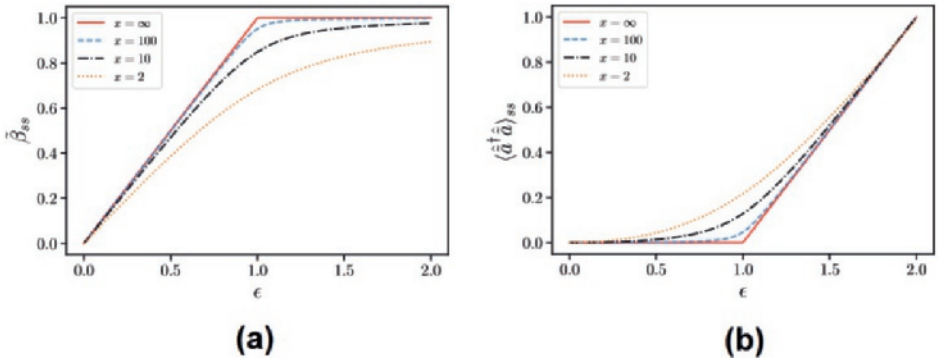

Figure 3.4: Scaled steady-state mechanical amplitude **(a)** and photon number **(b)** as function of driving. For lower $x = \mathscr{C}^{-1}$, the system exhibits a smoother transition near the threshold. When $\mathscr{C} \to 0$, the noiseless classical result is obtained.

Although the self-consistent linearization gives reasonable analytical results, its predictions differ qualitatively from our numerical results when both decay modes have roughly the same timescale. In order to obtain better results, a Focker-Planck (FP) equation in the complex P-representation [128] is employed. The complex P-representation is related to the density matrix by

$$\rho = \int_{\mathfrak{C},\mathfrak{C}'} e^{\frac{1}{2}|\alpha_1-\alpha_2^*|^2+2iIm\{\alpha_1,\alpha_2\}} P(\alpha_1,\alpha_2)|\alpha_1\rangle\langle\alpha_2^*|d\alpha_1 d\alpha_2\,, \tag{3.34}$$

where $\mathfrak{C},\mathfrak{C}'$ are contours in the complex plane. The coupling to the environment is carried out by the inclusion of the Lindblad super-operators in the master equation, and going from the Lindblad equation to a FP equation is a standard procedure in quantum open systems [84, 124], resulting in

$$\begin{aligned}\partial_t P(\Theta,t) = &\left\{\partial_{\alpha_1}\left[\frac{\kappa}{2}\alpha_1 - 2g\beta_1\alpha_2\right] + \partial_{\alpha_2}\left[\frac{\kappa}{2}\alpha_2 - 2g\beta_2\alpha_1\right] + \partial_{\beta_1}\left[\frac{\Gamma}{2}\beta_1 + g\alpha_1^2 + \mathscr{E}\right]\right.\\ &\left.+\partial_{\beta_2}\left[\frac{\Gamma}{2}\beta_2 + g\alpha_2^2 + \mathscr{E}\right] + g\left[\partial_{\alpha_1}^2\beta_1 + \partial_{\alpha_2}^2\beta_2\right] + \Gamma\bar{n}_B\partial_{\beta_1}\partial_{\beta_2}\right\}P(\Theta,t)\,,\end{aligned} \tag{3.35}$$

where $\Theta = (\alpha_1,\alpha_2,\beta_1,\beta_2)$. Using the same scaled variables as before, the FP equation becomes

$$\begin{aligned}\partial_\tau P(\tilde{\Theta},\tau) = &\left\{\frac{1}{\gamma}\partial_{\tilde{\alpha}_1}\left[\tilde{\alpha}_1 - \tilde{\beta}_1\tilde{\alpha}_2\right] + \frac{1}{\gamma}\partial_{\tilde{\alpha}_2}\left[\tilde{\alpha}_2 - \tilde{\beta}_2\tilde{\alpha}_1\right] + \partial_{\tilde{\beta}_1}\left[\tilde{\beta}_1 + \tilde{\alpha}_1^2 + \epsilon\right]\right.\\ &\left.+\partial_{\tilde{\beta}_2}\left[\tilde{\beta}_2 + \tilde{\alpha}_2^2 + \epsilon\right] + \frac{\mathscr{C}}{\gamma}\left[\partial_{\tilde{\alpha}_1}^2\tilde{\beta}_1 + \partial_{\tilde{\alpha}_2}^2\tilde{\beta}_2\right] + 2\mu^2\bar{n}_B\partial_{\tilde{\beta}_1}\partial_{\tilde{\beta}_2}\right\}P(\tilde{\Theta},\tau)\,.\end{aligned} \tag{3.36}$$

Eq.(3.36) is not easily solvable, and in order to make progress it must be brought to a simpler form. As before, the mechanical mode can be eliminated in the steady-state and the thermal noise of the mechanical oscillator can be disregarded. The validity of this approach can be seen from the stochastic differential equations (SDEs) corresponding to Eq. (3.36). Using the Itô rules, these are found to be [127]:

$$\gamma\partial_\tau \begin{bmatrix}\tilde{\alpha}_1\\ \tilde{\alpha}_2\end{bmatrix} = \begin{bmatrix}\tilde{\alpha}_2\tilde{\beta}_1 - \tilde{\alpha}_1\\ \tilde{\alpha}_1\tilde{\beta}_2 - \tilde{\alpha}_2\end{bmatrix} + \begin{bmatrix}\mathscr{C}\tilde{\beta}_1 & 0\\ 0 & \mathscr{C}\tilde{\beta}_2\end{bmatrix}^{\frac{1}{2}} \begin{bmatrix}\zeta_{A_1}\\ \zeta_{A_2}\end{bmatrix}, \tag{3.37}$$

$$\partial_\tau \begin{bmatrix}\tilde{\beta}_1\\ \tilde{\beta}_2\end{bmatrix} = \begin{bmatrix}\epsilon - \tilde{\alpha}_1^2 - \tilde{\beta}_1\\ \epsilon - \tilde{\alpha}_2^2 - \tilde{\beta}_2\end{bmatrix} + \begin{bmatrix}0 & 2\mu^2\bar{n}_B\\ 2\mu^2\bar{n}_B & 0\end{bmatrix}^{\frac{1}{2}} \begin{bmatrix}\zeta_{B_1}\\ \zeta_{B_2}\end{bmatrix}, \tag{3.38}$$

where $\langle\zeta_j\rangle = 0$ and $\langle\zeta_{i_1}\zeta_{i_2}\rangle = \delta(t-t')$. In the steady-state situation, the left-hand side of Eq.(3.38) is null, and for low phonon thermal occupations ($\bar{n}_B \ll \mu^{-2}$), the mechanical fluctuations can be disregarded, leading to the steady-state solution $\tilde{\beta}_{\mathrm{ss},i} = \epsilon - \tilde{\alpha}^2_{\mathrm{ss},i}$. Substituting $\tilde{\beta}_{\mathrm{ss},i}$ in Eq. (3.37) leads to a nonlinear stochastic equation for the microwave field. The steady-state of the new FP equation associated with Eq. (3.37) is

$$0 = \left\{\partial_{\tilde{\alpha}_1}\left[\tilde{\alpha}_1 - \left(\epsilon - \tilde{\alpha}_1^2\right)\tilde{\alpha}_2\right] + \partial_{\tilde{\alpha}_2}\left[\tilde{\alpha}_2 - \left(\epsilon - \tilde{\alpha}_2^2\right)\tilde{\alpha}_1\right] + \mathscr{C}\left[\partial^2_{\tilde{\alpha}_1}\left(\epsilon - \tilde{\alpha}_1^2\right) + \partial^2_{\tilde{\alpha}_2}\left(\epsilon - \tilde{\alpha}_2^2\right)\right]\right\} P_{\mathrm{ss}}(\tilde{\alpha}_1, \tilde{\alpha}_2). \tag{3.39}$$

Eq. (3.39) is equivalent to the one in [124, 127], (albeit it is derived in the adiabatic regime), and the solution is readily found to be

$$P_{\mathrm{ss}} = \mathscr{N}\left[\left(\epsilon - \tilde{\alpha}_1^2\right)\left(\epsilon - \tilde{\alpha}_2^2\right)\right]^{\frac{1}{2\mathscr{C}}-1} exp\left(\frac{\tilde{\alpha}_1\tilde{\alpha}_2}{\mathscr{C}}\right), \tag{3.40}$$

where $\mathscr{N}$ is a normalization constant. The photonic moments are defined as [128]

$$\langle\tilde{a}^{\dagger n}\tilde{a}^m\rangle = \int_{\mathscr{C}}\int_{\mathscr{C}'} d\tilde{\alpha}_1 d\tilde{\alpha}_2 \tilde{\alpha}_2^n \tilde{\alpha}_1^m P(\tilde{\alpha}_1, \tilde{\alpha}_2), \tag{3.41}$$

and with Eq.(3.40), they are found to be:

$$\langle\tilde{a}^{\dagger n}\tilde{a}^m\rangle_{\mathrm{ss}} = \mathscr{N}' \sum_{k=0}^{\infty} \frac{\epsilon^{\frac{m+n}{2}}}{k!}\left(\frac{\epsilon}{\mathscr{C}}\right)^k {}_2F_1\left(-(k+m), \frac{1}{2}\mathscr{C}^{-1}, \mathscr{C}^{-1}, 2\right) {}_2F_1\left(-(k+n), \frac{1}{2}\mathscr{C}^{-1}, \mathscr{C}^{-1}, 2\right), \tag{3.42}$$

where ${}_2F_1(u, v, w, z)$ is the hypergeometric function and $\mathscr{N}'$ a normalization constant. It is also possible to obtain an analytical expression for the steady-state mechanical amplitude as it is defined in terms of the second order moment $\langle a^2\rangle_{\mathrm{ss}}$. Fig. 3.5 shows the steady-state photon number as function of driving for the FP approach. The FP approach predicts an "undershooting" of the semiclassical prediction just above threshold, which becomes more pronounced as $\mathscr{C}$ increases; that is, when the coupling is large with respect to the dissipation rates. For $\mathscr{C} = 0.01$, the FP approach tends towards the noiseless classical prediction as the fluctuations of the mechanical and LC oscillator become

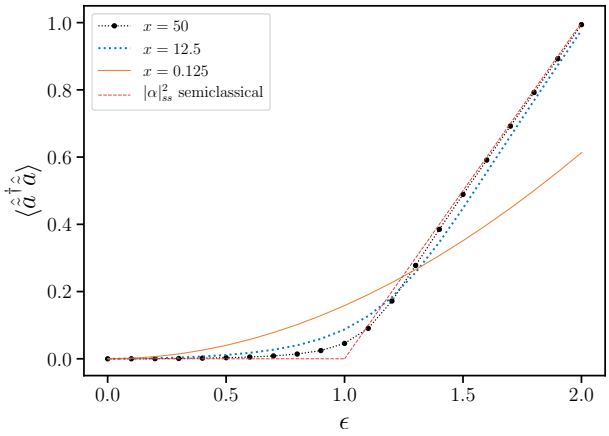

Figure 3.5: Steady-state scaled photon number as a function of driving for different values of $x = \mathscr{C}^{-1}$. For $x = 50$, the FP approach tends towards the semiclassical prediction as the fluctuations of the mechanical oscillator become small. For $x = 12.5$, the photon number "undershoots" the semiclassical prediction just above threshold. This behaviour is not predicted in the linearized approach. For $x = 0.125$, the quantum fluctuations introduced by ξ_A lead to a more pronounced undershooting.

negligible. For $\mathscr{C} = 0.04$, the undershooting is visible but it remains small. In contrast, for $\mathscr{C} = 4$, the quantum fluctuations are relatively large, and the undershooting is quite pronounced.

To check the performance of the FP approach outside the adiabatic regime, the FP results are compared to the results of numeric simulations. These simulations are done for $\kappa = \Gamma = 1$, $g = 0.1$ (where the system is still tractable numerically) and using QuTiP [129]. To obtain precise results for a given observable, the dimension of the matrix representing the operator should be significantly bigger than the expected outcome of the observable's value. Constructing a Fock-state basis containing $2N$ photons and N phonons requires all matrices to have size $2N^2 \times 2N^2$. We found that taking N=23 provides reasonable precision while avoiding memory issues. However, for higher values of driving, this dimension is not sufficient. In these cases, we used Shanks-extrapolation with as input the results of $N = 15, \ldots, 23$ to improve the results. The chosen region of parameter space lies neither in the adiabatic nor in the diabatic regime, so that the FP approach can be regarded at best as a linearization. However, as $\mathscr{C} = 0.04$ and $\mu = 0.4$, the noise contributions are expected to be negligible, and this linearization should be a reasonable approximation in the steady-state.

Fig. 3.6 shows the scaled steady-state mechanical amplitude and photon number obtained via different methods. The numerical result is shown in dotted-blue. The dashed-red line represents the semiclassical (mean-field) solution to the steady-state QLEs (3.27). The numerical behaviour of the system coincides roughly with the semiclassical result but it deviates from it around the threshold. The self-consistent linearization is shown in solid-orange, and it coincides with the semiclassical result for high and low driving power but connects these limits smoothly (in contrast with the semiclassical

result). However, it does not predict an overshooting of the mechanical amplitude (undershooting of the photon number) in comparison to the numerical predictions. The FP approach (dotted-black) does predict this undershooting and it is qualitatively similar to the numeric result. Upon close inspection, it is seen that the numerical results reach the semiclassical result for higher $\mathscr{E}$ somewhat faster than the FP result. This small discrepancy can have two origins. Firstly, the numerical simulations become less precise for higher values of the driving. Secondly, in the $\kappa = \Gamma$ regime, the FP method gives a linearized approximation of the true steady-state observables implying that the discrepancy could originate in the shortcomings of the analytical method.

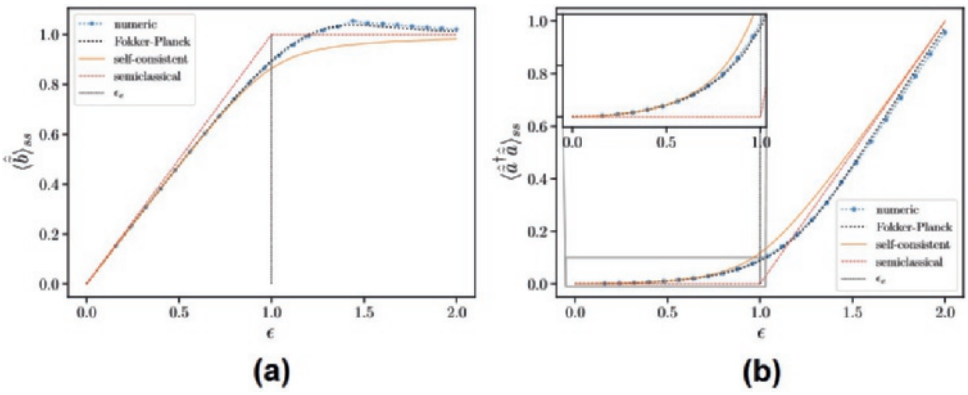

Figure 3.6: **(a)** Scaled mechanical amplitude as function of the normalized driving. Numerical simulations predict that the amplitude overshoots the self-consistent prediction in the intermediate driving regime;**(b)** Scaled photon number as function of the normalized driving. The FP approach matches the numerics rather well.

Fig. 3.7 shows the steady-state fluctuations of the photonic quadratures $X = a^\dagger + a$ and $Y = i(a^\dagger - a)$ for the different methods. The fluctuations for the $\tilde{X}$-quadrature display a behaviour qualitatively similar to the photon number. On the other hand, the fluctuations for the Y-quadrature drop below 1 for nonzero driving, indicating that the photonic state is squeezed. Above threshold, a clear discrepancy between the FP result and the self-consistent result can be seen. This discrepancy has been reported before [130], but has not yet been explained. The numerical result does not coincide with either one. The cause may be the issues discussed above. We could not check if the FP method provides accurate analytical results in the diabatic limit for the steady-state moments.

As a final note, the evolution of the stationary state of the system as a function of driving is numerically simulated, and as shown in Fig. 3.8, the Q function for the cavity goes from a Gaussian (squeezed) state below threshold into a mixture of coherent states above threshold.

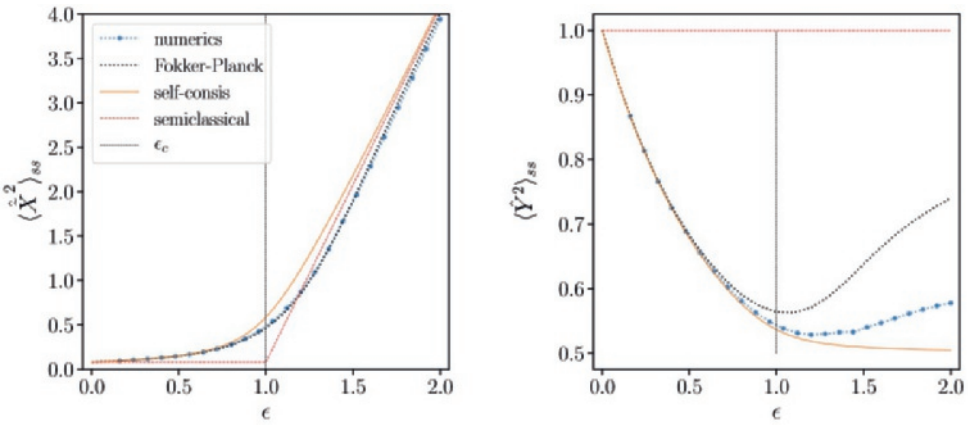

Figure 3.7: Steady-state fluctuations of the scaled photonic $\tilde{X}$- and unscaled Y-quadrature as a function of driving. The behaviour of $\langle \tilde{X}^2 \rangle$ is qualitatively similar to that of the photon number. For the Y-quadrature, the fluctuations decrease below Y^2_{ZPF} with driving, indicating the presence of squeezing. A yet unexplained discrepancy is observed between the numerical data, the self-consistent and the FP approaches.

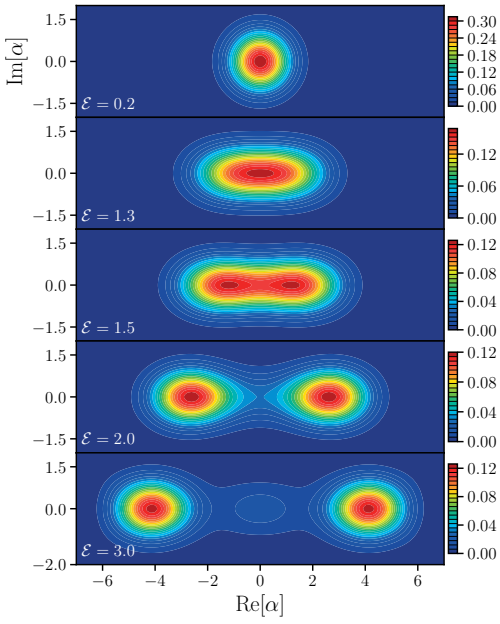

Figure 3.8: Q-function of the LC steady-state for different values of driving. For well-resolved density maxima, as for $\mathcal{E} = 3.0$, the centers of the maxima lie at the branches of the square root defined in Eq. 3.28.

3.3. CREATION AND INTERFERENCE OF MECHANICAL SUPERPOSITIONS [4]

Being able to control the quantum state of a macroscopic object, namely a mechanical resonator, is a current topic of interest because it supplies a tool to investigate fundamental questions in quantum mechanics. Besides testing quantum mechanics beyond atomic scales, another reason behind it is the hope that such massive superposition states suffer some form of collapse [131], particularly gravitationally-induced collapse [132]. If that is to be the case, these states would allow to test the foundations and limits of quantum mechanics, along with proposed extensions, namely the so called "collapse models".

To create such a superposition state, or any quantum state for the matter, the macroscopic object must to be coupled to a quantum element, whose properties can be controlled at will. A natural choice for the quantum element is a qubit, since its state can be fully manipulated through driving pulses. Several proposals for creating macroscopic superpositions by coupling mechanical resonators to qubits have been advanced [133–135], and a promising choice is to use NV centres in diamond as the qubit due to their long coherence times (a T_1 of ~ 5min was achieved in [136]).

The explicit form of the interaction depends on the geometry of the system, and different couplings lead to different ways of manipulating the mechanical state. Here, two forms of coupling are analyzed and compared. The first form of interaction considered is when the spin axis and the cantilever displacement are aligned. This coupling leads to a force acting on the resonator that is dependent of the spin state (i.e. proportional to σ^z). Therefore, if the spin is prepared in a superposition state, the coupling ensures that the cantilever evolves into a superposition. The second interaction considered is the case where the cantilever is aligned with the NV spin, but the motion is perpendicular to the axis. Due to the reflection symmetry, the coupling strength is approximately quadratic for small displacements. This interaction can be viewed as a spin-dependent bending potential for the cantilever. Likewise, if the spin is prepared in a superposition state, the cantilever will evolve into a superposition state due to the spin-state dependent mechanical frequency. A scheme illustrating the geometry enabling these forms of interaction is depicted in Fig. 3.9.

3.3.1. CREATION USING A LINEAR COUPLING

The geometry of the spin-cantilever system considered in this section is illustrated in Fig. 3.9. Because the spin axis is parallel to the cantilever motion (i.e. to the displacement of the fundamental bending mode), the coupling strength is proportional to the mechanical displacement and to the spin state (i.e. σ^z) [134]. Therefore, the Hamiltonian considered is

$$\mathcal{H} = \frac{\epsilon}{2}\sigma^z + \Omega b^\dagger b + g\sigma^z(b + b^\dagger), \tag{3.43}$$

where ϵ is qubit frequency, and g the coupling parameter. The reason why this type of interaction is suitable to create mechanical superposition states is simple: $g\sigma^z(b + b^\dagger)$

[4] The work presented in this section is part of a joint project with Oosterkamp Lab.

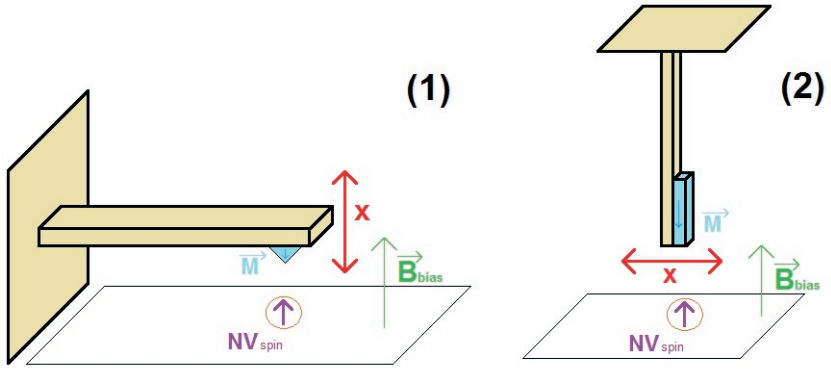

Figure 3.9: Schematics of different geometries for the cantilever+NV spin system. When the spin axis and the cantilever displacement are aligned (panel **(1)**), the force acting on the resonator is proportional to σ^z. If the cantilever is aligned with the NV spin, but the motion is perpendicular to the axis, this symmetry leads to an interaction proportional to x^2 (panel **(2)**).

can be seen as a potential of the type $\hat{F}.\hat{x}$, where $\hat{x} = b + b^\dagger$ is the displacement and $\hat{F}$ is a force. However, $\hat{F}$ is a force dependent on the spin state, and if the spin is in a superposition of $\uparrow$ and $\downarrow$, then the force acting on the cantilever is also a "superposition of forces" acting in opposite directions. Moreover, this Hamiltonian shares a few similarities with the standard optomechanical Hamiltonian, namely the spin plays the role of the photons in cavity optomechanics. This Hamiltonian can be diagonalized via the transformation $U = e^{\frac{g}{\Omega}\sigma^z(b^\dagger - b)}$ leading to the diagonalized Hamiltonian

$$\mathscr{H}_{diag} = U\mathscr{H}U^\dagger = \Omega b^\dagger b + \frac{\epsilon}{2}\sigma^z. \tag{3.44}$$

Note that, in comparison to the standard optomechanical system, there is no additional Kerr-like nonlinearity for the spin because for a spin $^1/_2$, $(\sigma^z)^2 = \mathbb{1}$. Furthermore, the time-evolution operator is given by

$$W(t) = U^\dagger e^{-i\mathscr{H}_{diag}t}U = e^{-i\eta^2\sin(\Omega t)}\mathscr{D}(\eta(e^{-i\Omega t}-1)\sigma^z)e^{-i\left(\frac{\epsilon}{2}\sigma^z + \Omega b^\dagger b\right)t}, \tag{3.45}$$

where $\eta = g/\Omega$ and $\mathscr{D}$ is the displacement (coherent state creator) operator. From Eq.(3.45), it is clear that, apart from a spin phase shift, the dynamics is periodic (with period $\frac{2\pi}{\Omega}$). Though the mechanical state returns to the initial state after a full period, at the middle of a mechanical period the state change caused by the interaction is most prominent, and after a half-period of oscillation,

$$W\left(t = \frac{\pi}{\Omega}\right) = \mathscr{D}(-2\eta\sigma^z)e^{-i\phi\sigma^z}(-1)^{b^\dagger b}, \tag{3.46}$$

with $\mathscr{D}(-2\eta\sigma^z) = e^{-2\eta\sigma^z(b^\dagger - b)}$ and $\phi = \frac{\pi\epsilon}{2\Omega}$. From Eq.(3.46), one can see that if the system starts in the mechanical ground state and in the spin state $\uparrow$ ($\downarrow$), a coherent mechanical state is created at $\beta = -2\eta$ ($\beta = 2\eta$). On the other hand, if the spin starts in a superposition state such that the initial state is $\frac{1}{\sqrt{2}}(|\downarrow\rangle + |\uparrow\rangle) \otimes |0\rangle$, after a half-period the state has

evolved into

$$|\psi\left(t=\frac{\pi}{\Omega}\right)\rangle=\frac{1}{\sqrt{2}}\left(e^{-i\phi}|\uparrow,-2\eta\rangle+e^{i\phi}|\downarrow,2\eta\rangle\right). \tag{3.47}$$

Therefore, this interaction enables the creation of a superposition state whose distance between the superposition branches is $4g/\Omega$. Two problems now arise: first, if the system is allowed to freely evolve in time, it will go back to the initial state and the superposition is lost. Second, the coupling is in general much smaller than the mechanical frequency, which means that the superposition is still within the zero-point uncertainty and it cannot be observed. These problems can be surpassed by applying a $\pi-$pulse on the qubit. Assuming that the duration of a pulse is much shorter than the mechanical period, the pulses can be regarded as instantaneous spin flips. Thus, if a π-pulse is applied and the system evolves for another half-period, the state becomes

$$|\psi^{\pi}\left(t=\frac{2\pi}{\Omega}\right)\rangle=\frac{1}{\sqrt{2}}\left(|\downarrow,4\eta\rangle+|\uparrow,-4\eta\rangle\right), \tag{3.48}$$

where the π upperscript in ψ is solely to mark that a $\pi-$pulse was applied at half-period. It is now clear that applying a π-pulse at the middle of the oscillation period not only prevents the system to go back to the initial state, but also increases the separation of the superposition (which is now 8η). Thus, a possible route to create macroscopic superpositions is to sent a succession of π-pulses at every mechanical half-period. If T_1 is the coherence time, the maximum possible number of π-pulses is $m\sim T_1\Omega/\pi$ and so, the maximal separation between the branches of the superposition is limited to $\approx gT_1$. Note that to create the superposition state, it is not required for the mechanics to start in the ground state. If for example, the initial mechanical state is a coherent state α, the only difference in the final state is that the superposition is now centred around α instead of 0. Additionally, one could also drive the mechanical resonator. Since including a driving term $(S(b^{\dagger}e^{-i\omega_d t}+be^{i\omega_d t}))$ in the Hamiltonian does not break the symmetry (σ^z is still a constant of motion), the diagonalization can be extended to include driving. This amounts to make the transformation

$$U=e^{\left(g\sigma^z+\frac{Se^{-i\omega_d t}}{\Omega+\omega_d}\right)b^{\dagger}-\left(g\sigma^z+\frac{Se^{i\omega_d t}}{\Omega+\omega_d}\right)b}. \tag{3.49}$$

However, driving only contributes to create a mechanical coherent state and to displace the centre of the superposition, and it does not give rise to new effects. Further, if a $\frac{\pi}{2}$-pulse is applied after a half-period, each branch of the superposition is split into two. Thus, different superposition states can be created by applying different pulse sequences.

In order to model the time-evolution in a realistic way, the interaction of the system with its environment must be considered. To account for the dissipative effects of the coupling to a thermal environment, a Fokker-Planck equation shall be employed. Besides the Schrödinger representation, quantum states can also be represented by quasiprobability distributions. Here and onwards, the Wigner functions

$$W_{j,l}(\alpha)=\frac{1}{\pi^2}\int Tr\left(e^{z(b^{\dagger}-\alpha)-z^*(b-\alpha)}\rho_{j,l}\right)d^2z, \tag{3.50}$$

shall be used, where $\rho_{j,l}$ is the full density matrix, (j,l) label the spin density matrix elements $\{\uparrow,\downarrow\}$, and Tr is the trace over both the spin and mechanical degrees of freedom. With the definition in Eq.(3.50) and the Lindblad equation, one can write a partial differential equation representing the quantum state evolution in phase-space, much like in the previous section. The Fokker-Planck equations describing the time-evolution encompassing the coupling to a thermal bath are

$$\begin{aligned}\partial_t W_{\pm,\pm} =& i\Omega(\alpha\partial_\alpha - \alpha^*\partial_{\alpha*})W_{\pm,\pm} \pm ig(\partial_\alpha - \partial_{\alpha*})W_{\pm,\pm} + \frac{\gamma}{2}(\alpha^*\partial_{\alpha^*} + \alpha\partial_\alpha)W_{\pm,\pm} \\ &+ \gamma W_{\pm,\pm} + \gamma(\bar{N}_{th} + {}^1\!/_2)\partial_\alpha\partial_{\alpha^*}W_{\pm,\pm}\,, \end{aligned} \tag{3.51}$$

where $\bar{N}_{th}$ is the thermal bath population, γ is the mechanical dissipation rate ($\gamma = \frac{\Omega}{2\pi Q_m}$, with Q_m the resonator's quality factor), and $\pm$ refers to $\{\uparrow,\downarrow\}$ respectively. Here the effects of spin relaxation were disregarded because the principle of creation of mechanical superpositions rests on the coherence of the spin. Past the T_1 time, the spin will be $\uparrow$ (or $\downarrow$), and the superposition will have vanished. Thus, the whole evolution is considered to take place well within T_1. Furthermore, the dephasing time T_2 only affects $W_{\pm,\mp}$, and unless a different pulse is applied (not a $\pi-$pulse), T_2 does not matter for the evolution of the mechanical superposition. Since the initial state is considered to be a Gaussian state, it is more appropriate to look for Gaussian solutions and determine the time-evolution of the coefficients from Eq.(3.51). The solutions found this way are

$$W_{\pm,\pm}(t) = \frac{\delta_0}{\pi D(t)} exp\left(-\frac{\left|\alpha - \alpha_0 e^{-i\Omega t - \frac{\gamma}{2}t} \pm \frac{g}{\Omega - i^{\gamma}/_2}(1 - e^{-i\Omega t - \frac{\gamma}{2}t})\right|^2}{D(t)}\right), \tag{3.52}$$

where α_0 is the centre of the initial Gaussian state, δ_0 is the initial broadening, and the diffusion coefficient is

$$D(t) = (N_{th} + 1/2)(1 - e^{-\gamma t}) + \delta_0 e^{-\gamma t}\,. \tag{3.53}$$

From this result one can see that dissipation counteracts the effects of the interaction, and so the separation between the superposition branches must now also overcome thermal broadening. Considering the π-pulses to be instantaneous (i.e. the duration is much shorter than all other relevant time-scales of the system), the action of a $\pi-$pulse is to make the swap $W_{\uparrow,\uparrow} \rightarrow W_{\downarrow,\downarrow}$ and $W_{\downarrow,\downarrow} \rightarrow W_{\uparrow,\uparrow}$. If the system starts in the state $\frac{1}{\sqrt{2}}(|\downarrow\rangle + |\uparrow\rangle) \otimes |0\rangle$ and a $\pi-$pulse is applied at the middle of a mechanical period, the quantum state after a mechanical period is

$$W^{\pi}_{\pm,\pm}\left(t = \frac{2\pi}{\Omega}\right) \approx \frac{1}{\pi\left(\frac{1}{2} + \frac{\bar{N}_{th}}{Q_m}\right)} exp\left(-\frac{\left|\alpha \pm 4\eta\left(1 - \frac{1}{4Q_m}(1 - \frac{i}{\pi})\right)\right|^2}{\frac{1}{2} + \frac{\bar{N}_{th}}{Q_m}}\right), \tag{3.54}$$

Comparing this result with Eq.(3.48), it is possible to notice that apart from thermal broadening, the distance between the branches is shortened by $\frac{2\eta}{Q_m}$ because of mechanical damping. Since in general mechanical resonators have huge quality factors, this effect is not very prominent. To create the largest mechanical superposition possible with

this type of coupling, we must apply a $\pi-$pulse every half-period. After n_c resonator cycles with this succession of pulses, the quantum state is

$$W_{\pm,\pm}\left(t=\frac{2\pi n_c}{\Omega}\right)\approx\frac{1}{\pi\left(\frac{1}{2}+\frac{\bar{N}_{th}}{Q_m}n_c\right)}exp\left(\frac{-\left|\alpha\pm 4n_c\eta\left(1-\frac{n_c}{4Q_m}\right)\right|^2}{\frac{1}{2}+\frac{\bar{N}_{th}}{Q_m}n_c}\right), \tag{3.55}$$

Therefore, the conditions for the superposition to be visible (i.e. when the separation is larger then thermal broadening and zero-point uncertainty) are

- $8g>\pi\gamma(\bar{N}_{th}+1)$ (separation rate overcomes thermalization rate) (3.56)
- $\frac{1}{16\eta}-\frac{\bar{N}_{th}}{256\eta^2Q_m}<n_c<4Q_m-\frac{\bar{N}_{th}}{4\eta}$ (interaction overcomes broadening) (3.57)

Using the values reported in [134] (Ω=7MHz, g=115kHz, $Q_m=10^5$, $\bar{N}_{th}\approx 300$), it is possible to create a visible superposition with 9 $\pi-$pulses. Visible here means that the superposition branches have overcome thermal broadening. Nevertheless, the superposition can still be quite small and it might require many more pulses to produce a large superposition. Sending several $\pi-$pulses means putting a large amount of power into the system, which might tamper with the coherence of the qubit. It is then desirable to have an interaction that does not require a large number of pulses to produce a large superposition.

3.3.2. CREATION USING A QUADRATIC COUPLING

Other types of coupling can be implemented by changing the geometry of the system. If the system has a reflection symmetry along the displacement axis of the resonator (see Fig. 3.9), then the coupling between the qubit and the resonator is quadratic in displacement [5], and the Hamiltonian modelling the system is

$$\mathscr{H}=\frac{\epsilon}{2}\sigma^z+\Omega b^\dagger b+\frac{\lambda}{2}\sigma^z(b+b^\dagger)^2, \tag{3.58}$$

where λ stands for the new type of qubit-resonator coupling. Here we have chosen the qubit axis to be perpendicular to the displacement axis. As the coupling is small in comparison to $\{\epsilon,\Omega\}$, it suffices to keep only the resonant interaction terms. With RWA, the Hamiltonian becomes

$$\mathscr{H}=\frac{\epsilon+\lambda}{2}\sigma^z+(\Omega+\lambda\sigma^z)b^\dagger b. \tag{3.59}$$

It is now evident that λ represents the frequency difference between a fast oscillating resonator state and the bare mechanical frequency. Thus, if the spin starts in a superposition state of $|\uparrow\rangle$ and $|\downarrow\rangle$, then the resonator evolves into a superposition of two states oscillating at different frequencies ($\Omega\pm\lambda$). An important consequence of this feature is that it is possible to create large superposition states with small coupling values.

[5] For sufficiently small displacements, such that only the magnetic field curvature plays a role and the tilting of the cantilever does not change the picture.

If the resonator starts in a large coherent state β and the spin in a superposition state $\frac{1}{\sqrt{2}}(|\uparrow\rangle - i|\downarrow\rangle)$, after a time t the system evolves into the state

$$|\psi(t)\rangle = \frac{1}{\sqrt{2}}(e^{-i\frac{\epsilon+\lambda}{2}t}|e^{-i(\Omega+\lambda)t}\beta,\uparrow\rangle - ie^{i\frac{\epsilon+\lambda}{2}t}|e^{-i(\Omega-\lambda)t}\beta,\downarrow\rangle). \tag{3.60}$$

Therefore, by simply letting the coupled system evolve freely in time, it is possible to create a superposition state. Note however that one branch of the superposition is entangled with the $|\uparrow\rangle$ state, whereas the other branch is entangled with the $|\downarrow\rangle$ state. To disentangle this superposition, one has to apply a $\pi/2$ pulse. Furthermore, Eq.(3.59) states that there is no single qubit frequency for the coupled system, but a distinct frequency for each phonon number. What are then the effects of a $\pi/2$ pulse? If we add a driving term $\frac{S}{2}(e^{-i\omega_d t}\sigma^+ + h.c.)$ in Eq.(3.59) and solve the Schrödinger equation, it is possible to see that the coupling between the spin and the resonator causes the mechanical state to change with the applied pulse (but maintaining its statistics). This state change can be avoided if $S \gg 2\lambda|\beta|^2$ which means that the duration of the applied pulse must be much shorter than $T = \frac{\pi}{2\lambda|\beta|^2}$. For $\lambda = 2\pi \times 15mHz$, and an amplitude of the cantilever motion of 10nm (and $x_{ZPM} = 0.2$pm), the state change is avoided if the pulses are much shorter than 5ns. Throughout this analysis, the pulses are considered instantaneous, and the state change negligible.

A constraint produced by this type of coupling is that the maximal separation between branches of the superposition is $2|\beta|$. The time necessary to achieve this separation is $\frac{\pi}{2\lambda}$ (see Eq.(3.60)), and for small coupling values relaxation, thermal broadening, decoherence and dephasing play a role before the maximum separation occurs. Thus, the coupling to the environment must be considered in order to have a realistic picture of the time-evolution. As before, the time-evolution considering the coupling to the environment can be evaluated by solving the Fokker-Planck equations for the Wigner functions representing the quantum state. These are now

$$\begin{aligned}\partial_t W_{\pm,\pm} &= i(\Omega \pm \lambda)(\alpha\partial_\alpha - \alpha^*\partial_{\alpha*})W_{\pm,\pm} + \gamma W_{\pm,\pm} \\ &+ \frac{\gamma}{2}(\alpha^*\partial_{\alpha^*} + \alpha\partial_\alpha)W_{\pm,\pm} + \gamma(\bar{N}_{th} + 1/2)\partial_\alpha\partial_{\alpha^*}W_{\pm,\pm}.\end{aligned} \tag{3.61}$$

$$\begin{aligned}\partial_t W_{\uparrow,\downarrow} &= i\Omega(\alpha\partial_\alpha - \alpha^*\partial_{\alpha*})W_{\uparrow,\downarrow} + \left(\gamma - \frac{1}{T_2} - i\epsilon - 2i\lambda|\alpha|^2\right)W_{\uparrow,\downarrow} \\ &+ \frac{\gamma}{2}(\alpha^*\partial_{\alpha^*} + \alpha\partial_\alpha)W_{\uparrow,\downarrow} + \left(\gamma(\bar{N}_{th} + 1/2) + i\frac{\lambda}{2}\right)\partial_\alpha\partial_{\alpha^*}W_{\uparrow,\downarrow}.\end{aligned} \tag{3.62}$$

If the mechanical resonator starts in a Gaussian state, it is best to look for a solution of the form

$$W_{j,l}(\alpha) = exp\left(c_{j,l}(t) + k_{j,l}(t)\alpha + q_{j,l}(t)\alpha^* + g_{j,l}(t)|\alpha|^2\right). \tag{3.63}$$

Plugging Eq.(3.63) into Eqs.(3.61),(3.62), leads to

$$g_{\pm,\pm}(t) = \frac{g_{\pm,\pm}(0)}{g_{\pm,\pm}(0)\left(\bar{N}_{th} + \frac{1}{2}\right)(e^{-\gamma t} - 1) + e^{-\gamma t}}, \tag{3.64}$$

$$k_{\pm,\pm}(t) = q^*_{\pm,\pm} = \frac{k_{\pm,\pm}(0)e^{(i(\Omega\pm\lambda)-\frac{\gamma}{2})t}}{g_{\pm,\pm}(0)\left(\bar{N}_{th}+\frac{1}{2}\right)(e^{-\gamma t}-1)+e^{-\gamma t}}, \tag{3.65}$$

$$c_{\pm,\pm}(t) = c_{\pm,\pm}(0) - \log\left(g_{\pm,\pm}(0)\left(\bar{N}_{th}+\frac{1}{2}\right)(e^{-\gamma t}-1)+e^{-\gamma t}\right) + \frac{\left(\bar{N}_{th}+\frac{1}{2}\right)k_{\pm,\pm}(0)\,q_{\pm,\pm}(0)(1-e^{-\gamma t})}{g_{\pm,\pm}(0)\left(\bar{N}_{th}+\frac{1}{2}\right)(e^{-\gamma t}-1)+e^{-\gamma t}}, \tag{3.66}$$

$$g_{+,-}(t) = \frac{g_{+,-}(0)(h_+e^{-\xi t}-h_-)+h_+h_-(1-e^{-\xi t})}{g_{+,-}(0)(e^{-\xi t}-1)-h_-e^{-\xi t}+h_+}, \tag{3.67}$$

$$q_{+,-}(t) = \frac{q_{+,-}(0)e^{(-i\Omega-\zeta/2)t}(h_+-h_-)}{g_{+,-}(0)(e^{-\xi t}-1)-h_-e^{-\xi t}+h_+}, \tag{3.68}$$

$$k_{+,-}(t) = \frac{k_{+,-}(0)e^{(i\Omega-\zeta/2)t}(h_+-h_-)}{g_{+,-}(0)(e^{-\xi t}-1)-h_-e^{-\xi t}+h_+}, \tag{3.69}$$

$$c_{+,-}(t) = c_{+,-}(0) + \left(-\frac{1}{T_2} - i\epsilon + i\lambda + \frac{\gamma-\xi}{2}\right)t + \frac{q_{+,-}(0)\,k_{+,-}(0)(1-e^{-\xi t})}{g_{+,-}(0)(e^{-\xi t}-1)-h_-e^{-\xi t}+h_+} + \log\left(\frac{h_+-h_-}{g_{+,-}(0)(e^{-\xi t}-1)-h_-e^{-\xi t}+h_+}\right), \tag{3.70}$$

where

$$h_\pm = \frac{-\gamma\pm\xi}{2\gamma\left(\bar{N}_{th}+\frac{1}{2}\right)+i\lambda}, \quad \text{and} \quad \xi = \sqrt{\gamma^2-4\lambda^2+8i\gamma\lambda\left(\bar{N}_{th}+\frac{1}{2}\right)}. \tag{3.71}$$

It is important to notice from Eq.(3.71) that the qubit-resonator coupling competes with the dissipation for both the effective decay rate and frequency. If the system starts in the state $\frac{1}{\sqrt{2}}(|\uparrow\rangle - i|\downarrow\rangle)\otimes|\beta\rangle$, after n_c resonator cycles and for short time scales ($t \ll \gamma^{-1}$), the Wigner functions that give the position of the mechanical resonator take the form

$$W_{\pm,\pm}\left(t=\frac{2\pi n_c}{\Omega}\right) \approx \frac{1}{\pi\left(\frac{1}{2}+\frac{\bar{N}_{th}}{Q_m}n_c\right)} exp\left(\frac{-\left|\alpha-\beta e^{\pm i\varphi-\frac{n_c}{2Q_m}}\right|^2}{\frac{1}{2}+\frac{\bar{N}_{th}}{Q_m}n_c}\right), \tag{3.72}$$

and $\varphi = 2\pi n_c\frac{\lambda}{\Omega}$. The separation between the superpositions is now given by $\approx 2\varphi|\beta|\left(1-\frac{n_c}{2Q_m}\right)$. Relaxation and thermal broadening affect the superposition created by the quadratic coupling in a similar way to the linear coupling, so comparing the creation of mechanical superpositions amounts to comparing $2g$ to $\pi\lambda|\beta|$. Considering the parameters $Q_m = 10^5$, $\lambda = 2\pi\times 45$mHz, $\Omega = 2\pi\times 3$ kHz, $T_2 = 100$ms, $|\beta| = 10^5$ (this can be obtained if the amplitude of the cantilever motion is 20nm and $x_{ZPM} = 0.2$pm), leads to $\pi\lambda|\beta| \approx 88.9$kHz which is quite close to the value for the linear coupling g presented above. Therefore, this provides a low power alternative to create a mechanical superposition with the same separation.

3.3.3. INTERFERING MECHANICAL SUPERPOSITIONS

Once macroscopic superposition states are created, the toolbox is open. But why are superposition states so important? Modelling the behaviour of an object whose position is unknown and which can be found indistinctively at two different places can already be done at a stochastic level (with the probability density distribution $\mathbb{P} = \frac{1}{2}(\delta(x-x_1)+\delta(x-x_2))$). The difference is that at the quantum level the rule of addition of probability amplitudes leads to interference effects in the probability of finding the resonator at a given place. It is this interference that holds a quantum nature, and not the states themselves. How to produce interference between the superposition states then? Consider the superposition state in Eq.(3.60). If after n_c resonator cycles a $\pi/2$-pulse is applied, after the same time interval $\tau = \frac{2\pi n_c}{\Omega}$, the state becomes

$$|\psi(2\tau)\rangle = \frac{1}{2}\Big(e^{-2i\theta}|\beta e^{-2i\varphi},\uparrow\rangle - i|\beta,\downarrow\rangle - |\beta,\uparrow\rangle - ie^{2i\theta}|\beta e^{2i\varphi},\downarrow\rangle\Big), \tag{3.73}$$

with the phases $\varphi = \frac{2\pi\lambda n_c}{\Omega}$ and $\theta = \frac{\pi\epsilon n_c}{\Omega}$. It is clear that sending a $\pi/2$-pulse allows to split each branch of the superposition into another two. By choosing the duration of the free evolution to be equal, two of the branches merge at the same position in phase-space, and there are now 3 possible positions for the resonator. However they are entangled with different spin states. If the system evolves further in time, the superposition branches would evolve separately, and if the state were measured at $t = 2\tau$, no interference would be visible. Yet, each component of the superposition of the mechanical resonator has a different phase, and it is this phase difference that enables interference between the superpositions of the resonator. Applying another $\pi/2$ pulse and letting the system evolve once more for a time τ, a true which-path experiment is built. The state for the situation described above is

$$|\psi(3\tau)\rangle = \frac{e^{-3i\theta}}{\sqrt{8}}\Big(|\beta e^{-3i\varphi},\uparrow\rangle - ie^{4i\theta}|\beta e^{-i\varphi},\downarrow\rangle - 2e^{2i\theta}|\beta e^{-i\varphi},\uparrow\rangle - e^{4i\theta}|\beta e^{i\varphi},\uparrow\rangle - ie^{6i\theta}|\beta e^{3i\varphi},\downarrow\rangle\Big), \tag{3.74}$$

and a scheme of the protocol to obtain this state is depicted in Fig. (3.10).

This proposal corresponds to a true which-path experiment because the position of mechanical resonator is uncertain (as each superposition branch moves in a different direction in the rotated frame), the possible paths of the resonator take place in real space, and interference between the possible paths enables to distinguish a quantum from a classical scenario. For very large superposition states ($2\varphi|\beta| \gg 1$), the probability of finding the resonator around $(\beta e^{-3i\varphi}, \beta e^{-i\varphi}, \beta e^{i\varphi}, \beta e^{3i\varphi})$ is $\sim (1/8, 5/8, 1/8, 1/8)$ respectively. It is possible to see that in a fully classical system where the spin is prepared with equal probabilities of being $|\uparrow\rangle$ or $|\downarrow\rangle$, the position of the mechanical oscillator would still disperse along the paths but the final probabilities would differ. As there are 3 out of 8 possible paths for the resonator to reach $\beta e^{-i\varphi}$ or $\beta e^{i\varphi}$, a purely stochastic evolution predicts the probability of finding the resonator at $(\beta, \beta e^{i\varphi}, \beta e^{2i\varphi}, \beta e^{3i\varphi})$ to be $(1/8, 3/8, 3/8, 1/8)$. Hence, this difference in the final probabilities allows to distinguish a fully classical stochastic evolution from a quantum one, as shown in Tab. 3.2.

The probability difference arises from the phase difference that each component acquires during the time-evolution, resulting in destructive/constructive interference between the identical components of the superposition created by the $\pi/2$ pulses. It is the

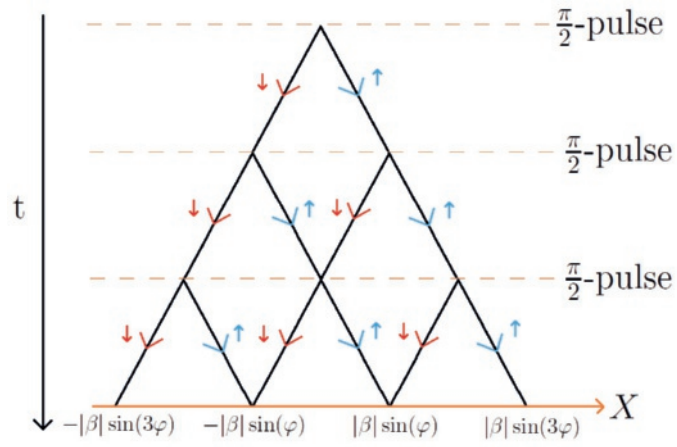

Figure 3.10: Schematics of the experimental proposal. The system starts in the state $\frac{1}{\sqrt{2}}(|\uparrow\rangle - i|\downarrow\rangle)\otimes|\beta\rangle$, and it evolves freely during a time τ leading to a physical separation of the resonator's position. At $t=\tau$, a $\frac{\pi}{2}$ pulse is applied in order to split again each of the superposition's branches, and the system evolves for another τ until a third $\frac{\pi}{2}$ pulse is applied. After a final free evolution of τ, the position of the cantilever is measured. The red (blue) arrows indicate that the mechanical branch is entangled to the spin $\uparrow$ ($\downarrow$) component. Because of the phase difference between the possible paths, the outcome probabilities to find the resonator around $(\beta e^{-3i\varphi},\beta e^{-i\varphi},\beta e^{i\varphi},\beta e^{3i\varphi})$ differ from the probabilities of a purely random process.

Position	$-\lvert\beta\rvert\sin(3\varphi)$	$-\lvert\beta\rvert\sin(\varphi)$	$\lvert\beta\rvert\sin(\varphi)$	$\lvert\beta\rvert\sin(3\varphi)$
Classical	1/8	3/8	3/8	1/8
Quantum	1/8	5/8	1/8	1/8

Table 3.2: Comparison between the fully classical and the quantum outcomes for the measurement of the cantilever's position. A histogram of the cantilever's position measurement outcomes enables to distinguish a classical from a quantum scenario.

accumulated phase difference that creates the asymmetry in the quantum outcome. For a superposition to exist, it is only required that the qubit can be found in both $\uparrow$ and $\downarrow$ states. However, the state $\frac{1}{\sqrt{2}}(|\uparrow\rangle + e^{i\phi}|\downarrow\rangle)$ is different from the statistical mixture $\frac{1}{2}(|\uparrow\rangle\langle\uparrow| + |\downarrow\rangle\langle\downarrow|)$, even though both states lead to a mechanical superposition. It is that difference that leads to the quantum asymmetry due to the interference created by the relative phase ϕ. Though it is possible to create a state with an equal probability of being $\uparrow$ or $\downarrow$ using a $\pi/2$ pulse, it is also possible to create a state with the same property using a $3\pi/2$ pulse. The choice of pulse sequence used leads to a different phase for each path $\left(\text{the } \phi \text{ in the } \frac{1}{\sqrt{2}}(|\uparrow\rangle + e^{i\phi}|\downarrow\rangle)\right)$, which ultimately leads to different outcomes for the position of the cantilever.

Once again, the effect of thermal relaxation and dephasing on the interference of the superpositions must be considered since the the spin-cantilever coupling is weaker than dephasing and mechanical relaxation rate, and thermal noise is quite substantial. The full exact dynamics is cumbersome and does not render the effects of the bath immediately clear. After γ^{-1}, the resonator relaxes, and the superpositions merge and become

broaden by thermal noise. Thus, the regime of interest is the short time scale regime ($\gamma\tau \ll 1$). The limits of a hot thermal bath ($\bar{N}_{th} \gg \max\{1, \gamma\lambda^{-1}\}$), and weak interaction $\lambda \ll \gamma\bar{N}_{th}$ are also considered. With Eqs.(3.63)-(3.71), after n_c resonator cycles ($\tau = \frac{2\pi n_c}{\Omega}$) and for an initial state $\frac{1}{\sqrt{2}}(|\uparrow\rangle - i|\downarrow\rangle)\otimes|\beta\rangle$, the quantum state of system becomes

$$W_{\pm,\pm}(t=\tau) \approx \frac{1}{\pi(2\gamma\bar{N}_{th}\tau+1)} exp\left(\frac{-2|\alpha-\beta e^{\mp i\varphi}|^2}{2\gamma\bar{N}_{th}\tau+1}\right), \tag{3.75}$$

$$W_{\uparrow,\downarrow}(t=\tau) \approx \frac{ie^{-\left(\frac{1}{T_2}+i\epsilon+\frac{\xi}{2}\right)\tau}}{\pi(2\gamma\bar{N}_{th}\tau+1)(1-\frac{\xi\tau}{2})} exp\left(\frac{2e^{-\frac{\xi\tau}{2}}(\beta\alpha^*+\beta^*\alpha)-(1+e^{-\xi\tau})(|\beta|^2+|\alpha|^2)}{2\frac{\gamma\bar{N}_{th}}{\xi}(1-e^{-\xi\tau})+\frac{1}{2}(1+e^{-\xi\tau})}\right), \tag{3.76}$$

where $\varphi = \lambda\tau$. For $\pi/2$-pulses much shorter than the mechanical period and decoherence rate, the effect of a $\pi/2$-pulse is

$$W_{\pm,\pm} \rightarrow \frac{1}{2}(W_{+,+}+W_{-,-}) \mp Im\{W_{\uparrow,\downarrow}\}, \tag{3.77}$$

and

$$W_{\uparrow,\downarrow} \rightarrow Re\{W_{\uparrow,\downarrow}\} + i\left[\frac{1}{2}(W_{+,+}-W_{-,-})\right]. \tag{3.78}$$

To clarify the effects of the bath, let us analyse what happens to the system after applying a $\pi/2$ pulse. The marginal distribution of $W_{\uparrow,\uparrow}(t=\tau^+)$ gives the probability of finding the spin in the $\uparrow$ state and the resonator at a point x in space. Considering $\beta = i|\beta|$, the probability is

$$\mathbb{P}(x, s=\uparrow, t=\tau^+) \approx \frac{1}{\sqrt{8\pi(2\gamma\bar{N}_{th}\tau+1)}}\left(exp\left(\frac{-2(x-|\beta|\sin\varphi)^2}{2\gamma\bar{N}_{th}\tau+1}\right)+exp\left(\frac{-2(x+|\beta|\sin\varphi)^2}{2\gamma\bar{N}_{th}\tau+1}\right)\right)$$
$$-Re\left\{\frac{e^{-\left(\frac{1}{T_2}+i\epsilon+\frac{\xi}{2}\right)\tau}}{\sqrt{\pi(2\gamma\bar{N}_{th}\tau+1)(1-\frac{3\xi\tau}{2})}} exp\left(\frac{-(1+e^{-\xi\tau})^2x^2+(1-e^{-\xi\tau})^2|\beta|^2}{\left(2\frac{\gamma\bar{N}_{th}}{\xi}(1-e^{-\xi\tau})+\frac{1}{2}(1+e^{-\xi\tau})\right)(1+e^{-\xi\tau})}\right)\right\}, \tag{3.79}$$

The first two terms of Eq.(3.79) are Gaussian functions that represent the superposition. They are centred at $\pm|\beta|\sin\varphi$ and broadened by thermal noise by $\gamma\bar{N}_{th}\tau$. The last term is an interference term, which is also affected by dephasing (produced by the spin bath, but also by an additional contribution from the thermal bath: the ξ term). In order for the interference to survive, the experiment must be performed within $\tau^{-1} \gg T_2^{-1} + Re\{\xi\}$. Apart from this temporal restriction, the interference is also suppressed for large coherent states (notice the factor $|\beta|^2$ in Eq.(3.79)), with the amplitude dependent dephasing given by

$$Re\left\{\frac{\left(h(\xi\tau)\right)^2}{2\frac{\gamma\bar{N}_{th}}{\xi}h(\xi\tau)+\frac{1}{2}}\right\}|\beta|^2 \quad \text{, with} \quad h(x) = \frac{1-e^{-x}}{1+e^{-x}}. \tag{3.80}$$

Since the time interval of interest is much shorter than $Re\{\xi\}^{-1}$, $h(x)$ can be expanded for small x and in the limit $\gamma\bar{N}_{th}\tau \gg 1$

$$Re\left\{\frac{\left(h(\xi\tau)\right)^2}{2\frac{\gamma\bar{N}_{th}}{\xi}h(\xi\tau)+\frac{1}{2}}\right\}|\beta|^2 \approx -4\lambda^2|\beta|^2\gamma\bar{N}_{th}\tau^3. \tag{3.81}$$

The separation between the peaks is given by $\lambda\tau|\beta|$ and the thermal broadening of the peaks in this limit is $\sqrt{\gamma\bar{N}_{th}\tau}$. For the superposition to be visible, the separation has to be larger than the broadening, but if that condition is satisfied, the interference vanishes because Eq.(3.81) becomes bigger than one. Therefore, for the interference effects to survive, the experiment must also take place before $(\gamma\bar{N}_{th})^{-1}$. Even for times smaller than $(\gamma\bar{N}_{th})^{-1}$, the interference suppression caused by the coupling to the environment is present. In the limit $\gamma\bar{N}_{th}\tau \ll 1$, this is

$$Re\left\{\frac{h(\xi\tau)^2}{2\frac{\gamma\bar{N}_{th}}{\xi}h(\xi\tau)+\frac{1}{2}}\right\}|\beta|^2 \approx -\frac{16}{3}\lambda^2|\beta|^2\gamma^2\bar{N}_{th}^2\tau^4. \tag{3.82}$$

For the interference to be visible, the above results show the number of oscillation cycles (or the amplitude of motion) allowed between the pulses is limited by 2 parameters: $\varsigma = 2\pi\lambda|\beta|/\Omega$, the separation per cycle in natural units, and $\varrho = \bar{N}_{th}/Q_m$, the thermal broadening per cycle. These limits are

$$\frac{1}{2\varsigma-\varrho} < n_c \ll \max\left\{\varrho^{-1}; \frac{\sqrt[4]{3}}{2\sqrt{\varsigma\varrho}}\right\}. \tag{3.83}$$

The lower limit for n_c comes from the condition that the separation must be larger than the position uncertainty, whereas the upper limit corresponds to the decoherence and interference suppression times. The latter is determined from Eq.(3.82) and corresponds to the point where the interference is suppressed by thermal noise. From the limits above, it is clear that ϱ should be small and ς large. ϱ is naturally small for a cold environment (so that the resonator is close to the ground state), but the mechanical quality factor can be increased to compensate for the rate at which thermal phonons affect the cantilever. It may be worth noticing that increasing the mechanical frequency might be advantageous because for a fixed temperature (and coupling to the environment), Q_m increases while $\bar{N}_{th}$ decreases. On the other hand, increasing the frequency decreases ς, which implies that more cycles are needed to separate the superpositions. Nevertheless, increasing ς can be done by driving the cantilever harder.

Consider the following feasible experimental values: $Q_m = 10^5$, $\lambda = 2\pi \times 45$mHz, $\Omega = 2\pi \times 3$ kHz, T_2 =100ms, $|\beta| = 10^5$ (this value can be obtained if the amplitude of the cantilever motion is 20nm and $x_{ZPM} = 0.2$pm), and let the resonator evolve freely during 5 cycles between each $\pi/2$ pulse. Note that the mechanical resonator may not start in a pure coherent state, but in a Gaussian state with a broadening δ. In the absence of a better choice for the broadening, δ is taken to be the detection uncertainty (≈ 760 phonons). The additional broadening modifies Eq.(3.83) to

$$\frac{4\delta^2}{4\delta\varsigma-\varrho} < n_c < \sqrt[4]{\frac{3}{8}}\sqrt{\frac{\delta}{\varrho\varsigma}}. \tag{3.84}$$

The result of evaluating the probability of finding the resonator at a position X after the described pulse sequence is displayed on Fig. 3.11, for different bath occupancies and for the parameters above. It is seen that the interference between the paths vanishes for hot thermal baths ($\bar{N}_{th}$=7500), leading to the classical prediction. Only for lower temperature baths ($\bar{N}_{th}$=7.5), it is possible to observe a deviation from the classical distribution.

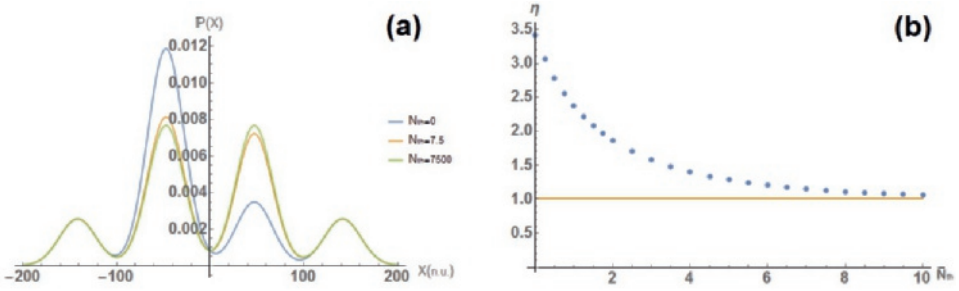

Figure 3.11: **(a)** Probability of finding the cantilever at a position X (in natural units) for several bath temperatures and for $Q_m = 10^5$, $\lambda = 2\pi \times 45$mHz, $\Omega = 2\pi \times 3$ kHz, T_2 =100ms, and $|\beta| = 10^5$, 5 cycles between the $\pi/2$ pulses, and an uncertainty of 760 phonons for the initial mechanical state. At T=0K, the expected 1-5-1-1 distribution appears, whereas at $\bar{N}_{th}$=7500 the 1-3-3-1 distribution prevails. A deviation from the classical 1-3-3-1 distribution can be observed at $\bar{N}_{th}$=7.5, though the difference is rather small; **(b)** Ratio between the probabilities (η, represented by dots) of finding the resonator at $X = -|\beta|\sin\varphi$ and $X = |\beta|\sin\varphi$ as a function of $\bar{N}_{th}$ for the same parameters. The continuous line marks the stochastic situation where no asymmetry exists. Note that at $\bar{N}_{th}$=0, $\eta < 5$ mainly because of residual interference suppression.

Fig. 3.11 also shows how the asymmetric quantum distribution tends to the classical one as the temperature increases. As the asymmetry is only present in the peaks located at $X = -|\beta|\sin\varphi$ and $X = |\beta|\sin\varphi$, and because the probability distribution is a set of Gaussian functions, the ratio η between the peak at $X = -|\beta|\sin\varphi$ and the one at $X = |\beta|\sin\varphi$ suffices to fully quantify the asymmetry. In the ideal case $\{T_2, Q\} \to \infty$, $\eta = 5$ while for the classical situation $\eta = 1$. It is visible from Fig. 3.11 that, for these parameter values, the asymmetry may be too small to be detected if $\bar{N}_{th} > 10$,.

To enhance the asymmetry, the resonator should be relatively closed to the ground state, or alternatively its quality factor should be increased such that the cantilever does not suffer so much with thermal decoherence. As seen in Fig. 3.12, this allows the observation of the asymmetry before the interference suppression settles in. However this increase in the quality factor has to compensate for the absence of further cooling, meaning for the above parameters an increase of 10^3 in the quality factor.

Another possibility mentioned is to increasing the mechanical frequency in order to decrease the broadening rate. For a given temperature, if the mechanical frequency increases, the number of thermal phonons decreases, which is beneficial. The problem with higher mechanical frequencies is that it requires more cycles to get the same degree of separation. One can see from Eq.(3.81), that the interference suppression grows with n_c^4, so it is desirable to have the least number of cycles possible. Thus, for the superposition to be visible while increasing Ω, one must have a better detection resolution. Considering the case of quantum limited sensitivity, and preparing the mechanical res-

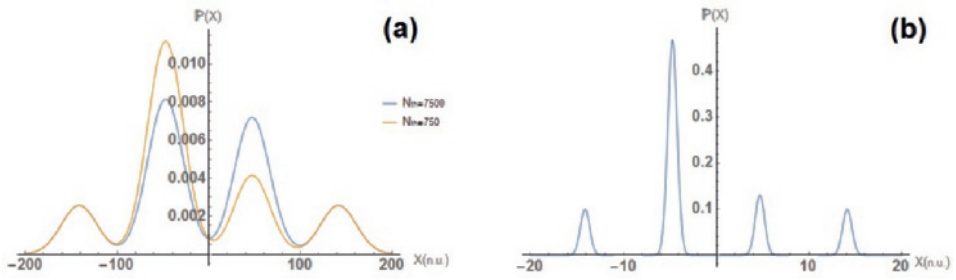

Figure 3.12: Probability of finding the cantilever at a position X (in natural units) for $\lambda = 2\pi \times 45$mHz, T_2 =100ms, and **(a)** $Q_m = 10^8$, $\Omega = 2\pi \times 3$ kHz, and $|\beta| = 10^5$, 5 cycles between the $\pi/2$ pulses, and for several bath temperatures and an uncertainty of 760 phonons for the initial mechanical state. Due to the high quality factor Q, the asymmetry exists even at $\bar{N}_{th} = 7500$. Cooling one order of magnitude leads to a completely resolved asymmetry; **(b)** $Q_m = 10^7$, $\Omega = 2\pi \times 30$ kHz, a pure coherent state with $|\beta| = 5 \times 10^4$, and 10 cycles between the $\pi/2$ pulses. For this higher mechanical frequency, a strong asymmetry is visible for $\bar{N}_{th} = 750$.

onator in a pure coherent state with $|\beta| = 5 \times 10^4$, it is also seen in Fig. 3.12 that after 10 resonator cycles (and for $Q_m = 10^7$ and identical remaining physical parameters), the superposition is fully resolved.

Note that for this type of interference experiment, the quantum behaviour stems from the qubit, and not from the mechanical resonator.

3.4. QUANTUM EFFECTS IN MIM [6]

The Membrane-In-the-Middle (MIM) geometry is a prime example of how symmetry is intertwined with the interaction between light and motion. As discussed in subsection 1.3.4, by placing a membrane at an optical node or anti-node, a quadratic coupling can be achieved. The interest around the quadratic coupling is due to proposals to use this type of interaction to directly observe mechanical quanta [138, 139]. Quadratic couplings have recently been implemented in MIM setups [140–145], ultracold atoms [146] and levitating dielectric particles [147]. Due to the direct dependence on the phonon number, this type of coupling is particularly suited to observe quantum jumps of the phonon number [138, 139], as well as to characterize the phonon statistics by a direct measurement of the cavity spectrum [139]. Other features enabled by this type of coupling are antibunching [148], and squeezing [149–151].

As the quadratic coupling strength is much weaker than the standard radiation pressure coupling, a stronger laser drive is required to enhance the interaction. The strong coupling regime has not yet been achieved for this type of coupling, and the majority of the studied effects for the driven system case rely only on linearized dynamics [152–154], or resonant interactions [138] together with adiabatic elimination [148, 149]. However, for an undriven cavity, an exact diagonalization for this quadratic coupling is possible. This undriven case has many interesting effects such as squeezing [150, 151], collapse and revivals of mechanical motion [150] and state engineering, such as the creation of

[6] The content of this section is based on a project with R. Slooter and it has been submitted for publication. A preprint can be found in [137].

star shaped Wigner function [151] (similar to the states created by the 3-photon down-conversion process).

3.4.1. ISOLATED DYNAMICS

The Hamiltonian modelling this optomechanical system (as discussed in subsection 1.3.4) is

$$\mathscr{H} = \omega_c a^\dagger a + \Omega b^\dagger b + g\Big(a^\dagger a + \frac{1}{2}\Big)(b^\dagger + b)^2 . \tag{3.85}$$

As the interaction preserves the photon number, Eq. (3.85) represents a quadratic form for the phonon operators, whose eigenfrequencies and eigenstates depend on the photon number. Thus, Eq.(3.85) can be diagonalized via a photon number dependent squeezing operator

$$S(\hat{r}(a^\dagger a)) = \sum_{n=0}^{\infty} e^{\frac{1}{2} r(n)((b^\dagger)^2 - b^2)} |n\rangle\langle n| , \tag{3.86}$$

where $|n\rangle$ refers to the photon Fock state. Using the short-hand notation $\hat{\chi} = g(a^\dagger a + \frac{1}{2})$ and choosing $r(n)$ to be real, the action of the squeezing operator defined in Eq.(3.86) on Eq.(3.85) leads to

$$\mathscr{H}_D = \omega_c a^\dagger a + \Big(\Omega \cosh(2\hat{r}) + 2\hat{\chi} e^{2\hat{r}}\Big)\Big(b^\dagger b + \frac{1}{2}\Big) . \tag{3.87}$$

The Hamiltonian in Eq.(3.87) is obtained by imposing that the terms containing bb and $b^\dagger b^\dagger$ vanish, which implies

$$(\Omega + 2\hat{\chi})\sinh(2\hat{r}) + 2\hat{\chi}\cosh(2\hat{r}) = 0 , \tag{3.88}$$

and determines the squeezing parameters to be (cf. [151])

$$r(n) = -\frac{1}{4}\log\left(1 + \frac{4g(n + {}^1\!/_2)}{\Omega}\right) . \tag{3.89}$$

Combining Eqs.(3.87) and (3.89) leads to (cf. [150])

$$\mathscr{H}_D = \omega_c a^\dagger a + \sqrt{\Omega^2 + 4g\Omega(a^\dagger a + {}^1\!/_2)}\Big(b^\dagger b + \frac{1}{2}\Big) . \tag{3.90}$$

Eq. (3.90) describes two harmonic oscillators whose frequencies depend on the quantum state of the other, making this system a paradigm for state sensitive quantum dynamics. With this transformation, it is possible to evaluate exactly the time-evolution of the quantum state for arbitrary coupling strengths, as well as any physical observable, via the time-evolution operator $W(t) = S^\dagger(\hat{r}(a^\dagger a))e^{-i\mathscr{H}_D t}S(\hat{r}(a^\dagger a))$ (a disentangled form for W can be found in [151]). The time-evolution of the displacement is

$$x(t) = W^\dagger(t)(b + b^\dagger)W(t) = \cos(\varpi t)x(0) + \frac{\Omega}{\varpi}\sin(\varpi t)p(0) , \tag{3.91}$$

where $\varpi = \sqrt{\Omega^2 + 4g\Omega(a^\dagger a + \frac{1}{2})}$, $x = b + b^\dagger$, and $p = i(b^\dagger - b)$. As ϖ depends on the photon number, $x(t)$ displays a different frequency for each $|n\rangle$, with a relative height dependent

of $|\langle n|\psi\rangle|^2$, where $|\psi\rangle$ is the cavity state. Thus, measuring the resonator's spectral density provides a direct way to determine the photon statistics in the optical domain.

A direct consequence of this photon number sensitivity for the mechanical motion is that these frequencies interfere, leading to collapse and revivals. When this interference occurs, the resonator's mean displacement quickly drops to 0 (the collapse), only to reappear again at a latter time (the revival) [150]. This behaviour is displayed in Fig. 3.13 for the initial coherent states $|\beta = 2, \alpha = 6\rangle$, where β (α) is the phonon (photon) state. In general, the mechanical motion is not periodic because of the incommensurability of the frequencies (see Eq.(3.90)). Consequently, each revival is smaller and broader than the previous one, and after several revivals, these start to overlap and interfere with each other. From that moment on, the motion exhibits a seemingly chaotic behaviour. The collapse and revival times can be estimated using well-known techniques from cavity QED [155–157]. For large coherent photon states ($|\alpha|^2 \gg 1$), the Poissonian distribution can be approximated by a Gaussian distribution, and in the single-photon weak coupling regime, $\bar{\omega}$ can be expanded in powers of g. Replacing the sum in the Fock basis by an integral via the Poisson summation formula, the mechanical displacement can be expressed as an oscillation, whose amplitude is modulated by Gaussian envelops of the form

$$\langle x(t)\rangle \approx 2\beta \sum_m \cos(\bar{\omega}_\alpha t + 2\pi|\alpha|^2 m) exp\left(-\frac{1}{2}\left(\frac{t - mT_{rev}}{T_{coll}}\right)^2\right), \tag{3.92}$$

where α is the initial cavity coherent state, the initial phonon coherent state β was taken to be real, and $\bar{\omega}_\alpha = \sqrt{\Omega^2 + 4g|\alpha|^2\Omega}$. The collapse and revival times (T_{coll} and T_{rev}, respectively) are given by

$$T_{rev} = 2\pi|\alpha| T_{coll} = \frac{\pi\sqrt{\Omega^2 + 4g|\alpha|^2\Omega}}{g\Omega}. \tag{3.93}$$

In contrast to cavity QED [155–157], the revival time in these optomechanical systems depends on the average photon number, whereas for high photon numbers ($4g|\alpha|^2 \gg \Omega$), the collapse time becomes independent of the mean photon number ($T_{coll}^{-1} \sim \sqrt{g\Omega}$). This collapse and revival behaviour is not restricted to the displacement, and it is visible for any mechanical observable as long as $2\pi|\alpha| > 1$. Namely, the displacement variance for a thermal phonon state and a coherent state α for the cavity is

$$\langle x^2(t)\rangle \approx (2n_{th} + 1)\left(\frac{\Omega + 2g|\alpha|^2}{\Omega + 4g|\alpha|^2} - e^{-|\alpha|^2}\sum_{n=0}^{+\infty}\frac{|\alpha|^{2n}}{n!}\frac{2gn}{\Omega + 4gn}\cos(2\bar{\omega}_n t)\right), \tag{3.94}$$

where n_{th} is the average phonon number of the thermal state. As seen from Fig. 3.13 and Eq.(3.94), the interaction creates squeezing, but for an initial coherent cavity state, the non-oscillating quadrature uncertainty can never be reduced to less than a half of the thermal uncertainty. Nevertheless, at the peak of each revival, the minimum uncertainty has no lower bound. Further, Fig. 3.13 shows that the appearance of collapse and revivals is not restricted to coherent states, and that the temporal envelope is characteristic of the cavity state. Particularly, for a vacuum squeezed photon state $|r\rangle$, the shape of the revival is elongated due to the superposition of the revival's echoes [157], with an envelope that changes in time.

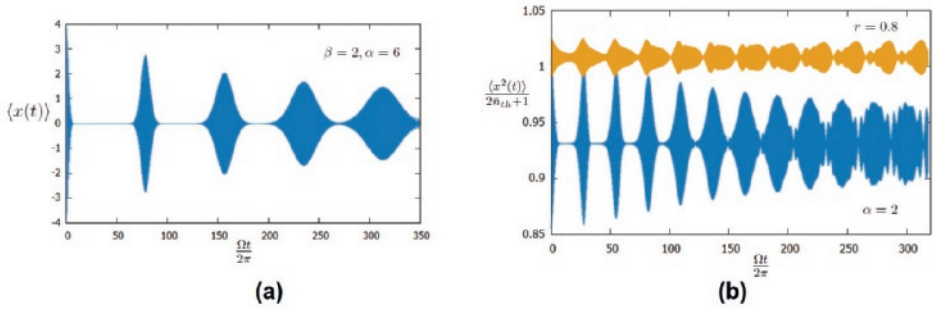

Figure 3.13: **(a)** Expected mechanical displacement for the initial coherent states $|\beta = 2, \alpha = 6\rangle$, and coupling $g = 0.01\Omega$. The mechanical displacement rapidly decays to 0 (the collapse event) and after ≈ 78 periods, the oscillation reappears (the revival). The revivals become smaller and broader with time, until interference between successive revivals occurs.**(b)** Collapse and revival behaviour of the displacement variance for an initial thermal state of the resonator, and for the cavity states $|\alpha = 2\rangle$ and $|r = 0.8\rangle$, where α and r denote coherent and vacuum squeezed states, respectively. The shape of the revivals is characteristic of the cavity state, and for a squeezed state, the revival's envelope changes with time.

As hinted in Eq.(3.94), the resonator experiences squeezing, and so the quantum state does not remain static. The time-evolution of the mechanical state for the initial phonon state $|0\rangle$ and cavity Fock state $|100\rangle$ is displayed in Fig. 3.14, where the Husimi Q-function for the resonator was computed using QuTiP [129]. For an initial cavity Fock state, the mechanical state is periodically squeezed, with the period determined by the effective phonon frequency in Eq.(3.91). Note that this feature solely depends on the initial cavity (Fock) state. The reason for this effect comes from the original form of the interaction (Eq.(3.85)), which comprises a photon-number dependent mechanical frequency, and squeezing interaction.

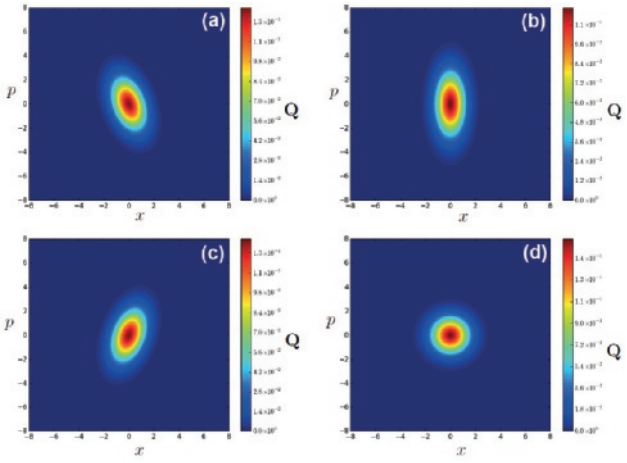

Figure 3.14: Time-evolution of Q-function of the mechanical state for $g = 0.01\Omega$, an initial cavity Fock state $N = 100$, and mechanical ground-state, after ($^1/_4, ^1/_2, ^3/_4, 1$) effective mechanical periods (panels (a),(b),(c), and (d), respectively). The interaction produces a periodic squeezing of the resonator.

Besides squeezed states, which have already been discussed in the literature [151], other quantum states can be created, depending on the initial cavity state. For a coherent cavity state $|\alpha = \sqrt{40}\rangle$ (and initial mechanical Fock state $|n = 2\rangle$), the mechanical state evolves into a superposition state after several periods (Fig. 3.15, panels (c,d)). The state undergoes rapid changes even within a period. As seen in Fig. 3.15, the state goes from a superposition-like state (panel (d)) to a state resembling a superposition of four coherent states (panel(e)), and afterwards to a seemingly distorted Fock state (panel (f)).

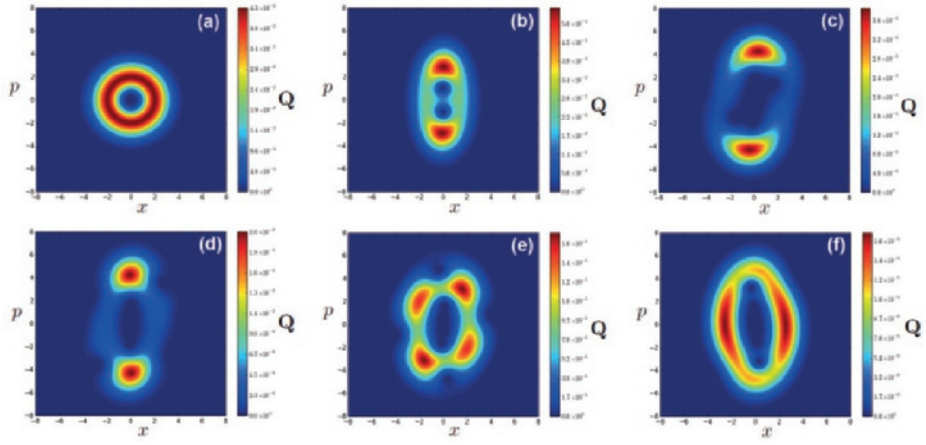

Figure 3.15: Time-evolution of Q-function of the mechanical state for $g = 0.01\Omega$, an initial phonon Fock state $n = 2$, and cavity coherent state $\alpha = \sqrt{40}$, after $(0, 1\,1/2, 130, 260, 260\,1/4, 261)$ effective mechanical periods (panels (a),(b),(c),(d),(e) and (f), respectively). After $1\,1/2$ periods, the Fock state (a) suffers a quadrature squeezing (b). Several periods later, the state evolves into a superposition-like state (c). The mechanical state undergoes rapid transformations within a period. This is seen from the superposition state (d) evolving to a state resembling a superposition of four coherent states (e), and afterwards to a seemingly distorted Fock state (f).

Note that even though the existence of two peaks in the Q function is insufficient to claim that the resonator is in a superposition state, it is clear from panel (d) of Fig. 3.15 that the quantum state is not a statistical mixture of coherent states. For the statistical mixture of coherent states $\rho = \frac{1}{2}(|i\beta\rangle\langle i\beta| + |-i\beta\rangle\langle -i\beta|)$, the Q function is

$$Q_{mixt}(\alpha) = \frac{1}{2\pi}\left(e^{-|\alpha - i\beta|^2} + e^{-|\alpha + i\beta|^2}\right), \tag{3.95}$$

which has two separate peaks like the aforementioned figure, but it is also Gaussian distributed along the line $Im\{\alpha\} = p = 0$. On the other hand, panel (d) of Fig. 3.15 displays a small deep around the origin and it has two maxima along the $p = 0$ line, and so the state cannot be a simple statistical mixture. The overall quantum state is quite complex because the mechanical state is entangled with the light state, but since no dissipation nor noise are present, this state is expected to display quantum correlations.

3.4.2. ZERO-POINT ENERGY EFFECTS

The analysis above considered only the coupling between one optical mode and the resonator. However, even if there are no photons for a given cavity mode, Eq.(3.90) shows

that this mode still plays a role due to the zero-point energy (ZPE). Due to conservation of the photon number, the multi-mode case can be easily approached for an arbitrary number of modes. With the substitution $g(a^\dagger a + 1/2) \rightarrow \sum_j g_j(a_j^\dagger a_j + 1/2)$, the transformation in Eq.(3.86) can be generalized to diagonalize the multi-mode Hamiltonian.

Even though g is small for most physical implementations of quadratic coupling, the contribution of several cavity modes enhances the mechanical frequency shift produced by ZPE. A simple way to measure this frequency shift is to place the membrane at a high symmetry point of the cavity (such as the centre of the cavity, where all optical modes couple quadratically to the membrane) and measure its frequency Ω_{centre}, and then shift the membrane to a point of low symmetry (such as close to one of the end mirrors) and measure the frequency Ω_{end} at this position. Note that the cavity should not be driven to prevent undesired contributions. Although it is not possible to monitor the membrane's position if the optics couples quadratically to the mechanics, the mechanical frequency can still be determined by a laser probe out of axes and independent of the cavity system, or by a mechanical probe. In the multi-mode single-photon weak-coupling regime, ZPE is responsible for the frequency difference

$$\Omega_{end} - \Omega_{centre} \approx 2 \sum_{j,even} g_j = G. \tag{3.96}$$

It is possible to implement this proposal with the existing technology [140, 141, 143], and it represents an alternative to force or displacement measurements of ZPE. In order for this scheme to be feasible, the frequency difference G must surpass the mechanical linewidth Γ, which does not require achieving the single-photon strong coupling regime. So far, G has never been determined, and the enhancement produced by all the even cavity modes is yet unknown. Apart from relatively high values for cold atoms implementations [146], the quadratic coupling for a single mode is in general quite small ($\sim 5\mu$Hz [143]). Although mechanical linewidths on the order of a few μHz exist [158], such small frequency differences may be difficult to detect. However, G is expected to increase by a few orders of magnitude with the use of low frequency resonators ($g \propto x_{ZPM}^2 \propto \Omega^{-1}$), and at least by another 2 orders of magnitude with the use of highly reflective membranes [159]. The combination of these improvements may bring the quadratic single-photon coupling to the Hz regime, where it can surpass existent mechanical linewidths, and ensure the feasibility of this proposal.

Note that despite the connection to ZPE, the nature of this frequency shift is not clear-cut. As remarked by [160], the fundamental interaction of the electromagnetic field with matter does not have ZPE terms, and so ZPE cannot have a direct physical effect. ZPE-like phenomena are known to arise as an asymptotic limit of detailed microscopic models [160, 161], and it may be the case for this frequency shift.

3.4.3. DRIVEN CAVITY

Physical systems experience dissipation and noise, and the cavity decay rate κ can easily surpass the effective interaction strength $g|\alpha|^2$. This implies that after the short timescale of κ^{-1}, most photons will have leaked out of the cavity and no longer interact with the mechanical resonator. To ensure a steady photon number, the cavity must be driven. As both driving and dissipation break the conservation of photon number present in the

isolated system case, it is difficult to obtain an exact solution for this situation. However, for weak driving (i.e. $|\alpha|^2 \ll \Omega/g$, with $|\alpha|^2$ the intracavity photon number created by the probe laser), one can disregard the off-resonant interaction term $a^\dagger a(bb+b^\dagger b^\dagger)$ invoking RWA. With this approximation, the effective Hamiltonian in the drive reference frame is

$$\mathscr{H} = -\Delta a^\dagger a + \Omega b^\dagger b + i\mathscr{E}(a-a^\dagger) + 2g a^\dagger a b^\dagger b, \tag{3.97}$$

where $\Delta = \omega_L - \omega_c - g$ is the detuning and $\mathscr{E}$ the driving strength. Within RWA, the interaction preserves the phonon number, and so the mechanical state can be identified by probing the cavity without any backaction. To take the effects of dissipation into account, we use the Fokker-Planck equation for the Husimi functions $Q_n(\alpha) = \frac{1}{\pi}\langle n,\alpha|\rho|n,\alpha\rangle$, where n refers to a phonon Fock state, and α to a photon coherent state. Using the standard master equation techniques [84], the Fokker-Planck equation for the system is

$$\begin{aligned}\partial_t Q_n = {} & i(-\Delta+2gn)(\alpha\partial_\alpha - \alpha^*\partial_{\alpha^*})Q_n - \mathscr{E}(\partial_\alpha + \partial_{\alpha^*})Q_n \\ & + \kappa Q_n + \frac{\kappa}{2}(\alpha\partial_\alpha + \alpha^*\partial_{\alpha^*})Q_n + \kappa\partial_\alpha\partial_{\alpha^*}Q_n\,.\end{aligned} \tag{3.98}$$

Since the timescale κ^{-1} is quite short, the interest lies not in the dynamics, but in the stationary properties. Additionally, we assume that the resonator is in a stationary state. This can be achieved by waiting until the steady-state is reached and optically probe the resonator afterwards. Even if the resonator is not in a steady-state, it can still be assumed that the mechanical state is stationary if the mechanical thermalization rate $\Gamma\bar{n}_{th}$ is much smaller than the inverse of the measurement time. The stationary solution of Eq. (3.98) is

$$Q_{n,ss} = \frac{1}{\pi} exp\left(-\left|\alpha - \frac{\mathscr{E}}{\frac{\kappa}{2} - i(\Delta - 2gn)}\right|^2\right), \tag{3.99}$$

which leads to the intracavity field amplitude

$$\langle a\rangle_{ss} = \int \alpha \sum_n Q_{n,ss} d^2\alpha = \sum_n \frac{\mathscr{E} p_n}{\frac{\kappa}{2} - i(\Delta - 2gn)}, \tag{3.100}$$

where p_n is the probability to find the mechanical resonator in the Fock state $|n\rangle$. A consequence of the interaction is that the phonon statistics leaves a signature on the cavity field. Eq. (3.100) features a set of peaks, each corresponding to a specific phonon number, and with a relative height of p_n. Therefore, the phonon statistics can be directly determined via the field amplitude, and measured by the cavity transmission $|t|^2$. The transmission is defined as the ratio between the coherent output power and the coherent input power

$$|t|^2 = \left|\frac{\langle a_{out}\rangle}{\langle a_{in}\rangle}\right|^2 = \left|\frac{\kappa_e\langle a\rangle}{2\mathscr{E}}\right|^2, \tag{3.101}$$

where κ_e is the decay rate through the output mirror (taken to be $\approx \kappa$ onwards). If the single-photon strong coupling is reached ($4g \gg \kappa$), each of the Fock peaks in the transmission is well-resolved and the phonon distribution can be immediately identified (see Fig. 3.16). Despite this regime being far from being achieved experimentally, there are still interesting features outside this regime. Particularly, one can still characterize the

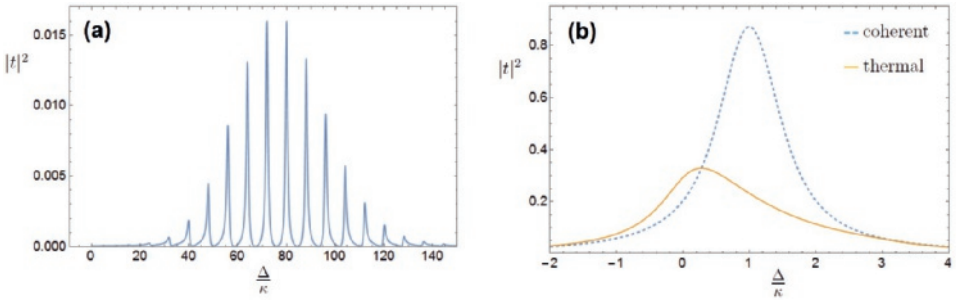

Figure 3.16: **(a)** Cavity transmission for $g = 4\kappa$ and a coherent mechanical state with $|\beta|^2 = 10$. In the single-photon strong coupling regime, the relative height of the n^{th} peak corresponds to the probability to find the mechanical resonator in a Fock state $|n\rangle$; **(b)** Comparison of the cavity transmission for a mechanical thermal state (thick yellow line) and for a coherent state (dashed blue line), with $g = 0.01\kappa$ and with an average of 50 phonons for both states. In this regime, the quantum state is not fully resolved, but the transmission lineshape still exhibits distinctive features characteristic of the mechanical state.

state without the peaks being fully resolved. In the strong coupling regime (defined here as $4g\bar{n}_b \gg \kappa$, with $\bar{n}_b$ the average phonon number), the transmission exhibits a lineshape characteristic of the mechanical state, as shown in Fig. 3.16.

Even if the average phonon number is the same, the transmission for a coherent state differs substantially from the transmission for a thermal state. The coherent state distribution for large average phonon number resembles a Gaussian, which is directly reflected in the transmission profile (note the deviation from $\Delta = 0$), whereas for a thermal state, we see that there is a strong asymmetry in the transmission. This asymmetry is a consequence of the Boltzmann exponential trend, and it can be used to determine the temperature of the resonator. For a thermal state, $p_n = \frac{1}{\bar{n}_{th}}\left(\frac{\bar{n}_{th}}{\bar{n}_{th}+1}\right)^{n+1}$, and using Eqs. (3.100,3.101), the transmission becomes

$$|t|^2 = \frac{\kappa_e^2}{\kappa^2 + 4\Delta^2}\left|{}_2F_1\left(1, -\frac{\kappa i + 2\Delta}{4g}, 1 - \frac{\kappa i + 2\Delta}{4g}, \frac{\bar{n}_{th}}{\bar{n}_{th}+1}\right)\right|^2 \tag{3.102}$$

where ${}_2F_1(a,b,c,z)$ is the Hypergeometric function. This transmission thermometry provides a simple method to determine the resonator temperature with the use of Eq.(3.102). The transmission asymmetry is in principle visible with a slight improvement on the state-of-the-art setups since for $g \sim 100\mu$Hz and for kHz resonators at room temperature, the multi-phonon strong coupling regime can be achieved for cavity linewidths up to the MHz range. Although we are mostly concerned about the properties of the mechanical resonator, the latter can also be used to change the cavity properties. As the area below the transmission lineshape is independent of the quantum state, and higher $\bar{n}_b$ lead to broader and smaller transmission profiles, the mechanical element can be employed as a switch controlling the light intensity exiting the cavity.

This mechanical state dependent cavity transmission behaviour (in particular the behaviour represented in panel (a) of Fig. 3.16) is much similar to the microwave spectral features found in circuit QED [162], and it is what makes MIM cavities the most promising optomechanical setup to observe the quantization of mechanical degrees of free-

dom, in a situation devoid of other potential quantum influences such as electronic excitations. Note however that the observation of a quantized behaviour is not necessarily a proof of a quantum nature (see [163]), and that a proper quantum-classical discussion must always have an unbiased comparison with possible non-quantum explanations.

4

HOW TO DISTINGUISH

Concerning the ontological repercussions of Quantum Theory, all its patriarchs have judged alike: it is nonsensical. Was it their pragmatism that led the neophytes to defend it so hardly? Since its birth, Quantum Theory has been a foreign and exotic land, sprouting with predictions and physical consequences that stood in direct contradiction with the everyday experience. To withstand the clash with the contemporary institutionalized theories, and to solidify its legitimacy, Quantum Theory had to define a frontier past which its singular features would vanish, and its position would be conceded to Classical Physics. The program to define a quantum-to-classical transition borderline was not particularly successful, and it was mostly abandoned with the subsequent quantum hegemony. For too long lingered such matters in slumber, and most attempts to address such problems were seen as theological speculations. The current trend on quantum systems with macroscopic mechanical elements has revived the interest, but this time with an agenda for reclaiming additional vital space for Quantum Theory.

The loose thoughts composing this last chapter are not intended to solve the quantum-to-classical transition problem, but to advert to recurring issues of presumed solutions to this problem, as well as other issues in distinguishing and defining whether an object has a quantum nature or not.

4.1. DISTINGUISHING QUANTUM FROM CLASSICAL

In the previous chapters, a thorough discussion on the nature of diverse phenomena was carried out. Several of them were shown to have a classical nature, while others were deemed quantum due to the absence of a classical explanation. But how is it possible to know in general if a given phenomenon has a truly quantum nature or not?

In subsection 3.4.1, it was shown that collapse and revivals of mechanical motion can occur in the MIM geometry. This effect arises due to the discreteness of the Fock basis, which strongly suggests a quantum nature. It is commonly stated without proof that the collapse event is a purely stochastic feature while the revivals are a true manifestation of a quantum nature [164]. To analyse this assertion, consider the case of an optical

cavity with a nonlinear medium inside (a Kerr medium). The Hamiltonian describing the system is

$$\mathscr{H} = \omega a^\dagger a + K a^\dagger a^\dagger a a, \tag{4.1}$$

where K is the Kerr nonlinearity parameter. The time-evolution is given by

$$a(t) = e^{-i(\omega + 2K a^\dagger a)t} a(0). \tag{4.2}$$

For a coherent state β ($\beta \in \mathbb{R}$ for simplicity), the average field quadrature $\langle a + a^\dagger \rangle$ evolves in time as

$$\langle a + a^\dagger \rangle(t) = 2\beta exp\Big(-|\beta|^2(1-\cos(2Kt))\Big)\cos\Big(\omega t + |\beta|^2 \sin(2Kt)\Big) \tag{4.3}$$

4

This leads to the standard collapse and revivals behaviour presented before, with the single exception that if ω/K is an integer, the system is periodic and there is no breakdown of the revivals. To compare the quantum behaviour with the classical one, it is considered the case where the electromagnetic field has a stochastic nature (i.e. the optical mode has an associated probability distribution for the amplitude and phase of the respective classical field) with a time-evolution analogous to Eq.(4.4), i.e.

$$\alpha(t) = e^{-i(\omega + 2K|\alpha|^2)t} \alpha(0), \tag{4.4}$$

where α is the complex amplitude of the field. As the Wigner (or Q) function for a coherent state is a Gaussian function, the classical probability distribution representing the state of the field is also chosen to be a Gaussian: $\mathbb{P}(\alpha) = (2\pi\delta^2)^{-1} exp\Big(-\frac{|\alpha-\beta|^2}{2\delta^2}\Big)$. With this choice, the time-evolution of the average electric field is governed by

$$\begin{aligned}\langle \alpha + \alpha^* \rangle(t) &= \int (\alpha + \alpha^*)\mathbb{P}(\alpha) d^2\alpha = \frac{2\beta}{(1+16K^2t^2\delta^4)^2} exp\left(-\frac{8K^2|\beta|^2 t^2\delta^2}{1+16K^2t^2\delta^4}\right) \times \\ &\times \left[(1-16K^2t^2\delta^4)\cos\left(\omega t + \frac{2K|\beta|^2 t}{1+16K^2t^2\delta^4}\right) - 8Kt\delta^2 \sin\left(\omega t + \frac{2K|\beta|^2 t}{1+16K^2t^2\delta^4}\right)\right].\end{aligned} \tag{4.5}$$

When $\delta \to 0$, the system behaves simply as a harmonic resonator of frequency $\omega + 2K|\beta|^2$. However, provided that there is a nonnull uncertainty in the field, Eq.(4.5) reveals that $\langle \alpha + \alpha^* \rangle \to 0$ as $t \to +\infty$. In particular, for $\delta = |\beta|$ (an uncertainty reminiscent of the Poissonian distribution), Eq.(4.5) simplifies to

$$\langle \alpha + \alpha^* \rangle(t) = \frac{2\beta exp\left(-\frac{2\varphi^2}{1+4\varphi^2}\right)}{(1+4\varphi^2)^2}\left[(1-4\varphi^2)\cos\left(\omega t + \frac{\varphi}{1+4\varphi^2}\right) - 4\varphi \sin\left(\omega t + \frac{\varphi}{1+4\varphi^2}\right)\right], \tag{4.6}$$

where $\varphi = 2K|\beta|^2 t$. The resulting behaviour for $|\beta|^2 = 10$, $\omega = 100K$ and for a quantum coherent state and classical Gaussian state is shown in Fig.4.1. In this classical case, the field oscillations decay with a Gaussian envelope (see Eq.(4.6)), never to reemerge again.

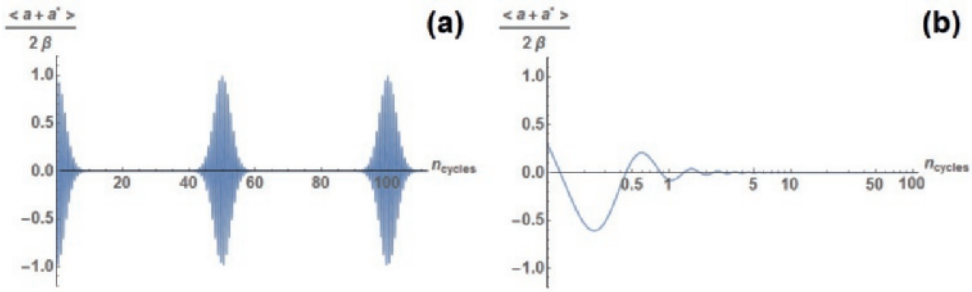

Figure 4.1: Time evolution (in number of cycles) of the field amplitude $\langle a + a^* \rangle$ for $|\beta|^2 = 10$ and $K = 0.01\omega$. For a coherent quantum state **(a)**, there is a periodic revival of the oscillations, whereas for a classical Gaussian state of variance $|\beta|^2$ **(b)**, after the initial collapse, no revival ever occurs. Note also that the collapse for the classical case takes place considerably before the quantum case.

This example provides a simple distinctive difference between the quantum and classical frameworks. However, this relied on the choice of a particular probability distribution. Could there be a probability distribution $\mathbb{P}$ such that revivals occur in a classical situation? To answer this question, consider the long time behaviour of the field quadrature $E = \alpha + \alpha^*$

$$\begin{aligned}\langle E(t)\rangle &= Re\left\{\int d^2\alpha\, \alpha \mathbb{P}(\alpha,\alpha^*)e^{-iK|\alpha|^2 t}\right\}\\ &= Re\left\{\int_0^{2\pi} d\phi \int_0^{+\infty} dr\, r^2 e^{i\phi - iKr^2 t}\mathbb{P}(r,\phi)\right\},\end{aligned} \tag{4.7}$$

where the change of variables $\alpha e^{-i\omega t} \to \alpha$ and the polar coordinates $\alpha = re^{i\phi}$ were used. Writing $f(r) = \int_0^{2\pi} e^{i\phi}\mathbb{P}(r,\phi)d\phi$ and integrating by parts leads to

$$\langle E(t)\rangle = Re\left\{\frac{1}{2iKt}\int_0^{+\infty} dr\, e^{-iKr^2 t}\partial_r\big(rf(r)\big)\right\}. \tag{4.8}$$

Further, the field amplitude decays with time since

$$\begin{aligned}|\langle E(t)\rangle| &\le \frac{1}{2Kt}\left|\int_0^{+\infty} dr\, e^{-iKr^2 t}\partial_r\big(rf(r)\big)\right|\\ &\le \frac{1}{2Kt}\left(\left|\int_0^{+\infty} dr\, e^{-iKr^2 t} f(r)\right| + \left|\int_0^{+\infty} dr\, re^{-iKr^2 t}\partial_r f(r)\right|\right)\\ &\le \frac{1}{2Kt}\left(1 + \frac{1}{2Kt}\left(\big|\partial_r f\big|(0) + \left|\int_0^{+\infty} dr|\partial_r^2 f(r)|\right|\right)\right)\\ &\le \frac{1}{2Kt}\left(1+\frac{\xi}{Kt}\right),\end{aligned} \tag{4.9}$$

where

$$\xi = \big|\partial_r f\big|(0) + \sum_{x_i}|\partial f|(x_i) \quad \text{with} \quad \{x_i : \partial^2 f(x_i) = 0\}. \tag{4.10}$$

Thus, for any "well-behaved" probability distribution (ξ finite), the average field amplitude decays with at least t^{-1} as $t \to \infty$. In a quantum picture, the system can be periodic,

and as Eq.(4.9) predicts an amplitude decay for a classical probability function, the two situations are never alike. Note that it was not proven that revivals cannot occur classically, but only that the field amplitude must always decay in time. The only implication is the impossibility of periodic revivals for well-behaved distributions. The possibility of decaying revivals in a classical picture is still open. It is also tempting to believe that the existence of periodical revivals provides a signature of a purely quantum nature. But it is not the case. To be able to display a revival, the decay induced by the uncertainties must be overcome, which is accomplished if the probability distribution breaks the good behaviour condition assumed above. If the distribution is composed by a set of δ peaks, the field amplitude is shielded from the decay induced by uncertainty in phase space. In particular, computing the average field quadrature $\langle E\rangle$ for the probability distribution

$$\mathbb{P}(\alpha,\alpha^*) = e^{-|\beta|^2}\sum_{n=0}^{+\infty}\frac{|\beta|^{2n}}{n!}\delta(\alpha-\sqrt{n})\delta(\alpha^*-\sqrt{n}) \tag{4.11}$$

leads to

$$\langle E(t)\rangle = e^{-|\beta|^2}\sum_{n=0}^{+\infty}\frac{|\beta|^{2n}}{n!}\sqrt{n}\cos\big((\omega+2Kn)t\big). \tag{4.12}$$

The time-evolution of Eq.(4.12) is displayed in Fig. 4.2 for the same parameters as the previous cases ($\omega = 100K$ and $|\beta|^2 = 10$). It is clear from the figure that it is possible for revivals to occur with a classical probability distribution (in this case the one in Eq.(4.11)), and for the collapse and revivals times to be (at least approximately) the same as their quantum counterparts.

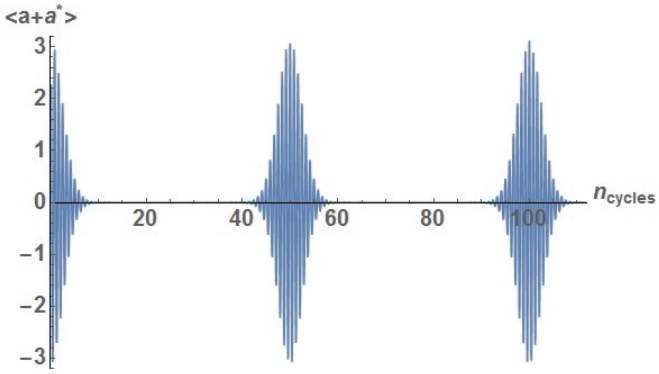

Figure 4.2: Time-evolution of the average electric field as given in Eq.(4.12) for $K = 0.01\omega$ and $|\beta|^2 = 10$. It is visible from the plot that not only collapse and revivals occur in a classical framework, but they also have the same characteristic times as the quantum ones displayed in Fig. 4.1.

It is thus possible for revivals to exist in a classical framework provided that the chosen distribution mimics the discreteness of a quantum basis. What is not possible is to match all statistical properties of the system for both quantum and classical frameworks. Although Eq.(4.12) is able to provide a classical description of revivals, its prediction differs from the quantum case (Eq.(4.3)). The differences between the two situations become slightly more prominent as one evaluates higher order moments. Namely, for the

quantum case, $\langle E^2 \rangle$ is given by

$$\langle E^2 \rangle_{quant}(t) = 2\beta^2 + 1 + 2\beta^2 exp\Big(-|\beta|^2(1-\cos(4Kt))\Big)\cos\Big(2(\omega+K)t+\beta^2\sin(4Kt)\Big), \quad (4.13)$$

while for the classical case with revivals

$$\langle E^2 \rangle_{class}(t) = 2\beta^2 + 2\beta^2 exp\Big(-|\beta|^2(1-\cos(4Kt))\Big)\cos\Big(2(\omega+2K)t+\beta^2\sin(4Kt)\Big). \quad (4.14)$$

The qualitative behaviour is the same for both scenarios, but there a few quantitative differences. Specifically, zero-point fluctuations give an additional contribution to $\langle E^2 \rangle$, and the classical and quantum cases differ in the frequency of the fast oscillating component ($2(\omega+2K)$ and $2(\omega+K)$ respectively). This frequency difference comes from the commutation relations between $exp(-2iKa^\dagger a t)$ and a, and it provides a way to distinguish between the classical and quantum scenarios since K can be determined from the revival time $\tau_{rev} = \pi K^{-1}$. The difference between the classical and quantum descriptions can also be found in the equations governing the (quasi)probability distribution describing the state of the system. In the quantum case, for the $\mathscr{P}$ distribution for example, there are additional terms stemming from the nonlinearity (such as $K(\alpha^2\partial_\alpha^2 - (\alpha*)^2\partial_{\alpha*}^2)\mathscr{P}$) which produce a different time-evolution. Such differences can only arise when there is a form of nonlinearity present, and it is the only way for the classical and quantum cases to be distinguishable.

Another reason behind the overall differences between the classical and quantum predictions is that for revivals to occur in a classical framework, the probability distribution must be a set of δs like the one in Eq.(4.11). For this distribution, the measurement outcome of the field amplitude is a discrete set of values associated with each sharp peak in phase space. For the quantum framework, the Wigner function for a coherent state is a Gaussian function in phase space, implying that the probability distribution for the measurement of the field amplitude is also a Gaussian. Thus, even if the occurrence of revivals is possible to mimic in a classical framework, it is impossible to match all physical outcomes and higher order correlations with the quantum scenario.

An interesting property of the collapse and revivals effects is that their qualitative behaviour (Gaussian shaped revival, static behaviour of the dynamical revival between the collapse and the revival events) is the same independently of the specific form of the nonlinearity used to create them. If a harmonic oscillator starts in a coherent state, the collapse and revivals are all alike whether the oscillator is coupled to another oscillator (the cavity and the mechanical element in the MIM geometry), to an atomic 2-level system (the standard textbook situation [26]) or to itself via a nonlinear medium (as discussed above). The universality of this effect, allied with its unique quantum features, provides a sturdy reference point to test whether a system does have a quantum nature. There have been several claims of observation of collapse and revivals in very distinct systems [164–167], but the observed behaviour not only differs among the experimental observations, it is also qualitatively different from the theoretical prediction. The primary obstacle preventing the observation of this effect is that for the majority of physical implementations, the relaxation rate of the system is much larger than the coupling rate (the revival time is of the order of g^{-1}, whereas the cavity photon lifetime is of $\kappa^{-1} \ll g^{-1}$). Thus, light will leak out of the cavity before the revival occurs, unless the resonantly strong coupling regime is achieved.

What the preceding analysis tells is that to determine whether the nature of a given phenomenon is quantum or not, one must always test if there is a probability distribution $\mathbb{P}$ that can describe the measured outcomes, and look for correlations that cannot have a classical counterpart.

4.2. DEQUANTIZATION ISSUES AND THE CLASSICAL LIMIT

Due to the longstanding and successful tradition of classical physics to model the majority of everyday phenomena, the presupposed ubiquity of quantum mechanics implies the existence of a limit where the predictions of classical physics can be derived from a quantum framework. But what is that limit?

The previous example of light propagating in a nonlinear medium provides a good starting point to analyse the so-called quantum-to-classical transition. A common statement is that quantum mechanics reduces to classical physics in the limit of high average particle number. The average particle number in the quantum situation of light propagation in a Kerr medium (as in Eq.(4.3)) is given by $|\beta|^2$, but the limit $|\beta| \to +\infty$

$$\lim_{|\beta|\to\infty} \langle a + a^\dagger \rangle(t) = 0\,, \quad \text{for } t \neq \frac{\pi n}{K}\,, \tag{4.15}$$

does not correspond to an oscillation with an amplitude dependent frequency. It does match the limit $|\beta| \to +\infty$ of its stochastic version (for example Eq.(4.5)) *presque partout* simply because when there is a finite amount of uncertainty, the field experiences an amplitude dependent decay. But even for this situation, the quantum limit is

$$\lim_{|\beta|\to\infty} \langle a + a^\dagger \rangle \left(t = \frac{\pi n}{K} \right) = 2\beta \cos\left(\frac{2\pi n \omega}{K} \right), \tag{4.16}$$

whereas its stochastic counterpart is still 0. And apart from these particular points, the general qualitative behaviour of both situations is not altered with the limit $|\beta| \to +\infty$. Moreover, if there is a limit where both situations match at all times, that limit is $|\beta| \to 0$. In this opposite limit, the quantum and the classical scenarios (namely Eqs.(4.3) and (4.6) respectively) merge into

$$\lim_{|\beta|\to 0} \frac{\langle a + a^\dagger \rangle(t)}{2\beta} = \cos(\omega t)\,. \tag{4.17}$$

However, this limit describes a simple harmonic oscillation, which does not portrait any of the interaction effects. The view that $|\beta|^2 \to \infty$ constitutes the classical limit implies that $|\beta| \to 0$ should be the full quantum limit, but Eq. (4.17) does not display any quantum behaviour of any kind nor it is different from a purely classical harmonic oscillator. This reverse limit is actually closer to the classical case, which makes the hypothesis of a high particle number to be the classical limit nonsensical. The flaws of considering $|\beta|^2 \to \infty$ the classical limit are not restricted to this particular situation. A similar reasoning applies to other remarkably distinct situations, such as for example antibunching of Fock states with a high excitation number, and bunching of thermal states with a low excitation number.

Another common statement is that quantum mechanics reduces to classical mechanics in the limit $\hbar \to 0$. However, directly computing the limit $\hbar \to 0$ gives null results for any physical observable. For a simple harmonic oscillator, the average energy $\epsilon = \hbar\omega\bar{n}$, the average momentum $p = \sqrt{\frac{\hbar m\omega}{2}}\, i\langle a^\dagger - a\rangle$, as well as any other observable scale with $\hbar^\alpha$ (with $\alpha > 0$), which makes them all vanish in the limit $\hbar \to 0$. One could think, that the limit should be understood in the sense of the expected values in terms of their zero-point uncertainties, i.e. the limit of the ratio between the physical observable and its zero-point fluctuation value. But what is then the limit of Eq.(4.3)? The Kerr nonlinearity arises from the propagation of electromagnetic fields in nonlinear media. The quantization of such nonlinearity implies that $K \propto E_{ZPF}^4 \propto \hbar^2$. Thus, under this reasoning, the classical limit of Eq.(4.3) should occur when $K \to 0$. However, $K \to 0$ makes $\langle a + a^\dagger\rangle(t)$ in Eq.(4.3) a simple oscillation of frequency ω, which is not the purely classical case nor the result in Eq.(4.5). This problem occurs for any type of nonlinearity, since the quantization rules imply that any nonlinearity vanishes when $\hbar \to 0$.

A latent problem when taking the limit $\hbar \to 0$ and comparing to the classical situation is what objects are exactly being compared. The above comparison, much like most similar comparisons, assumes that the mapping between quantum and classical objects (operators and canonical variables, the Poisson bracket and the commutator) remains unchanged with $\hbar$. However, the subtleties and pathologies of the different quantization schemes suggest that the mapping might have an intricate dependence on $\hbar$ [2]. As this mapping problem remains unsolved, not much can be further added.

If $\bar{n} \to +\infty$ and $\hbar \to 0$ do not provide good criteria for defining a classical limit, where else to look for a classical limit? As mentioned in Chapter 2, it is possible to construct inequalities that cannot be violated in a classical context. The reason why they can be violated in a quantum context is because there is no true probability distribution representing the state of the system. Namely, there must be a quasiprobability function representing the system with regions (of non-null measure) where the function is negative. It is then tempting to define a nonclassicality criterion based on these negative regions, and the classical limit via some metric between the quasiprobability distribution and some positive probabilistic state.

Apart from the possible arbitrariness associated with the choices of metric and probability functions involved, it must be clarified first why is a negative quasiprobability distribution a good indicator of a quantum nature. Before establishing a classical limit, it must first be established what is intrinsically quantum. The critical question over what is nonclassical must then be revisited.

4.3. ISSUES WITH DEFINING THE QUANTUM FRONTIER

As discussed in subsection 2.2.1, the standard photodetection model places a classical boundary for the second order correlation function: $g^{(2)} \geq 1$. In this detection model, n-folded coincidences, i.e. coincidence detections between $2n$ detectors, are proportional to the normal ordered product $\langle (a^\dagger)^{2n} a^{2n}\rangle$. The quasiprobability distribution describing normal ordered statistics is the $\mathscr{P}$-distribution. If the coincidence detection has a n-folded correlation function

$$g^{(2n)} = \frac{\langle (a^\dagger)^{2n} a^{2n}\rangle}{\langle (a^\dagger)^n a^n\rangle^2} < 1\,, \tag{4.18}$$

then a classical bound is broken. This can be confirmed by replacing the operators $(a, a^\dagger)$ by their scalar counterparts (α, α^*) and realize that the variance of $|\alpha|^{2n}$ must be negative if $g^{(2n)}_{class} < 1$. This inequality violation implies that $\mathscr{P}$ must have negative regions, which is impossible for a classical probability distribution.

The act of judging whether something is nonclassical or not is often done by finding negative regions in quasiprobability distributions (although it has also been proposed that finding the zeros of the Q function is an equivalent path [168]). Building upon these negativity foundations, hierarchies for the "intensity" of nonclassicality have been proposed [168, 169]. However, defining $\mathscr{P} < 0$ (or any other function for that matter) as a nonclassicality criterion is problematic because not all quasiprobability distributions with negative regions display nonclassical behaviour. To see that, consider the Diósi mixture [170]

$$\rho = \sum_{n=1}^{+\infty} 2^{-n} |n\rangle\langle n| . \tag{4.19}$$

The $\mathscr{P}$-distribution representing this state is

$$\mathscr{P}(\alpha) = \frac{2}{\pi} e^{-|\alpha|^2} - \delta(\alpha) . \tag{4.20}$$

Although $\mathscr{P} < 0$ at the origin, the classical bound is never violated because

$$g^{(2n)} = \frac{2^n (2n)!}{(n!)^2} > 1 , \forall n > 0 . \tag{4.21}$$

Therefore, no antibunching of any sort ever occurs. Obviously this reasoning is restricted to a particular type of measurements. There are other types of measurements that can be performed, which have different classical bounds. However, the $g^{(2)}$ bound is the one specific to normal ordered operators, whose statistics are described by the $\mathscr{P}$ distribution. Consequently, there is no equivalence between antibunching and a negative $\mathscr{P}$ distribution. There could still be other classical bounds that could be violated with a negative $\mathscr{P}$ distribution, but for such situations, $\mathscr{P}$ would not be a preferred quasiprobability distribution. For a given quantum state, there are multiple quasiprobability distributions representing it, and the negativity of a particular quasiprobability distribution function cannot fully account for the overall nonclassical features.

A stricter criterion for nonclassicality is the negativity of the Wigner function, since the Wigner function is related to the $\mathscr{P}$-function by

$$W(\alpha) = \frac{2}{\pi} \int \mathscr{P}(\beta) e^{-2|\alpha-\beta|^2} d^2\beta . \tag{4.22}$$

Because the convoluting Gaussian is always positive, $W(\alpha)$ can only be negative if $\mathscr{P}$ is negative as well. Using the negativity of W as a nonclassical criterion is a popular choice since the Wigner function can easily be inferred experimentally with quantum tomography techniques [167, 171, 172]. Although the state can be uniquely reconstructed from its marginal distributions, such uniqueness for systems with continuous variables (like bosonic systems) requires an infinite amount of precise measurements. In practice, the finite amount of possible measurements along with errors or uncertainties for the measurements, break this uniqueness and requires inversion strategies like maximization of

a likelihood function. This in turn can lead to unphysical outcomes such as an unnormalized Wigner function or density matrix (or probability distribution) as well as negative probabilities for the system to be found in a given state ψ [167, 173]. However, discovering a negative Wigner function as a result is usually not seen as pathological. The problem is in the significance of these negativities since negative probabilities already occur in classical reconstruction algorithms as a defect of the algorithm's convergence. As a side note, the negative regions of the overall Wigner functions are usually in a small region centred around the origin, which inspires to look for a connection between antibunching and other nonclassical phenomena relying on negative Wigner functions.

As the marginal distributions of W are the probability distributions for the quadratures, W is often seen as the quantum counterpart of a classical probability distribution in phase-space. Under this view, the existence of negative regions for W is a sign of a nonclassical nature. It is then said that W cannot represent a true probability distribution because of its negative regions. But independently of W being positive or not, W can never be seen as a probability distribution. And the same applies to all other quasiprobability distributions. As discussed in Section 4.1, a Gaussian probability distribution does not lead to revivals, whereas a Gaussian Wigner function does. Moreover, although the marginal distributions of W represent the probability distribution of the quadratures, other types of marginals, such as $\mathscr{R}(r) = \int d\theta r W(r,\theta)$, do not represent probability distributions of any sort.

The Wigner function for the state in Eq.(4.19) is

$$W(\alpha) = \frac{2}{3\pi} e^{-2|\alpha|^2} (2e^{\frac{4}{3}|\alpha|^2} - 3), \tag{4.23}$$

which is negative close to the origin. One might now be tempted to look for an effect or test where this negativity would lead to a fully nonclassical behaviour. In subsection 2.1.3, a classical bound was demonstrated for the CHSH inequality for quadrature measurements, but this and other Bell-like inequalities rely on systems with two independent degrees of freedom, and so they cannot be addressed. One could then think of a test involving measurements of position and momentum. Because they are conjugate variables, quantum theory states that the state of the system is not defined for particular values of (q,p). As a consequence, it is not possible to predict within a quantum framework what would be the outcome of simultaneous measurements of (x,p).

However, it is still physically possible to simultaneously measure both quadratures. For the LC circuit case, placing a voltmeter in parallel with the capacitor and an ammeter in series enables the simultaneous measurement of (q,p). Suppose now that for this situation, one measures simultaneously (q,p) and is able to repeat the measurement many times for the same state (whether by being in a stationary state or by reinitializing the state before each new measurement). How to describe the average outcome for this situation? Is it $\langle qp\rangle$, $\langle pq\rangle$, $\frac{1}{2}\langle qp+pq\rangle$, or something else? An alternative to simultaneous measurements would be conditional measurements. However, as the conditional Wigner function does not represent a conditional probability distribution, and because of the collapse postulate, it is not clear how the negativity of the Wigner function plays role in these type of measurements.

Apart from the issue that a negative Wigner function may not violate any classical bound, the negativity of the Wigner function is generally not a a necessary nor sufficient

condition for nonclassicality [174]. It is possible to observe antibunching with fully positive Gaussian states [175], and it is also possible for Bell-like inequalities to be violated with positive Wigner functions [176–178]. Therefore, the negativity of the Wigner function as a criterion for nonclassicality should be abandoned.

The reason why the negativity of quasiprobability distributions fails to be a consistent criterion for nonclassicality is because no quasiprobability distribution can ever represent a true probability distribution due to the inequivalence between quantum mechanics and a classical stochastic process. As shown in [179], contradictions arise when attempting to model quantum mechanics in such a way. Specifically, symmetric combinations of positive-valued operators can lead to negative correlations [179], impossible to mimic in any classical theory. It is nevertheless quite instructive to see what phenomena can be reproduced from classical approaches, and the best way to fully understand quantum theory is to find what is not characteristically quantum. An interesting related attempt is the reproduction of certain effects in Gaussian quantum mechanics with probability distributions with the restrictions on the minimum of uncertainty for the variables and on the precise knowledge of the value of conjugate variables [180].

The lesson to learn from all of this, is that rules of thumb to discern quantum from classical situations are an act of intellectual sloth. To be able to distinguish a truly quantum from a possibly classical situation, one must always consider the physical system together with the measurements being performed on it, and attempt to model the outcomes with the widest possible classical formalisms. Only when no classical model describes the measured observations, and if quantum theory is able to do so, then one can speak of a truly nonclassical quantum effect. And by following such procedure, quantum theory will progressively lose its mysteries, and its nature will become comprehensible. Because deep down, it is just a trick.

EPILOGUE

It takes time, but a lot of time, until a wrong idea fades away from the collective mind of a community. And in Physics, the land of step-by-step, it took several centuries for the most basic physical phenomena to be fully understood. We no longer learn from history, but if we did, we would recall that the current ardor and frenzy surrounding the "fundamental physics" of today are not unique to our time. And if we made use of history of science beyond the erection of an Olympus, we would also recall that from all the fundamental theories of the past, none still stands as such. Because what truly hampers the advance of science is not skepticism nor criticism, but the unshaken belief in idols, in canons and in theories themselves.

Ingenuity is something that we can no longer wear. Quantum Theory is already an institution in itself. It has gained widespread appeal and it has conquered its own position, thus ensuring eternal existence. Besides its premature indoctrination, its strength resides in its unity. The nature and mechanisms behind phenomena such as superconductivity or nuclear binding are completely distinct from each other as well as from any quantum optics' effect. Nevertheless, the successes of one are perceived as a general achievement of Quantum Theory. As long as this cohesion persists, sloppy theories and distorted physical notions can safely subsist under the roof of a great foundation.

Science, as an institution that zeals for owning the monopoly of *veritas aeterna*, should have as primary interest the constant reassessment and validation of its laws, as well as the excommunication of any metaphysical and paranormal dissents. Otherwise we will find that the promised golden eggs are actually made from pyrite. And instead of engaging in the ideological warfare of scientific speculations, we should simply return to the factual touchstones.

Just like men have ages, so do theories, and there is always a time when these become obsolete or recognised as ludicrous. What is the caterpillar to the butterfly but the reminder of an ignominious origin? Despite giving birth to important scientific fields and having been practiced by men of science, astrology and alchemy are now seen as a distant shameful relative by their offspring. And the same must be the present to the future. The wise men of tomorrow will diagnose our contemporary beliefs and perceptions about the Universe as a primitive desire for the supernatural, as a cunning tool for intellectual exhibitionism, as ideological zealotry, as simply, human. The path that goes from the caterpillar to the cocoon is already traversed, but there is still something very larval in us. And only with such recognition, can Physics cleanse itself from the current mysticisms. Because after each zenith, there is always a sunset.

REFERENCES

[1] P.A.M. Dirac, Principles of Quantum Mechanics. USA: Oxford University Press (1982)

[2] S.T. Ali and M. Engliš , Rev. Math. Phys. 17, 391 (2005)

[3] R. Arens and D. Babbitt , J. Math. Phys. 6, 1071 (1965); M. Engliš , Comm. Theor. Phys. 37, 287 (2002)

[4] H.J. Groenewold, Physica 12, 405 (1946)

[5] G.A. Goldin, R. Menikoff and D.H. Sharp, J. Math. Phys. 21, 650 (1980); G.A. Goldin, R. Menikoff and D.H. Sharp, J. Math. Phys. 22, 1664 (1981); G.A. Goldin and D.H. Sharp, Phys. Rev. Lett. 76, 1183 (1996)

[6] J.M. Leinaas and J. Myrheim, Nuovo Cimento B 37, 1, (1977)

[7] G.M. Tuynman, Geometric quantization, Proceedings Seminar 1983-1985: Mathematical structures in field theories, Vol.1, CWI Syllabus, vol.8 Math Centrum, CWI, Amsterdam, 1985

[8] https://physics.aps.org/story/v13/st8

[9] A.H. Compton, Phys. Rev. 21, 483 (1923)

[10] O. Klein, Z. Phys. 41, 407 (1927)

[11] G.Wentzel, Z. Phys. 43, 1 (1927)

[12] O. Klein, Y. Nishina, Z. Phys. 52 (11-12), 853 (1929)

[13] J. Barwick, Phys. Rev. A 17, 1912 (1978)

[14] S.D. Bosanac, Eur. Phys. J. D 1, 317 (1998)

[15] A. Einstein, Ann. Physik 17, 132 (1905).

[16] G. Beck, Z. Phys. 41, 443 (1927)

[17] G. Wentzel, Z. Phys. 41, 828 (1927)

[18] W.E. Lamb, Jr. and M.O. Scully, Polarization, Matière et Rayonnement (Presses University de France, Paris, 1969); H.Fearn and W.E. Lamb Jr., Phys. Rev. A 42, 2124 (1991)

[19] L. Mandel, E.C.G. Sudarshan, and E. Wolf, Proc. Phys. Soc. 84, 435 (1964)

[20] R.E.B. Makinson, Phys. Rev. 75, 12, 1908 (1949)

[21] A. Komech, Scattering of Light and Particles. In: Quantum Mechanics: Genesis and Achievements. Springer, Dordrecht, pp 117-144 (2013)

[22] P. Warszawski and H.M. Wiseman, J. Opt. B 4, 1 (2002); P. Warszawski, and H.M. Wiseman, J. Opt. B. 5, 15 (2003)

[23] O. Costin, R.D. Costin, and J.L. Lebowitz, J. Stat. Phys. 116, 283 (2004)

[24] P.A.M. Dirac, Proc. Roy. Soc. A114 (767), 243 (1927)

[25] V. Weisskopf, Naturwissenschaften 23, 631 (1935)

[26] Quantum Optics, M. O'Scully and Zubairy, Cambridge University Press (2008)

[27] E.T. Jaynes and F.W. Cummings, Proc. IEEE 51, 89 (1963)

[28] M.D. Crisp and E.T. Jaynes, Phys. Rev. 179, 1253, (1969)

[29] C.R. Stroud Jr. and E.T. Jaynes, Phys. Rev. A 1, 106, (1970)

[30] R.K. Nesbet, Phys. Rev. A 4, 259 (1971)

[31] K. Shimoda, T.C. Wang, and C.H. Townes, Phys. Rev. 102, 1308 (1956)

[32] W.E. Lamb Jr., Phys. Rev. 134, A1429 (1964)

[33] T.A. Welton, Phys. Rev. 74, 1157 (1948)

[34] W.E. Lamb Jr. and R.C. Retherford, Phys. Rev. 72, 241 (1947)

[35] H. Bethe, Phys. Rev. 72, 339 (1947); N.H. Kroll and W.E. Lamb, Jr., Phys. Rev. 75, 388 (1949); J.B. French and V. F. Weisskopf, Phys. Rev. 75, 1240 (1949); J. Barwick, J. Math. Phys. 24, 12 (1983)

[36] R.Pohl et al., Nature 466, 213 (2010); R. Pohl et al., Science 353 (6300), 669 (2016)

[37] Classical Electrodynamics, J.D. Jackson, Wiley & Sons, Inc. New York (1962)

[38] H.J. Kimble, M. Dagenais, and L. Mandel, Phys. Rev. Lett. 39, 691 (1977); M. Dagenais and L. Mandel, Phys. Rev. A 18, 2217 (1978)

[39] H.J. Carmichael et al., J. Phys. A 11, L121 (1978)

[40] P. Grangier, G. Roger and A. Aspect, Europhys. Lett. 1 (4), 173 (1986)

[41] R. Hanbury Brown and R. Q. Twiss., Proc. Roy. Soc. A. 242 (1230), 300 (1957)

[42] S.J. Freedman and J. Clauser, Phys. Rev. Lett. 28, 938 (1972)

[43] E.S. Fry and R.C. Thompson, Phys. Rev. Lett. 37, 465 (1976)

[44] J.F. Clauser, Phys. Rev. D 9, 853 (1974)

[45] R.E. Slusher, L.W. Hollberg, B. Yurke, J.C. Mertz, and J.F. Valley, Phys. Rev. Lett. 55, 2409 (1985); L.-A. Wu, H.J. Kimble, J.L. Hall, and H. Wu, Phys. Rev. Lett. 57, 2520 (1986)

[46] R.M. Shelby, M.D. Levenson, S.H. Perlmutter, R.G. DeVoe and D.F. Walls, Phys. Rev. Lett. 57, 691 (1986)

[47] S. Deléglise, et al., Nature 455, 510 (2008)

[48] A. Ourjoumtsev, H. Jeong, R. Tualle-Brouri and P. Grangier, Nature 448, 784 (2007); G. Kirchmair, et al., Nature 495, 205 (2013); B. Vlastakis, et. al, Science 342 (6158), 607 (2013)

[49] K. Hammerer: www.uibk.ac.at/th-physik/optmech2013/hammerer_innsbruck.pdf

[50] M. Aspelmeyer, T.J. Kippenberg, and F. Marquardt, Rev. Mod. Phys. 86, 1391 (2014)

[51] T. P. Purdy, R. W. Peterson, and C. A. Regal, Science 339 (6121), 801 (2013)

[52] Schliesser et al., New J. Phys. 10, 0955015 (2008); G. Anetsberger, O. Arcizet, Q. P. Unterreithmeier, R. Rivière, A. Schliesser, E. M. Weig, J. P. Kotthaus and T. J. Kippenberg, Nat. Phys. 5, 909 (2009)

[53] J. D. Teufel, T. Donner, M. A. Castellanos-Beltran, J. W. Harlow and K. W. Lehnert, Nat. Nanotechnol. 4, 820 (2009); T. Westphal, et al., Phys. Rev. A 85, 063806 (2012)

[54] I. Mahboob, H. Okamoto, K. Onomitsu, and H. Yamaguchi, Phys. Rev. Lett. 113, 167203 (2014)

[55] D.W.C. Brooks, et. al., Nature 488, 476 (2012); A.H. Safavi-Naeini et al., Nature 500, 185 (2013); T. P. Purdy, P.-L. Yu, R. W. Peterson, N.S. Kampel, and C. A. Regal, Phys. Rev. X 3, 031012 (2013)

[56] T.A. Palomaki, J.D. Teufel, R.W. Simmonds, and K.W. Lehnert, Science 342, 710 (2013)

[57] T.A. Palomaki, J.W. Harlow, J.D. Teufel, R.W.Simmonds, and K.W. Lehnert, Nature 495, 210 (2013)

[58] A.H. Safavi-Naeini, J. Chan, J. T. Hill, T.P.M. Alegre, A. Krause, and O. Painter, Phys. Rev. Lett. 108, 033602 (2012)

[59] J. Chan, T.P.M. Alegre, A.H. Safavi-Naeini, J.T. Hill, A. Krause, S. Gröblacher, M. Aspelmeyer, and O. Painter, Nature 478, 89 (2011)

[60] A.J.Weinstein, C.U. Lei, E.E. Wollman, J. Suh, A. Metelmann, A.A. Clerk and K.C. Schwab, Phys. Rev. X 4, 041003 (2014)

[61] N. Brahms, T. Botter, S. Schreppler, D.W.C. Brooks, and D.M. Stamper-Kurn, Phys. Rev. Lett. 108, 133601 (2012)

[62] T.P. Purdy, P.-L. Yu, N.S. Kampel, R.W. Peterson, K. Cicak, R.W. Simmonds, and C.A. Regal, Phys. Rev. A 92 031802, (2015); M. Underwood, D. Mason, D. Lee, H. Xu, L. Jiang, A.B. Shkarin, K. Børkje, S.M. Girvin, and J.G.E. Harris, Phys. Rev. A 92, 061801 (2005)

[63] S. Hong, R. Riedinger, I. Marinkovic, A. Wallucks, S. G. Hofer, R. A. Norte, M. Aspelmeyer, and S. Gröblacher, Science 358, 203 (2017)

[64] O'Connel et al., Nature London 464, 697 (2010)

[65] S. Girvin in "Circuit QED: superconducting qubits coupled to microwave photons", from "Quantum Machines: Measurement and Control of Engineered Quantum Systems, Lecture Notes of the Les Houches Summer School, Volume 96, 2011", Oxford Univerity Press (2014)

[66] J.C. Sankey, C. Yang, B.M. Zwickl, A.M. Jayich, and J.G.E. Harris, Nat. Phys. **6**, 707 (2010)

[67] Quantum Optics, J.C. Garrison and R.Y. Chiao, Oxford University Press (2008)

[68] C. Schori, J.L. Sørensen, and E.S. Polzik, Phys. Rev. A 66, 033802 (2002); W.P. Bowen, R. Schnabel, and P.K. Lam, Phys. Rev. Lett. 90, 043601 (2003);

[69] X. Jia, X. Su, Q. Pan, J. Gao, C. Xie, and K. Peng, Phys. Rev. Lett. 93, 250503 (2004); A. Villar, L.S. Cruz, K.N. Cassemiro, M. Martinelli, P. Nussenzveig, Phys. Rev. Lett. 95, 243603 (2005)

[70] Z. Y. Ou, S.F. Pereira, H.J. Kimble, and K.C. Peng, Phys. Rev. Lett. 68, 3663 (1992);

[71] M. D. Reid and P. D. Drummond, Phys. Rev. Lett. 60, 2731 (1988); M.D. Reid, Phys. Rev. A 40, 913 (1989)

[72] L.-M. Duan, G. Giedke, J.I. Cirac, and P. Zoller, Phys. Rev. Lett. 84, 2722 (2000)

[73] R. Simon, Phys. Rev. Lett. 84, 2726 (2000)

[74] A.E. Allahverdyan, A. Khrennikov, and Th. M. Nieuwenhuizen, Phys. Rev. A 72, 032102 (2005)

[75] N.D. Mermin, Rev. Mod. Phys. 65, 803 (1993)

[76] D.M. Greenberger, M.A. Horne, A. Shimony, and A. Zeilinger, Am. Journ. Phys. 58, 1131 (1990)

[77] E.G. Cavalcanti, J.C. Foster, M.D. Reid, and P.D. Drummond, Phys. Rev. Lett. 99, 210405 (2007)

[78] Z. Y. Ou and L. Mandel, Phys. Rev. Lett. 61, 50 (1988)

[79] A. Aspect, J. Dalibard, and G. Roger, Phys. Rev. Lett. 49, 1804 (1982)

[80] J.F. Clauser, Phys. Rev. A 6, 49 (1972)

[81] Y. H. Shih and C. O. Alley, Phys. Rev. Lett. 61, 2921 (1988)

[82] L. Mandel, Phys. Rev. 152, 438 (1966)

[83] Quantum Theory of Optical Coherence: Selected Papers and Lectures, R. J. Glauber (2007)

[84] Statistical Methods in Quantum Optics 2, H.J. Carmichael, (2008) ISBN 978-3-540-71319-7 Springer Berlin Heidelberg New York

[85] C.W. Gardiner, Quantum Noise, Springer, Berlin (1991)

[86] J.J. Thorn, M.S. Neel, V.W. Donato, G.S. Bergreen, R.E. Davies, and M. Beck, Am. Journ. Phys. 72, 1210 (2004)

[87] J.D. Cresser, Phys. Rep. 94, 47 (1983)

[88] R. Ghosh and L. Mandel, Phys. Rev. Lett. 59, 1903 (1987)

[89] Z. Y. Ou and L. Mandel, Phys. Rev. Lett. 62, 2941 (1989)

[90] P.G.Kwiat et al., Phys. Rev. A 41, R2910 (1990)

[91] Z.Y. Ou, X.Y. Zou, L.J. Wang, and L. Mandel, Phys. Rev. Lett. 65, 321 (1990)

[92] U. Eichmann et al., Phys. Rev. Lett. 70, 2359 (1993)

[93] Yoon-Ho K., R. Yu, S.P. Kulik, Y. Shih, and M.O. Scully, Phys. Rev. Lett. 84, 1 (2000)

[94] S.P. Walborn, M.O. Terra Cunha, S. Pá and C.H. Monken, Phys. Rev. A. 65, 033818 (2002)

[95] J.D.P. Machado and Ya.M. Blanter, "Absence of quantum features in sideband asymmetry", arXiv:1805.02952

[96] F. Diedrich, J.C. Bergquist, W.M. Itano, and D.J. Wineland, Phys, Rev. Lett. 62, 403 (1989); C. Monroe, D.M. Meekhof, B.E. King, S.R. Jefferts, W.M. Itano, D.J. Wineland, and P. Gould, Phys, Rev. Lett. 75, 4011 (1995)

[97] P.S. Jessen, C.Gerz, P.D. Lett, W.D. Phillips, S.L.Rolston, R.J.C. Spreeuw, and C.I. Westbrook, Phys, Rev. Lett. 69, 49 (1992)

[98] F. Ya. Khalili, H. Miao, H. Yang, A.H. Safavi-Naeini, O. Painter, and Y. Chen, Phys. Rev. A 86, 033840 (2012)

[99] I. Wilson-Rae, N. Nooshi, W. Zwerger, and T.J. Kippenberg, Phys. Rev. Lett. 99, 093901 (2007); F. Marquardt, J.P. Chen, A.A. Clerk, and S.M. Girvin, Phys. Rev. Lett. 99, 093902 (2007); D.J. Wineland, W.M. Itano, J.C. Bergquist, and R.G. Hulet, Phys. Rev. A 36, 2220 (1987); A. A. Clerk, M. H. Devoret, S. M. Girvin, F. Marquardt, and R. J. Schoelkopf, Rev. Mod. Phys. 82, 1155 (2010)

[100] A.H. Safavi-Naeini, J. Chan, J.T. Hill, S. Gröblacher, H. Miao, Y. Chen, M. Aspelmeyer, and O. Painter, New J. Phys. 15, 035007 (2013)

[101] A.M. Jayich et al., New J. Phys. 14 (2012) 115018

[102] M. Tsang, Quantum Measurements and Quantum Metrology 1, 84-109 (2013)

[103] K. Børkje, Phys. Rev. A 94, 043816 (2016)

[104] H.P.Yuen, and V.W.S. Chan, Optics Letters 8, 3, 177-179 (1983); B.L. Schumaker, Optics Letters 9, 5, 189-191 (1984); Quantum Optics, J.C. Garrison, and R.Y. Chiao, Oxford University Press (2008)

[105] M.O. Scully, and W.E. Lamb Jr., Phys. Rev. 166, 246 (1968)

[106] L. Diósi, Phys. Lett. A 129, 419 (1988); K. Jacobs, and D.A. Steck, Contemporary Physics 47, 279 (2006)

[107] R.K. Nesbet, Phys. Rev. Lett. 27, 553 (1971)

[108] J.D.P. Machado and Ya.M. Blanter, Phys. Rev. A 94, 063835 (2016)

[109] S. Mancini, V.I. Man'ko, and P. Tombesi, Phys. Rev. A 55, 3042 (1997)

[110] S. Bose, K. Jacobs, and P.L.Knight, Phys. Rev. A 56, 4175 (1997)

[111] A. Nunnenkamp, K. Børkje, and S.M. Girvin, Phys. Rev. Lett. 107, 063602 (2011); P.Rabl, Phys. Rev. Lett. 107, 063601 (2011)

[112] M. Ludwig, B. Kubala, and F. Marquardt, New J. Phys. 10, 095013 (2008); A.D. Armour and D.A. Rodrigues, C.R. Physique 13, 440 (2012); D.A. Rodrigues and A.D. Armour, Phys. Rev. Lett. 104, 053601 (2010)

[113] P.D.Nation, Phys. Rev. A 88, 053828 (2013); J. Qian, A.A. Clerk, K. Hammerer, and F. Marquardt, Phys. Rev. Lett. 109, 253601 (2012); N. Lörch, J. Qian, A. Clerk, F. Marquardt, and K. Hammerer, Phys. Rev. X 4, 011015 (2014)

[114] K. Børkje, A. Nunnenkamp, J.D. Teufel, and S.M. Girvin, Phys. Rev. Lett. 111, 053603 (2013)

[115] M.A. Lemonde, N. Didier, and A. A. Clerk, Phys. Rev. Lett. 111, 053602 (2013)

[116] M.A. Lemonde and A. A. Clerk, Phys. Rev. A 91, 033836 (2015); Yong-Chun Liu, Yun-Feng Xiao, You-Ling Chen, Xiao-Chong Yu, and Qihuang Gong, Phys. Rev. Lett. 111, 083601 (2013)

[117] R. Leijssen and E. Verhagen, Nature Sci. Rep. 5, 15974 (2015)

[118] D.W.C. Brooks, T. Botter, S. Schreppler, T.P. Purdy, N. Brahms, and D.M. Stamper-Kurn, Nature 488, 476 (2012)

[119] X. Sun, K.Y. Fong, C. Xiong, W.H.P. Pernice, W. H. P. and H. X. Tang, Opt. Express 19, 22316 (2011); W.C. Jian, X. Lu, X. J. Zhang and Q. Lin, Opt. Express 20, 15991 (2012); H. Pfeifer,T. Paraïso, L. Zang, L. and O. Painter, Opt. Express 24 (11), 11407 (2016)

[120] Y. Chu, P. Kharel, W.H. Renninger, L.D. Burkhart, L. Frunzio, P.T. Rakich, and R.J. Schoelkopf, Science 358, 199 (2017);M. Kervinen, I. Rissanen, and M. Sillanpää, Phys. Rev. B 97, 205443 (2018)

[121] M. Horowski et al., J. Physics A: Math. Gen. 37.23, 6115 (2004); G. Chadzitaskos, M. Horowski, A. Odzijewicz, and A. Tereszkiewicz, Czech. J. Phys. 53: 1015 (2003)

[122] E. Jansen, "The Degenerate Parametric Amplifier in Electromechanics", master thesis, Delft University of Technology (2018)

[123] E. Jansen, J.D.P. Machado, and Ya.M. Blanter, Phys. Rev. B 99, 045401 (2019)

[124] D.F. Walls and G.J. Milburn, *Quantum Optics*, Springer Verlag, Berlin Heidelberg (1994)

[125] J. D. Teufel et al., Nature (London) 475, 359 (2011)

[126] O. Veits and M. Fleischhauer, Phys. Rev. A 52, R4344 (1995)

[127] P.D. Drummond , K.J. McNeil and D.F. Walls, Opt. Act. 28, 211 (1981)

[128] P. D. Drummond and C. W. Gardiner, J. Phys. A: Math. Gen. 13, 2353 (1980)

[129] QuTiP 2.2.0; J.R. Johansson, P.D. Nation, and F. Nori, Comp. Phys. Comm. 183, 1760 (2012)

[130] C. Navarrete-Benlloch, E. Roldán, Y. Chang, and T. Shi, Opt. Express 22, 24010 (2014)

[131] P. Pearle, Phys. Rev. D 13, 857 (1976); G. C. Ghirardi, A. Rimini, and T. Weber, Phys. Rev. D 34, 470 (1986)

[132] L. Diósi, Phys. Lett. A 105, 199 (1984)

[133] A.D. Armour and M.P. Blencowe, New. J. Phys. 10, 095004 (2008)

[134] P. Rabl et al., Phys. Rev. B 79, 041302(R) (2009)

[135] K. E. Khosla, M. R. Vanner, N. Ares, and E. A. Laird, Phys. Rev. X 8, 021052 (2018)

[136] A. Jarmola, V. M. Acosta, K. Jensen, S. Chemerisov, and D. Budker, Phys. Rev. Lett. 108, 197601 (2012)

[137] J.D.P. Machado, R.J. Slooter, and Ya.M. Blanter, "Quantum signatures in quadratic optomechanics", arXiv:1808.01658

[138] A.A. Gangat, T.M. Stace, and G.J. Milburn, New. J. Phys. 10, 095008 (2008)

[139] M Ludwig, A.H. Safavi-Naeini, O. Painter, and F. Marquardt, Phys. Rev. Lett 109, 063601 (2012)

[140] J.D. Thompson, B.M. Zwickl, A.M. Jayich, F. Marquardt, S.M. Girvin, and J.G.E. Harris, Nature 452, 72 (2008)

[141] A.M. Jayich, J.C. Sankey, B.M. Zwickl, C. Yang, J.D. Thompson, S.M. Girvin, A.A. Clerk, F. Marquardt, and J.G.E. Harris, New. J. Phys. 10, 095008 (2008)

[142] J.C. Sankey, C. Yang, B.M. Zwickl, A.M. Jayich, and J.G.E. Harris, Nature Physics 6, 707 (2010)

[143] M. Karuza, M. Galassi, C. Biancofiore, C. Molinelli, R. Natali, P. Tombesi, G. Di Giuseppe, and D. Vitali, J. Opt. 15, 025704 (2013)

[144] C. Reinhardt, T. Müller, A. Bourassa, and J.C. Sankey, Phys. Rev. X 6, 021001 (2016)

[145] D.J. Wilson, C.A. Regal, S.B. Papp, and H.J. Kimble, Phys. Rev. Lett. 103, 207204 (2009)

[146] T.P. Purdy, D.W.C. Brooks, T. Botter, N. Brahms, Z.-Y. Ma, and D.M. Stamper-Kurn, Phys. Rev. Lett 105, 133602 (2010)

[147] Zhang-qi Yin, Andrew A. Geraci, and Tongcang Li, Int. J. Mod. Phys. B 27, 1330018 (2013)

[148] H. Seok and E. M. Wright, Phys. Rev. A 95, 053844 (2017)

[149] A. Nunnenkamp, K. Børkje, J.G.E. Harris, and S.M. Girvin, Phys. Rev. A 82, 021806 (2010)

[150] A. Rai and G.S. Agarwal, Phys. Rev. A 78, 013831 (2008)

[151] H. Shi and M. Bhattacharya, Phys. Rev. A 87, 043829 (2013)

[152] M. Bhattacharya, H. Uys, and P. Meystre, Phys. Rev. A 77, 033819 (2008)

[153] H. Seok, L.F. Buchmann, S. Singh, and P. Meystre, Phys. Rev. A 86, 063829 (2012)

[154] C. Biancofiore, M. Karuza, M. Galassi, R. Natali, P. Tombesi, G. Di Giuseppe, and D. Vitali, Phys. Rev. A 84, 033814 (2011)

[155] N.B. Narozhny, J.J. Sanchez-Mondragon, and J.H. Eberly, Phys. Rev. A 23, 236 (1981)

[156] H-I Yoo, J.J. Sanchez-Mondragon, and J.H. Eberly, J. Phys. A 14, 1383 (1981); P. Filipowicz, J. Phys. A 19, 3785 (1986)

[157] M. Fleischhauer and W.P. Schleich, Phys. Rev. A 47, 4258 (1993)

[158] B. D. Cuthbertson, M. E. Tobar, E.N. Ivanov, and D. G. Blair, Rev. Sci. Inst. 67, 2435 (1996)

[159] P. Piergentili et al., New J. Phys. 20, 083024 (2018)

[160] H. Nikolić Phys. Lett. B 761, 197 (2016); H. Nikolić Ann. Phys. 383, 181 (2017)

[161] J. Schwinger, L.L. DeRaad, Jr., and K.A. Milton, Ann. Phys. 115, 1 (1978); R.L. Jaffe, Phys. Rev. D 72, 021301 (2005)

[162] D.I. Schuster et al., Nature 445, 515 (2007)

[163] P.K. Tien and J.P. Gordon, Phys. Rev. 129, 647 (1963)

[164] G. Rempe, H. Walther and N. Klein, Phys. Rev. Lett. 58, 353 (1987)

[165] O.V. Misochko, M. Hase, K. Ishioka, and M. Kitajima, Phys. Rev. Lett. 92, 197401 (2004)

[166] D.N. Matsukevich, T. Chanelière, S.D. Jenkins, S.-Y. Lan, T.A.B. Kennedy and A. Kuzmich, Phys. Rev. Lett. 96, 033601 (2006)

[167] D. Liebfried, D.M. Meekhof, C. Monroe, B.E. King, W.M. Itano and D.J. Wineland, J. Mod. Opt. 44, 11, 2485 (1997)

[168] N. Lütkenhaus and S.M. Barnett, Phys. Rev. A 51, 3340 (1995)

[169] Th. Richter and W. Vogel, Phys. Rev. Lett 89, 283601 (2002)

[170] L. Diósi, Phys. Rev. Lett. 85, 2841 (2000)

[171] A.I. Lvovsky, and J.H. Shapiro, Phys. Rev. A, 65, 033830 (2002)

[172] A. Zavatta, V. Parigi, and M. Bellini, Phys. Rev. A 75, 052106 (2007)

[173] A.I. Lvovsky and M.G. Raymer, Rev. Mod. Phys. 81, 299 (2009)

[174] R.W. Spekens, Phys. Rev. Lett. 101, 020401 (2008)

[175] M.-A. Lemonde, N. Didier, and A. A. Clerk, Phys. Rev. A 90, 063824 (2014)

[176] M. Revzen, P.A. Mello, A. Mann, and L.M. Johansen, Phys. Rev. A 71, 022103 (2005)

[177] K. Banaszek and K. Wódkiewicz, Phys. Rev. A 58, 4345 (1998)

[178] L.M. Johansen, Phys. Lett. A 236, 173 (1997)

[179] H. Grabert, P. Hänggi, and P. Talkner, Phys. Rev. A 19, 2440 (1979)

[180] S.D. Barlett, T. Rudolph, and R.W. Spekkens, Phys. Rev. A 86, 012103 (2012)

Acknowledgements

I would like to thank everyone who played a role in the work leading to this thesis, particularly Yaroslav for his patience and trust, and the Dutch Science Foundation (NWO/FOM) for its financial support.

CVRRICVLVM VITAE

João Duarte PEREIRA MACHADO

07-01-1991	Geboren ter Lisboa, Portugal.
2006–2009	Lyceum Escola Secundária da Amadora
2009–2014	BSc.& MSc. in Physics Engineering Instituto Superior Técnico, Lisboa
	Thesis: Fractionalization in low-dimensional systems *Promotor:* Prof. P.D.S. Sacramento

PUBLICATIONS PERTAINING TO THIS THESIS

7. J.D.P. Machado and Ya.M. Blanter,“Existence of classical revivals and the quantum-to-classical transition problem” (in preparation)

6. J.D.P. Machado and Ya.M. Blanter, ”Origin and nature of state-transfer, squeezing and entanglement“ (in preparation)

5. J.D.P. Machado, F.G. Hoekstra, T.H. Oosterkamp, and Ya.M. Blanter, “Towards an interferometry experiment demonstrating superposition of a quantum force sensor coupled to a single spin” (in preparation)

4. E. Jansen, J.D.P. Machado, and Ya.M. Blanter, Phys. Rev. B 99, 045401 (2019)

3. J.D.P. Machado, R.J. Slooter, and Ya.M. Blanter, "Quantum signatures in quadratic optomechanics", arXiv:1808.01658 (submitted)

2. J.D.P. Machado and Ya.M. Blanter, "Absence of quantum features in sideband asymmetry", arXiv:1805.02952

1. J.D.P. Machado and Ya.M. Blanter, Phys. Rev. A 94, 063835 (2016)